2017

Synthesis and characterization of CdY (Y= Te/O/Se) nanoparticles by wet chemical process

A Thesis Submitted in Fulfillment of the requirements for the Degree of

MAGISTER SCIENTIAE (M.Sc.)

By Kiprotich Sharon

(BSC Hons (Physics))

Student Number: 2013107749

Faculty of Natural and Agricultural Sciences

Department of Physics, University of the Free State (QwaQwa campus), South Africa, ZA 9866

Supervisor: Prof. F.B Dejene

Co-supervisor: Prof. M.O. Onani

July 2017

Dedication

This thesis is dedicated to my lovely family and my dear parents.

Acknowledgements

- Above all I would like to express my most special heartfelt and sincere thanks to **almighty God** for His sufficient grace, love, favor and mercy for me. His continuous renewal of my strength and everlasting guidance helped me to overcome even the most difficult and trying times.
- I would like to express my sincere gratitude to my supervisor, **Prof. F.B. Dejene** and my co-supervisor, **Prof. M.O. Onani** who with their advices, constructive criticisms, valuable comments, suggestions, guidance and support throughout the study made my research a success. This study could not have been a success without them.
- I am also thankful to all my UFS QwaQwa campus research colleagues **Dr. L.F. Koao, Dr. K.G. TShabalala, Mr. J. Ungula, Mr. S.J. Motloung, Mr. R. Ocaya, Mr. J.T. Leta, Mr. N. Debelo, Ms M.A. Lephoto, Mr. P.C. Korir** and **Ms L. Meiki** of the physics department for their continuous support during my period of study.
- I am thankful to the University of Western Cape (UWC) research colleagues (chemistry department); **Mr**. **Ayabei Kiplagat** for his unfailing support throughout my synthesis and assisting me access the PL, UV-vis reflection and HRTEM equipment for characterization. Also, **Mr. Garvin**, **Ms. Rose, Mr. Hillary, Ms. Laundrea and Ms. Zuran** for their continuous encouragement and co-operation in helping me complete my experiments in their laboratories.
- I also want to thank the members of the UFS-QwaQwa campus physics department academic staff for their constant advice on various academic matters relevant to my thesis.
- I am grateful to the UFS QwaQwa campus chemistry department for letting me use their equipment in doing part of the characterization of my samples.

- I want to express my gratitude also to the South African National Research Foundation (NRF) and the University of the Free State for the financial support I benefited from them.
- Lastly, I want to express my indebted appreciation to my beloved family (my husband Jatani and our son Jayden) for their enormous support and our dear parents for their continuous prayers throughout this project. May the Almighty God bless them abundantly

Abstract

Semiconductor quantum dots are nanoparticles with unique tuneable properties. For instance, water soluble nanocrystals which have been synthesized by wet chemistry in open air environment are highly luminescent. They possess well-resolved absorption maxima, high stability and narrow emission bands. This thesis presents several aspects about the synthesis of highly luminescent water soluble, CdTe nanoparticles (NPs) and their near infrared emitting counterpart such as $CdTe_xSe_{1-x}$ and CdO_xTe_{1-x} NPs. It also investigates the synthesis of highly luminescent NPs specifically engineered to be used for biomedical applications.

Here in a novel approach to synthesize CdY (Y = O/Te/Se) with tunable material properties are presented. The surface morphologies of the as-prepared NPs displayed by SEM micrographs depended strongly on their growth kinetics, probably due to the variation of reaction time, growth temperature or Te concentration. Differences in shape and size were observed depending on the growth conditions. Spherical, rod-like, oval-like and blade-like morphologies were obtained for different reaction parameters. There was observable change in size and shape at longer growth time or higher Te molar ratio. The representative HRTEM analysis showed that the as-obtained CdTe NPs appeared as spherical particles with excellent monodispersity. The images also displayed clear lattice fringes that were an indication of enhanced crystallinity. The X-ray diffraction (XRD) pattern displayed polycrystalline nature of the NPs. XRD pattern confirmed the formation of wurtzite (JCPDS no. 19-0193) and zinc blende (75-2086) phases for the CdYsamples prepared. The type of phase formed depended greatly on the composition, the molar ratios of the consequent elements and reaction conditions of the NPs. The average crystallite sizes estimated from Scherrer equation were found to increase with increase in reaction time, which was in agreement with the HRTEM measurement. The crystallite sizes of the NPs were in the range of 3 to 40 nm depending on the reaction conditions and composition of the NPs formed. Crystallinity of the samples was enhanced up to certain extent as shown by highest peak intensity of the XRD pattern. Variation in the XRD peak intensities was very much dependent on the reaction parameters. Results from XRD also showed a systematic shift in peak positions towards lower and higher 2θ degrees values for CdTe or and CdO_XTe_{1-X} NPs, respectively with an increase/decrease in reaction parameters.

Results from PL showed sharp excitonic band edges of the CdTe, which loses its shoulder during the growth of the NPs. The PL spectra of all the prepared samples indicated a drastic shift in emission window of the core to longer wavelength (500 to 650 nm) which was simultaneously accompanied by variation in emission intensity with different reaction conditions. The position of the emission band was observed to shift towards the lower

wavelength side for shorter durations of synthesis, lower growth temperatures and lower tellurium concentrations. Some difference in absorption edges were observed due to variation in reaction conditions of CdTe NPs. The ultraviolet and visible analysis (UV-Vis) displayed well-resolved absorption maxima which were red shifted upon increase in reaction time, growth temperature and Te concentration. There was an inverse relation between the bandgap and the reaction parameters under study (reaction time, growth temperature and tellurium concentration). The CdTe bulk band gap of 1.5 eV was tuned to even above 3.0 eV while the CdTe counterparts displayed band gap from 1.7 to 2.6 eV.

A pH of 11, reaction temperature of 100 ^{o}C and Cd:Te ratio of 1:0.4 were found to be the optimum conditions so far for the preparation of CdY NPs. This method of preparation is simple, sensitive, low cost, easy to execute and efficient with profound advantages such as low reaction temperatures, broad range of pH value and wide PL emission wavelength range thus making it reliable for practical applications.

Declaration

I (**Sharon Kiprotich**) declare that the thesis hereby submitted by me for the Master's degree at The University of the Free State is my own independent work and has not previously been submitted by me at another university/faculty. I furthermore, cede copyright of the thesis in favour of the University of the Free State.

Signature……..Date……..

Key words

- Cadmium Telluride
- Nanoparticles
- Quantum Dots
- Morphology
- Excitation
- Band Gap
- Luminescence
- Particle Size
- Emission
- Absorption Edges
- Red Shift
- Crystallinity
- Lattice Fringes
- Growth temperature
- X-ray diffraction
- Precursor pH
- Tellurium
- Concentration
- Morphology
- Crystallite size
- Wet-chemical process

Acronyms

- **EDS**- Energy Dispersive x-ray Spectroscopy
- **PL**- Photoluminescence
- **SEM**- Scanning Electron Microscopy
- **TEM**- Transmission Electron Microscopy
- **XRD**- X-Ray Diffraction
- **NPs**- Nanoparticles
- **QDs-** Quantum dots
- **QWs-**Quantum wells
- **HRTEM-** High resolution transmission electron microscopy
- **CIE**- Commission Internationale de l'Eclairage
- **LEDs**- Light emitting diodes
- **NIR**- near infra-red
- **M_e**- Effective mass of an electron
- **M_h**- effective mass of a hole
- **ICDD**- International Centre of Diffraction Data
- **UV-vis-** Ultraviolet and visible
- **JCPDS**- Joint Committee on Powder Diffraction Standards
- **CdTe**- Cadmium telluride
- **CdO**- cadmium oxide
- **CdSe**- cadmium selenide

Table of Contents

Chapter 1

Introduction

1.1 General background

Semiconductor nanoparticles (NPs) or quantum dots (QDs) have drawn a lot of attention recently due to their novel properties such as their size-tunable emission, high photoluminescence (PL) intensity, narrow emission spectra or broad excitation, reasonable photochemical stability, high quantum yields, controllable spectroscopic properties, and the ability to provide specific color fluorescence when excited with a single excitation wavelength and their stability against photo bleaching [1-3]. These properties have been studied for various biomedical and industrial applications such as photonic crystals, light-emitting devices (LEDs), nonlinear optical devices and biological label QDs [4-6]. A QD is a semiconductor core commonly known to be surrounded by a layer of organic ligands. The smallest QDs (< 1 nm in diameters) are nearly molecular (<100 atoms) whereas the largest QDs (>20 nm in size) can be composed of over 100,000 atoms.

The growth of NPs is in the size focusing region when a certain range is considered since smaller particles need less material to grow a shell whereas larger particles need more materials to achieve a shell of the same thickness. When monomer concentration is extremely low, as will always happen when monomers are depleted from the reaction, Ostwald ripening happens. Small particles dissolve to compensate the growth of large particles. Nanoparticles made of metals, semiconductors, or oxides are specifically studied due to their special features regarding their electrical, magnetic, mechanical, chemical, optical and other properties. For further applications nanoparticles (1-20 nm) also referred to as quantum dots have been used in nanomaterial-based catalysts where the nanoparticles act as chemical catalysts. Recently, a range of nanoparticles were extensively investigated for biomedical applications including biolabelling, bioimaging and biosensors [7].

For quantum dots, their emission colors vary depending on the size of the nanoparticles obtained. These nano-sized QDs also show stimulating properties such as an inverse relation of the band gap with the particle sizes, ultra-fast recombination time and PL with high quantum efficiency [8]. Usually, the material properties of nanoregime are considerably different from those of bulk material form. The unique nanomaterial properties are known to be due to the very large surface area -to- volume ratio of the as-prepared NPs (Fig. 1.1) [9, 10].

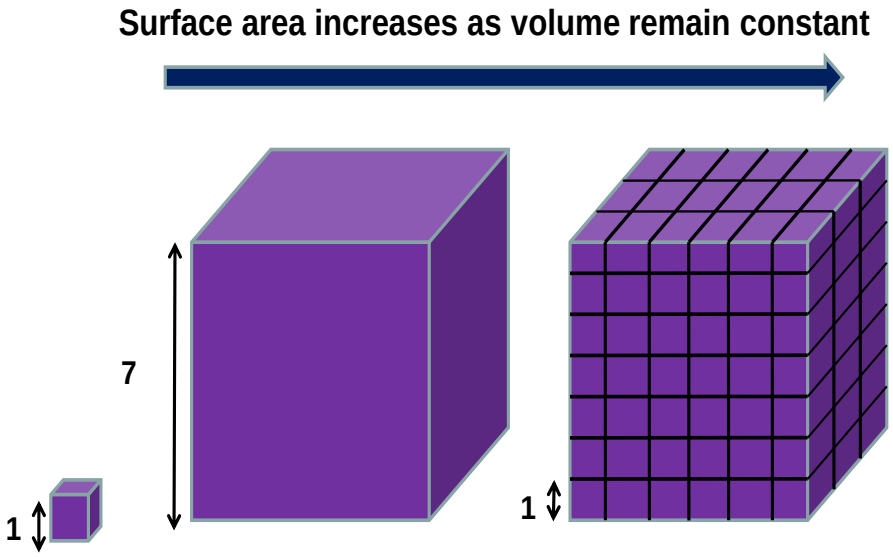

Figure 1.1 Surface area-to-volume ratio.

There are very few reports for L-cysteine capped CdTe and their near infrared (NIR) emitting counterpart nanocrystals in the biological field. This thesis reports the study of L-cysteine capped CdTe and its counterparts NPs using potassium telluride as stable tellurium source while sodium borohydride was used as a reductant. L-cysteine used as a capping agent can also act as an antioxidant and is widely known to protect cells against oxidative stress and cytotoxicity induced by the QDs. It is also an aminophenol which is friendly to human body since it has no any cytotoxin and it has been considered to be the most suitable stabilizer that promotes the production of spectra which possess very narrow emission and long fluorescence lifetime [11, 12].

1.2 Basis and scope of this work

1.2.1 Motivation

The main motivation of this research is that growth parameters of CdTe NPs can be controlled and engineered by monitoring the shape, size and size distribution of the as-synthesized NPs among other material features. In biological tissues research, the NIR light travel through and is enfeebled very little due to the fact that the absorbance of the NIR photons by biological tissues is quite low. This implies that penetration of the NIR photons into biological tissues is quite deep, which makes them very useful in biological detection and bioimaging [13]. The various applications of semiconductors are critically reliant on the band gap energy value of the material. Therefore, the ability to tune (or engineer) the band gap is essential for the fabrication of bio-imaging materials with widely varying properties. Selenium being group VI element as sulphur, can easily make an isovalent ternary semiconductor alloys ($AB_{1-x}C_x$). It has also attracted attention because of its antioxidant properties which yield highly stable nanoparticles [14]. The capability of tailoring material properties promotes production of NPs with various electrical, optical, structural and chemical properties which suit desired applications. Most importantly, is to be able to produce stable and highly crystalline NPs via a facile and less expensive method in large scale. The main objective of this project is to produce NIR emitting NPs because of their vast superior properties.

1.2.2 Statement of the problem

Researchers have been focusing on bridging the gap between the macro, micro and nano regime. This is because the material properties of nanocrystals differ so much from those of the bulk solids. The nanoparticles are also greatly affected by their size and surface chemistry. In the recent years, achievements have mainly focused on the synthesis and characterization of high-quality nanoparticles for various applications in electrical, optoelectronic devices and medication. Researchers have been trying to find ways of using quantum dots inside the human body. Doctors for many years have used dyes to aid the detection of cancer and other ailments. These dyes concentrate in certain parts of the body like where the cancer cells are located. The quantum dots are excited into emitting light that can be detected outside the human body. This light which is detected is turned into a detailed image of tissues which can easily be analysed. Dots of various sizes could be used simultaneously to image different parts of the body because quantum dots emit light at a particular frequency.

Nevertheless, a main concern has been searching for suitable means to produce nanoparticles which are stable and water-soluble. Different kinds of solvents and stabilizers have been studied and used in preparation of the NPs but producing water-soluble NPs has been a major challenge since it required other procedures like ligand exchange in order to make them soluble in water. This research tries to solve the stabilizer and water-solubility problem in that the method used produces highly stable and water-soluble. L-cysteine which if used in this research is human body and environmental friendly. It prevents the NPs from oxidation and associate well with the body since it is part of the proteins found in the human body. Controlling the growth process of CdTe NPs by varying reaction parameters such as reaction time, growth temperature, concentration of the precursor molar ratios and composition is explored in order to form reproducible NPs with desired structure, morphology, size and size distribution for specific optical, chemical, electrical and medical applications. Since the material properties of CdTe NPs can be tailored, NPs of any size and morphology can be produced to emit light at various wavelengths.

1.2.3 Objectives of the study

The specific objectives of the study include:

- To prepare CdY QDs by simple one-pot wet chemical process.
- To characterize and analyse the as-prepared nanoparticles.
- To investigate the influence of reaction times on the morphological, structural and optical properties of the as-prepared samples.
- To study the effect of growth temperature on the morphological, structural and optical properties of the as-prepared samples.
- To study the effect of different tellurium concentration on the morphological, structural and optical properties of the as-prepared samples.
- To estimate the particle sizes of the as-prepared samples with High Resolution Transmission Electron Microscopy (HRTEM).
- To study the surface morphology of the as-prepared samples using scanning electron microscope (SEM).
- To define quality of the as-prepared samples through their chemical compositions using Energy Dispersive X-Ray spectroscopy (EDS).
- To establish the crystal structure and crystallite size with X-Ray Diffraction (XRD).
- To measure the absorption and reflection intensities of the samples and determine their corresponding band gap energies from spectral data by using UV-vis equipment.

- To study and compare the material properties of CdTe NPs ternary compounds.
- Optimization of the material quality of the as-prepared nanoparticles.

1.4 Thesis Layout

Chapter 1 commences with a general background of nanoparticles outlining their properties, development and presents the basis and scope of this study including the statement of the problem and objectives of this undertaking.

Chapter 2 gives general information on quantum dots, its history over the past decades, gives brief definitions of some common terminologies and applications for the same.

Chapter 3 discusses briefly on the toxicity concerns of QDs used in biomedical applications.

Chapter 4 gives short explanation of the experimental equipment/ techniques used to design, synthesize and characterize transition metal compound quantum dots. A summary of various characterization techniques used are also given. This includes a description of the operation of each of the techniques such as UV-vis, PL, XRD, HRTEM, SEM and EDX-S.

In *Chapter 5*, reports detailed information about the high luminescent L-cysteine capped CdTe quantum dots prepared at different reaction times. This involves the synthesis, analysis and characterisation of CdTe QDs.

In *chapter 6*, effect of growth temperature on the optical, structural and luminescence properties of CdTe NPs were investigated.

Chapter 7 discusses the effect of tellurium concentration on the optical and structural properties of CdTe NPs were examined using several systems.

Chapter 8 gives a detailed information on a comparison investigation of optical, structural and luminescence properties of CdO_xTe_{1-x} and $CdTe_xSe_{1-x}$ nanoparticles prepared by a simple one pot method.

List of figures, tables, publications, conferences and possible future suggestions are summarized at the end of *chapter 9*.

References

[1] W.R. Algar, K. Susumu, J.B. Delehanty, I.L. Medintz, "Semiconductor Quantum Dots in Bioanalysis: Crossing the Valley of Death", Anal. Chem. 2011, 83, 8826.

[2] M. Gao, C. Lesser, S. Kirstein, H. Mçhwald, A. L. Rogach, H.Weller, "Electroluminescence of different colors from polycation/CdTe nanocrystal self-assembled films", J. Appl. Phys. 2000, 87, 2297.

[3] N. N. Mamedova, N. A. Kotov, A. L. Rogach, "Albumin−CdTe Nanoparticle Bioconjugates: Preparation, Structure, and Interunit Energy Transfer with Antenna Effect", J. Studer, Nano Lett. 2001, 1, 281.

[4] F. Chen, D. Gerion, "Fluorescent CdSe/ZnS Nanocrystal−Peptide Conjugates for Long-term, Nontoxic Imaging and Nuclear Targeting in Living Cells", Nano Lett. 2004, 4, 1827.

[5] F. Fleischhaker, R. Zentel, "Photonic Crystals from Core-Shell Colloids with Incorporated Highly Fluorescent Quantum Dots", Chem. Mat. 2005, 17, 1346.

[6] H. Huang, A. Dorn, G. Nair, V. Bulovic, M. Bawendi, "Bias-Induced Photoluminescence Quenching of Single Colloidal Quantum Dots Embedded in Organic Semiconductors", Nano Lett. 2007, 7, 3781.

[7] K.K. Nanda, F.E. Kruis, H. Fissan, M. Acet, "Band-gap tuning of PbS nanoparticles by in-flight sintering of size classified aerosols", J. Appl. Phys, 2002, 91, 2315.

[8] M.S. Dhlamini, PhD Thesis, University of the Free State, South Africa "Luminescence Properties of Synthesized PbS Nanoparticles", 2008.

[9] Y. Gogotsi, Nanomaterials Handbook, "Materials Science at the Nanoscale", Routledge Publishers, USA 2006, 5.

[10] Z. Liu, Y. Liu, J. Zhang, J. Rong, L. Huang, D. Yuan, "Long afterglow in Pr^{3+} and Li^{+} co-doped $CaZrO^{3}$", Optics Com. 2005, 251, 388.

[11] A.O. Choi, S.J. Cho, J. Desbarats, J. Lovric, D.J. Maysinger, "Quantum dot-induced cell death involves Fas upregulation and lipid peroxidation in human neuroblastoma cells", Nanobiotechn. 2007, 5, 1.

[12] J. Lovric, H.S. Bazzi, Y. Cuie, G.R.A. Fortin, F.M. Winnik, D.J. Maysinger, "Differences in subcellular distribution and toxicity of green and red emitting CdTe quantum dots", J. Mol. Med. Heidelberg, Ger., 2005, 83, 377.

[13] P. Yang, M. Ando, T. Taguchi, N. Murase, “Highly Luminescent CdSe/$Cd_xZn_{1-x}S$ Quantum Dots with Narrow Spectrum and Widely Tunable Wavelength”, J. Phys. Chem. C, 2011, 115, 14455.

[14] M. Kieliszek, B. Stanisław, “Selenium: Significance, and outlook for supplementation”, Nutrition 2013, 29, 713.

Chapter 2

Literature review on quantum dots

2.1 Brief history on quantum dots

QDs are nano-sized semiconductor particles composed of II-VI group or III-V main group elements. Normally, the size of the quantum dots is between 1 ~ 100 nm. When the electrons and holes within are quantum confined in all the three dimensions, the continuous bandgap structures of the bulk material would become discrete if excited to higher energy states. A photon of a frequency characteristic of that material is emitted when the QDs return to their ground state. This behaviour results in possession of properties intermediate between those of bulk materials and those of discrete molecules.

The history of QDs is known to have begun in the early 1970s with nanometer-thick foils called QWs. Charge carriers (electrons and holes) in QWs become trapped in a few-nanometers-thick layer of wells. The band gap of such QWs is smaller than in the neighbouring barrier layers. Changing the material composition led to the variation of the band gap was achieved in the compound semiconductor. These first low dimensional structures QWs were then followed by invention of quantum wires and QDs. The QD history commenced when Russian physicist Ekimov first discovered the glass crystals in 1980 [1]. Progressive expansion in the science and technology of QDs after 1984 was motivated by derivation of a relation between particle size and bandgap of semiconductor NPs by Luis Brus when he applied the particle in a sphere model approximation to the wave function for bulk semiconductors [2, 3]. Even though it took a long time for new advancement in QDs research, Murray et al. eventually developed QDs with size-tuneable band-edge absorption and emissions [4].

Enormous preparation approaches have been established used to synthesize QD. These methods are divided into two classifications which include the physical approach and chemical approach. The physical approach was commonly known as the epitaxial growth.

However, the main disadvantages of this method are defection formation, size non-uniformity, poor interface quality and even damage to the bulk of the crystal itself. Pyrolysis of organometallic and chalcogen precursors and the main processes that this method relies on where rapid nucleation followed by slower and steady growth is desired [5].

Quantum dots have so many applications in solar cells, light emitting devices, photo bio-chemo labelling technologies because of their enormous reasons: tunable absorbance and emissions, high quantum yields, wide excitation window but narrow Gaussian emission peaks, great opposition to photobleaching when compared to organic dyes, minimal interference and possible functionality with different bio-active agents [6-8].

2.2 Quantum Confinement

The quantum confinement effect causes the optical properties of QDs to evolve dramatically with their size. The quantum confinement effect is described as the phenomenon which causes widening of the bandgap energies of the semiconductor materials when its size is shrunk to nanoscale. The energy required to create an electron and a hole with zero kinetic energy at a distance far enough apart that their Coulombic attraction could be ignored is known as bandgap of that material. If one carrier approaches the other, a bound electron-hole pair (exciton) would is created. This electron-hole pair acts typically like a hydrogen atom, except that a hole, which is not a proton, forms the nucleus. The distance between the electron and hole is referred to as exciton Bohr radius (r_B) expressed by the equation below;

$$r_B = \frac{\hbar^2 \varepsilon}{e^2}\left(\frac{1}{m_e} + \frac{1}{m_h}\right) \qquad (1)$$

The m_e and m_h are the effective masses of electrons and holes, respectively, while ε, $\hbar$ and e are the dielectric constant, reduced Planck constant and the charge of an electron respectively [9]. If the size of a QD shrinks in such a way that its radius (R) is $R < r_B$, then the material in question is said to be strongly confined since the motion of the electrons and holes in the QD is confined to the QD dimensions. This size dependent effect was firstly observed in thin films of semiconductor materials (quantum wells) synthesized using molecular beam epitaxy approach [10]. The thickness of the thin film is equivalent to the exciton Bohr radius so that the exciton is confined, which modifies the density of states such that there are fewer band edge states and the bandgap is shifted to the blue [11]. Later studies led to quantum wires/rods and quantum dots. As the QD size is smaller than the material's exciton Bohr radius, the dimensions of the crystal become so small that the photo excited carriers feel the

boundary, causing the continuous density of states in the bulk to collapse into discrete electronic states. In addition, the more confined the carriers are, the higher the bandgap energy is, and correspondingly the potential photoluminescence should blue-shift [12].

2.3 Applications of quantum dots

2.3.1 Solar cells

The ability to produce dots of different sizes allows quantum dots to possess tunable bandgaps across a wide range of energy levels. Semiconductors were used to make traditional solar cells. This however had a disadvantage in that they were expensive to produce. A reported theoretical upper limit value of 33% efficiency is achieved when sunlight is converted to electricity using these solar cells. Tunable band edge offers the possibility to harvest light energy over a wide range of visible-IR light with selectivity. A quantum dot solar cell is a solar cell designed to use QDs as the absorbing PV material. It endeavors to substitute the bulk materials like copper indium gallium selenide (CIGS) or silicon [13].

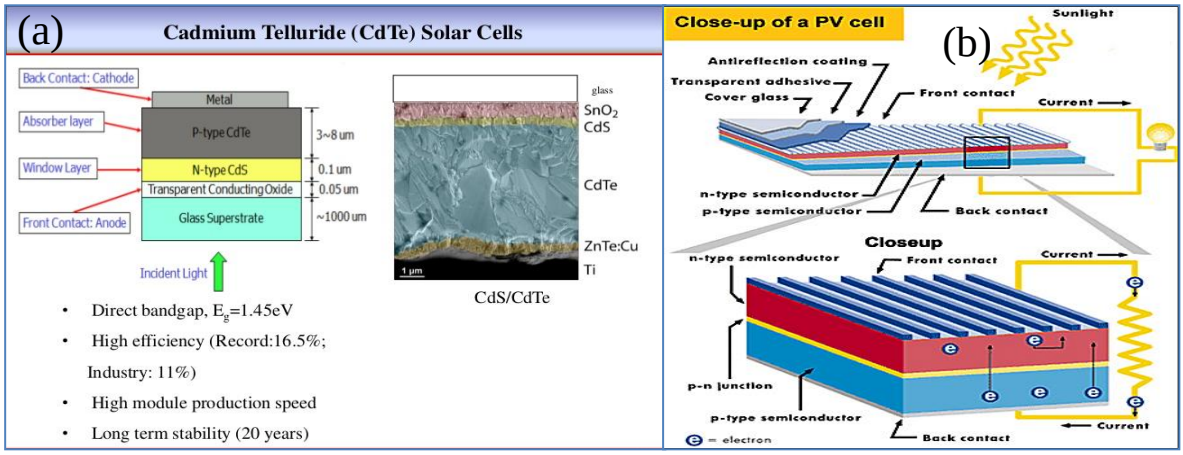

Figure 2.1: image of cadmium telluride (a) solar cell and (b) photovoltaic cell [14]

2.3.2 QD-lasers

QD laser structure is fabricated in a way similar to the QW lasers and can be treated like QW lasers in principle. The only main difference arise from the optically active medium where QDs are used instead of QWs. Fig. 2.2 shown below displays a simple laser structure, consisting of an active layer embedded in a waveguide, surrounded by layers of lower refractive index to ensure light confinement. The optically active material medium consists of quantum wells or quantum dots where the bandgap is lower than that of the waveguide material [15].

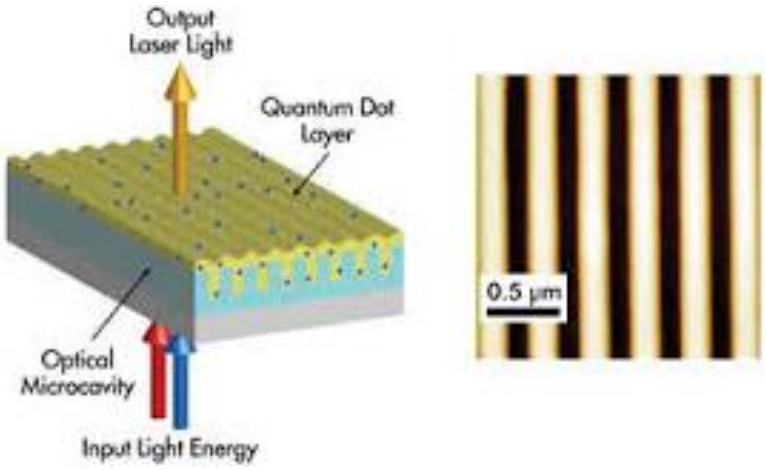

Figure 2.2: Schematic diagram of a quantum dot lasing device [16]

2.3.3 Indicators

Nanoparticles can be applied in making safety displays for example exit signs which still operate even when there are current blackout cases (Fig. 2.3).

Figure 2.3: (a) Luminescent signs (b) a neon sign and (c) traffic light signs [17, 18]

2.3.4 Quantum dots LEDs

The main characteristics of QD LEDs are that they consist of pure and saturated emission colours with narrow bandwidth. By changing the size of the QDs, their emission colours or wavelength is easily tuned. They offer high durability and colour purity with high efficiency and flexibility. Moreover, it has an advantage of low processing cost when producing the organic light-emitting devices. Making use of the tunablity of the QDs' emissions over the entire visible wavelength range from 460 nm (blue) to 650 nm (red) the structure of the QD LED can be engineered. The design of QD-LED is comparable to the structure of O-LED except for fact that the light emitting centres are cadmium telluride nanocrystals in this case. Cadmium-telluride QDs layer is inserted between layers of electron-transporting and hole-transporting organic materials. An applied electric field causes electrons and holes to move into the QD layer, where they are captured in the quantum dot and recombine, and emitting photons. The spectrum of photon emission is narrow, characterized by its full width at half the maximum value. [19, 20]

Figure 2.4: LED display and devices [21]

2.3.5 Textiles

The field of textiles, focus is given in two main areas; firstly, upgrading existing materials and performances of textiles materials and secondly, developing intelligent textiles with completely new characteristics and functions. The application of nanotechnology in the field of textiles has led to the evolution of nanocompositions, nanofibers, nanopolymers, nanofinishes, etc. In the field of textiles, nanotechnology has been employed in the synthesis of quantum dot (semiconductor nanocrystals). A spray-on coating that mimics the way lotus leaves repel water droplets and particles of dust wasdeveloped by a leading German chemical manufacturer. Lotus plants have super hydrophobia surface and this effect arises because they are coated with hydrophobic wax crystals of around 1 nm (nanometer) in diameter. This lotus effect had led a very significant development in textile technology. The first commercial application of nano technology in textile and clothing industry is found in the form of nano particle (sometimes called nano bead) through a finishing process, which is generally known as nano finishing. One of the developments of nanotextiles is nano fibers [22].

2.3.6 Biological applications

Concerning the QDs in biological applications, two main groups may be discussed; biosensors and labels in biological imaging [23].

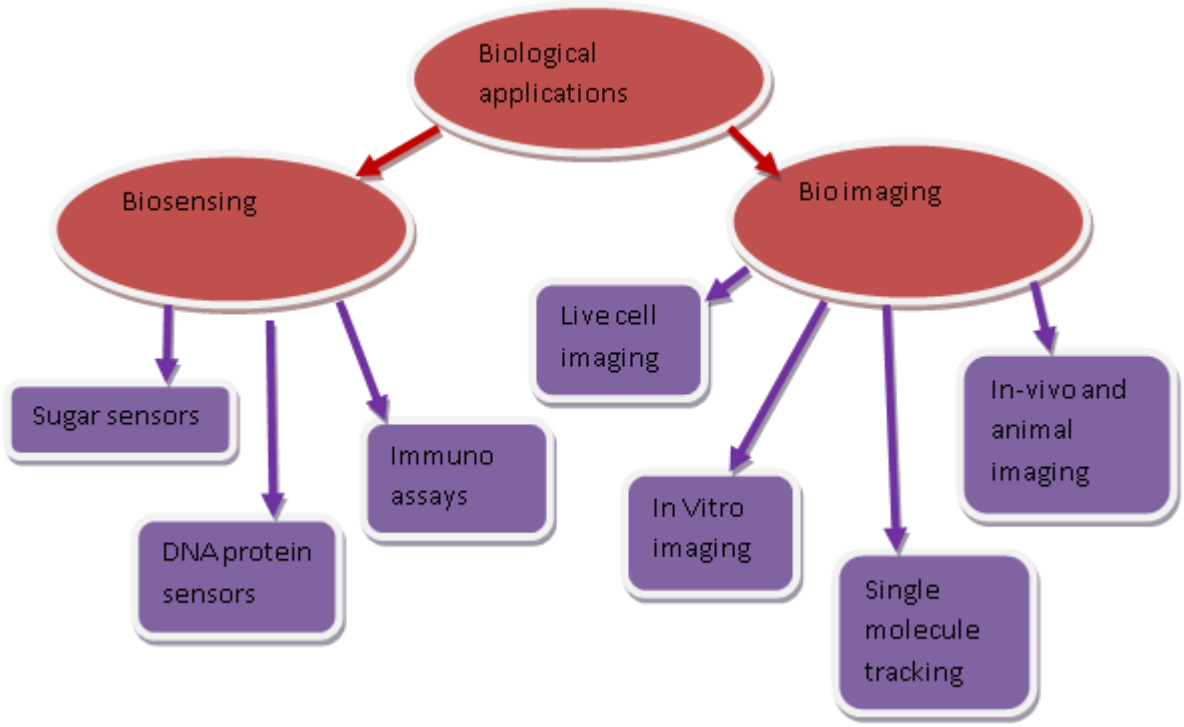

Figure 2.5: A diagram showing examples of QDs bioanalytical and biomedical application.

A few examples of each group can be seen on the diagram below (Fig. 2.5). For in vivo biological imaging applications of QDs, the fluorescent emission wavelength ideally should be in a region of the spectrum where blood and tissue absorb minimally but still detectable by the instruments. Thus the QDs should emit at approximately 700-900 nm in the NIR region to minimize the problems of indigenous fluorescence of tissues. Moreover, the spectroscopic properties of NIR QDs would allow imaging at a deeper penetration than conventional near-infrared dyes [24].

References

[1] A.I. Ekimov, and A.A. Onushchenko. “Green synthesis of ZnO nanoparticles via Agathosma betulina natural extract”, Jetp Lett 34, 1981, 345.

[2] L.E. Brus, “Electron-electron and electron-hole interactions in small semiconductor crystallites: The size dependence of the lowest excited electronic state” J. chem. Phy. 80, 1984, 4403.

[3] L. Brus, “Electronic wave functions in semiconductor clusters: experiment and theory”, J. Phy. Chem 90, 1986, 2555.

[4] C.B. Murray, D.J. Norris, and M.G. Bawendi. “Synthesis and characterization of nearly monodisperse CdE (E=sulfur, selenium, tellurium) semiconductor nanocrystallites”, J. American Chem Society 115, 1993, 8706.

[5] S.Y. Kaya, E. Karacaoglu, and B. Karasu, “Effect of Al/Sr ratio on the luminescence properties of $SrAl_2O_4$: $Eu^{2+,}$ Dy^{3+} phosphors”, Ceramics International 38, 2012, 3701.

[6] S. Santra, R.P. Bagwe, D. Dutta, J.T. Stanley, G.A. Walter, W. Tan, B.M. Moudgil, and R.A. Mericle. “Synthesis and characterization of fluorescent, radio-opaque, and paramagnetic silica nanoparticles for multimodal bioimaging applications”, Advanced Materials 17, 2005, 2165.

[7] S. Santra, H. Yang, J.T. Stanley, P.H. Holloway, B.M. Moudgil, G. Walter, and R.A. Mericle. “Rapid and effective labelling of brain tissue using TAT-conjugated CdS: Mn/ZnS quantum dots”, Chemical communications 25, 2005, 3144.

[8] H. Yang, S. Santra, G.A. Walter and P.H. Holloway. “Gd III-Functionalized Fluorescent Quantum Dots as Multimodal Imaging Probes”, Advanced Materials 18, 2006, 2890.

[9] P.N. Prasad, Nanophotonics. John Wiley & Sons, 2004.

[10] D.S. Chemla, "Nonlinear optics in quantum-confined structures." Physics Today 46, 1993, 46-52.

[11] D.S. Chemla and D.A.B Miller. “Room-temperature excitonic nonlinear-optical effects in semiconductor quantum-well structures”, JOSA B 2, 1985, 1155.

[12] P. Guyot-Sionnest, M. Hines, “Intraband transitions in semiconductor nanocrystals”, Appl. Phys. Lett. 1998, 72, 686.

[13] Solar cell, [online]. Available from; http://www.solarcellcentral.com/solarpage.html. [Accessed 13 March 2017].

[14] Quantum dot laser, [online]. Available from; https://en.wikipedia.org/wiki/Quantum_dot_laser. [Accessed 13 March 2017].

[15] Lasers online. Available from; http://freshscience.org.au/2010/print-your-own-lasers-lights-and-tv-screens. [Accessed 13 March 2017].

[16] Signs & Tape, [online]. Available from; http://www.glonation.com/signs-and-tape.html [Accessed 17 March 2016].

[17] Neon 'open' sign, [online]. Available from http://www.neonclick.de/index.html. [Accessed 10 June 2016].

[18] P.O. Anikeeva, J.E. Halpert, M.G. Bawendi, and V. Bulovic. "Quantum dot light-emitting devices with electroluminescence tunable over the entire visible spectrum", Nano letters 9, 2009, 2532.

[19] S. Coe, W.K. Woo, M.G. Bawendi, and V. Bulovic. "Electroluminescence from single monolayers of nanocrystals in molecular organic devices", Nature 420, 2002, 800.

[20] LED applications, [online]. Available from; https://en.wikipedia.org/wiki/Light-emitting_diode. [Accessed 17 June 2016].

[21] Quantum dot textile applications, [online]. Available from; http://style2designer.com/textile-techniques/nano-textiles/. [Accessed 17 March 2017].

[22] P. Majzlík, J. Prásek, L. Trnková, J. Zehnálek, V. Adam, L. Havel, J. Hubálek, and R. Kizek. "Biosensors for detection of heavy metals", Listy cukrovarnicke a reparske 126, 2010, 413.

[23] J. Drbohlavova, V. Adam, R. Kizek, and J. Hubalek. "Quantum dots—characterization, preparation and usage in biological systems", International journal of molecular sciences 10, 2009, 656.

[24] J. Gao, and B. Xu. "Applications of nanomaterials inside cells", Nano Today 4, 2009, 37.

Chapter 3

Material properties of cadmium telluride

3.1 Outline

Among the group II–VI semiconductor is cadmium telluride (CdTe) with a commonly known Zinc blende/wurtzite crystalline structure, Bohr exciton radius of approximately 6.5 nm with tunable bulk band gap energy corresponding to 1.5 eV at room temperature. They possess superior qualities of long-term stability and brightness which make them ideal candidates for live animal targeting and bioimaging. A study on how to reduce accumulation of NPs in the liver and bone marrow when focusing on long-term imaging of live mice showed the importance of coating NPs with high molecular weight polyethylene glycol (PEG) molecules to [1]. It was discovered that after several months the NPs were still visible in the bone marrow and lymph nodes of the animals which was an indication of high stability of these investigations. Most organic fluorophores used in imaging for extended periods are prone to metabolic and chemical degradation and photodamage. These make them hard to label cells for extended time. Means to overcome these shortcomings are hunted and the use of genetically encoded organic fluorophores which are constantly prepared and replaced in the cell (L-cystiene) like fluorescent proteins are recommended. After their introduction into cells it takes long period of time before they are detected in the body and cause very long delays when they are faced by photobleaching and other demerits. These shortcomings are minimised when NPs that are resistant to photodamage, degradation by enzymes in live cells and chemical damage are used [2, 3] like CdTe QDs. Thus, NPs have aided the monitoring of molecules in live cells for several hours [4-6], and watching over the cell fate for a whole period of development of an organism [7, 8].

3.2 CdTe crystal structure

The crystal structure of the CdTe nanocrystals formed depend greatly on the growth conditions like the concentration of precursors , growth temperature, reaction time, pH and molar ratios of the precursor elements. The nanocrystals grown had a wurtzite and zinc blende structure depending on the growth conditions. High reaction temperatures favored the formation of zinc blende. Reaction time showed slight changes in crystal structure.

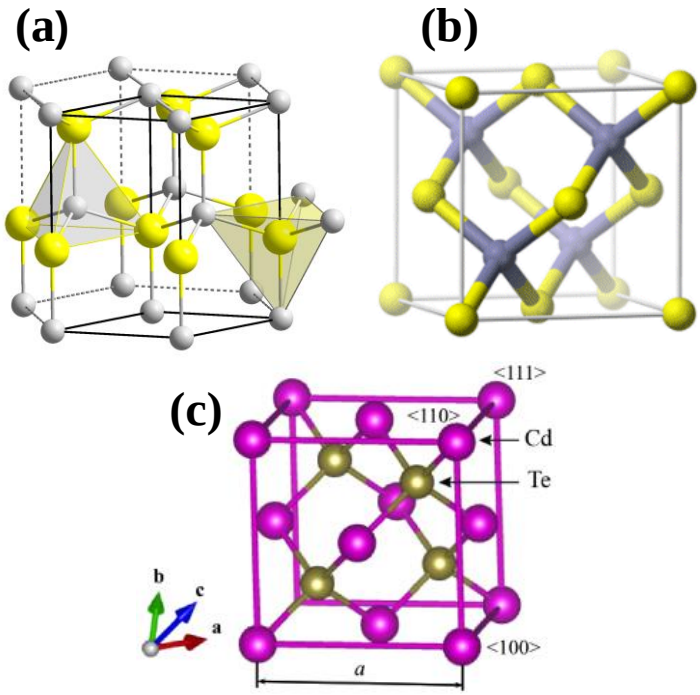

Figure 3.1(a): wurtzite - hexagonal (b) zinc blende - cubic structure of CdTe NPs and (c) crystal structure displaying the planes and the lattice parameter of the CdTe NPs [9].

3.3 Electronic band structure of CdTe

The CdTe is extensively studied because of the well-known direct band gap energy which ranges from 1.4 to 1.5 eV and can be tuned to a desired value for various applications. The direct materials are differentiated from the indirect gap materials from their relative positions of the conduction band minimum and the valence band maximum in the Brillouin zone. Brillion zone is defined as the volume of k space containing all the values of k up to π/a where a is the unit lattice cell dimension. Both the conduction band minimum and the valence band maximum occur at the zone center where k=0 for a direct gap material while for an indirect gap material the conduction band minimum does not occur at k=0, but rather at some other values of k which is usually at the zone edge or close to it.

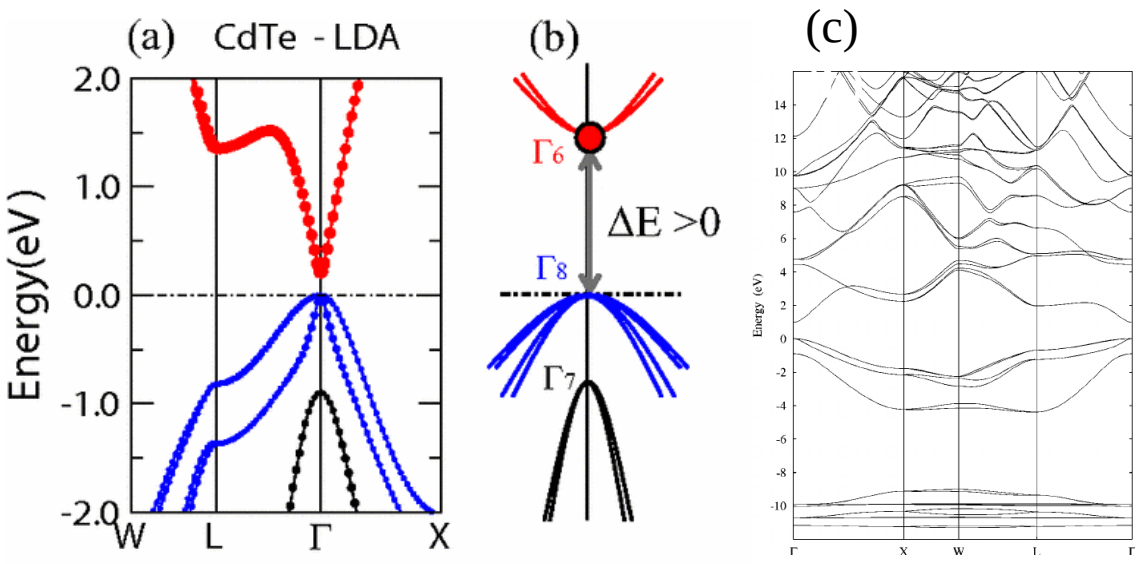

Figure 3.2: (a) LDA band structure (b) is schematically experimental band structure of CdTe and (c) LDA band structure of CdTe obtained with a semi- empirical shift of Cd 4d states and including spin-orbit interaction. The red solid dots denote the s-orbit originated Γ6 state [10].

3.4 Luminescence in CdTe

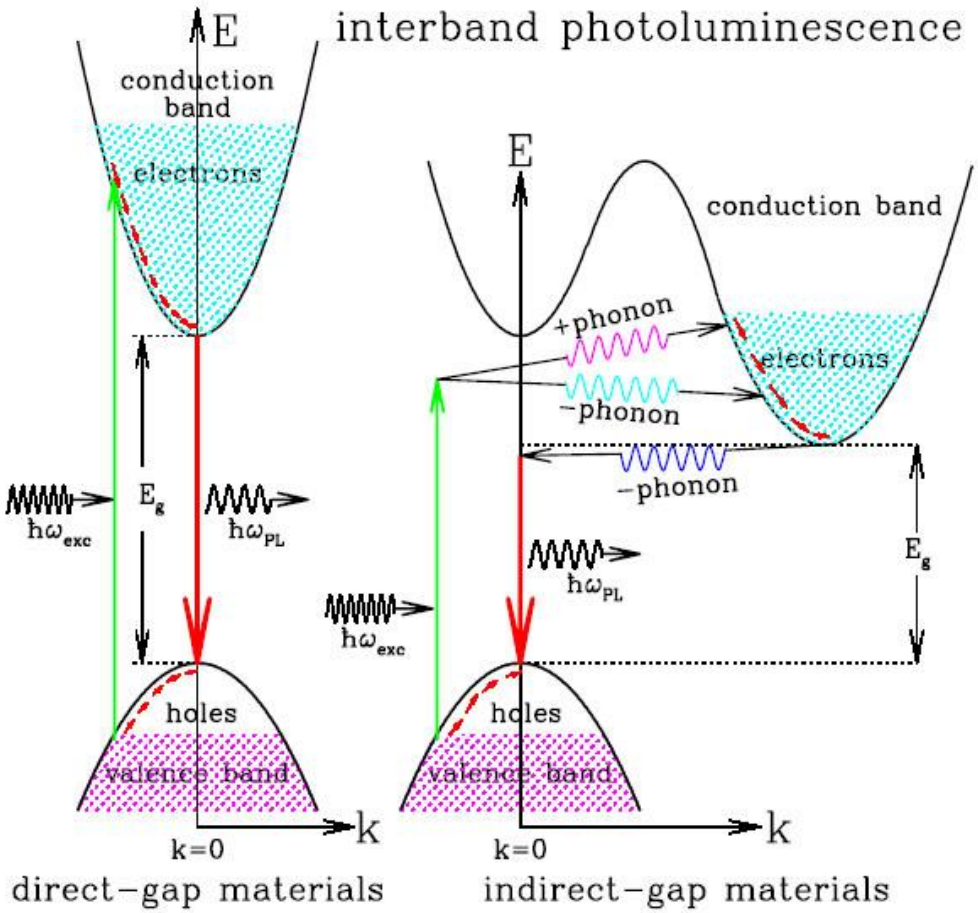

Figure 3.3: E-k diagrams for a direct band gap material and indirect gap material for the photoluminescence processes [11].

The PL mechanism in semiconductors is graphically demonstrated in Fig. 8, E-k diagrams for a direct band gap material and indirect gap material plots are shown. E and k are the kinetic energy and wave vector (or "momentum vector") of the electron or hole respectively. The absorption of photons energizes the material causing the generation of electrons at the bottom of the conduction band and the holes at the top of the valence band. The movements of the electrons and holes within the conduction and valence bands are due to the rapid thermalization of the excited electrons and holes through phonon emission. The conduction band minimum and the valence band maximum of a direct band gap material (left) occur at the same k values. The momentum of the absorbed or emitted photon is very small (negligible) compared to the momentum of the electron thus the photon absorption and emission (the electron-hole recombination) processes can conserve momentum without the assistance of phonons. On the other hand, an indirect gap material (right) has its conduction band minimum at different k value with the valence band maximum. Therefore, for it to conserve momentum, other processes ere involved for instance the photon absorption process must involve either absorption or emission of a phonon and that the PL process needs the emission of a phonon whose energy (~ 0.01 eV) is much smaller than the energy of the PL photon. The PL peak wavelength approximately gives the band gap of a material.

However, for luminescence to occur in a material a semiconductor structure with a nonzero band gap, Eg should be present in the luminescent material (for example metals do not luminesce because they have no band gap) and that it requires an external source of energy to excite the material before luminescence can occur [11].

3.5 Toxicity in CdTe

The issue of toxicity in QDs presents a major concern when it comes to search of their in vivo application in biomedical imaging. The key source of this toxicity are; the semiconductor materials that commonly constitute the QD core (and sometimes the shell) which can leach under certain circumstances and the generation of reactive and free radical species during excitation [12, 13]. Furthermore, the unique QD nanoscale structure presents a complex set of physiochemical characteristics that further compound any simple studies or conclusions in this direct toxicity issue. As presented in detail in literature, the nanocrystalline cores can be created from various amalgamations of binary semiconductors such as CdTe, InP, CdSe and CdS, just to mention but a few. To further curb the toxicity issue, the cores are normally encapsulated with an ancillary semiconductor material which they are coated with variety of ligands or larger amphiphilic polymers for aqueous compatibility [14, 15]. Moreover, the NPs

can have a wide range of sizes with diameters ranging from 2 nm to greater than 10 nm even though the physical dimensions are on the nanoscale. However, studies done by Ye et al. showed that severe venomousness can be minimised in the as-prepared in-vivo QDs. They demonstrated that the blood and biochemical markers remained within normal ranges following treatment of major organs when rhesus macaques was injected with phospholipid micelle-encapsulated CdSe/CdS/ZnS QDs [16]. No palpable toxicity of QDs and abnormalities observed in mice even at long-time exposure as reported in other biochemical analysis and body weight measurement studies [17]. For biological use, combination of materials and physical properties of QDs can be further modified with either proteins, such as neutravidin, or other biomolecules such as DNA in order to confound any systematic study of toxicity and other issues such as dosage or exposure time can be looked into.

3.6 Absence of cytotoxicity

Extensive research has been conducted concerning the toxicity of QDs to be used for imaging of live cells and organisms for long durations. For such QDs to be used in living organisms it is imperious that QDs are not toxic to cells. Cadmium, tellurium and selenium present in the core of QDs have led to the conviction that the QDs are toxic [18]. However, studies on QDs revealed no toxicity whatsoever in live animals when injected into the bloodstream of pigs and for up to 4 months in mice [1]. No toxicity was detected also when QDs were laden in cells growing in vitro. Furthermore, no trace toxic effects of QDs in cells have been observed in vivo in experiments using Xenopus, Dictyostelium and mouse [19, 20 and 21].

Nevertheless, whenever a new approach for QD synthesis or coating is used, or if QDs are used in an extreme environment that could compromise their integrity, it is important to test for their cytotoxicity. Suitability for multicolor in vivo imaging QDs have facilitated the simultaneous imaging of at least five populations of live cells, each labeled with a different colored QD [22].

Visible light is limited by the fact that they have high absorbance and scatter easily hence hindering imaging in tissue beyond a depth of 100 mm. QDs on the other hand have been found to be orders of magnitude brighter than the conventional fluorescent probes used in multiphoton microscopy. Thus, the use of QDs is highly recommended since they offer significant advantages when a probe requiring simultaneous imaging of multiple fluorophores is conducted. The ability to synthesize QDs that emit in the near-infrared spectrum has also facilitated in vivo imaging not only in mice, but also in bigger animals such as pigs [23-25].

References

[1] B.B. Ballou, C. Lagerholm, L.A. Ernst, M. P. Bruchez, A.S. Waggoner, “Noninvasive Imaging of Quantum Dots in Mice”, Bio conjugate chemistry 15, 2004, 79.

[2] J.K. Jaiswal, M. Hedi, J.M. Matthew, M.S. Sanford, “Long-term multiple color imaging of live cells using quantum dot bioconjugates”, Nature biotechnology 21, 2003, 47.

[3] E.B. Voura, J.K. Jaiswal, M. Hedi, M.S. Sanford, “Tracking metastatic tumor cell extravasation with quantum dot nanocrystals and fluorescence emission-scanning microscopy”, Nature medicine 10, 2004, 993.

[4] D.S. Lidke, P. Nagy, R. Heintzmann, D.J. Arndt-Jovin, J.N. Post, H.E. Grecco, E.A. Jares-Erijman, and T.M. Jovin. "Quantum dot ligands provide new insights into erbB/HER receptor-mediated signal transduction", Nature biotechnology 22, 2004, 198.

[5] M. Dahan, L. Sabine, L. Camilla, R. Philippe, R. Beatrice, T. Antoine, “Diffusion dynamics of glycine receptors revealed by single-quantum dot tracking”, Science 302, 2003, 442.

[6] X. Wu, H. Liu, L. Jianquan, K.N. Haley, A.T. Joseph, J.L. Peter, N. Ge, P. Frank, P.B. Marcel, “Immunofluorescent labeling of cancer marker Her2 and other cellular targets with semiconductor quantum dots”, Nature biotechnology 21, 2003, 41.

[7] B. Dubertret, P. Skourides, D.J. Norris, N. Vincent, A.H. Brivanlou, A. Libchaber, “In vivo imaging of quantum dots encapsulated in phospholipid micelles”, Science 298, 2002, 1759.

[8] A. Hoshino, K. Hanaki, K. Suzuki, K. Yamamoto, “Applications of T-lymphoma labeled with fluorescent quantum dots to cell tracing markers in mouse body”, Biochemical and biophysical research communications 314, 2004, 46.

[9] Crystal structure online; http://en.wikipedia.org/wiki/wurtzite, cubic crystal structure [Accessed 22 Feb 2017].

[10] Electronic band structure online; http://en.wikipedia.org/wiki/electronic band structure structure [Accessed 23 Feb 2017].

[11] Luminescence online; https://ned.ipac.caltech.edu/level5/Sept03/Li/Li4.html. [Accessed 24 Feb 2017].

[12] E.R. Goldman, E.D. Balighian, H. Mattoussi, M.K. Kuno, J. M. Mauro, P.T. Tran, G.P. Anderson, "Avidin: a natural bridge for quantum dot-antibody conjugates", J. American Chem Society 124, 2002, 6378.

[13] M. Bruchez, M. Moronne, P. Gin, S. Weiss, A.P. Alivisatos, "Semiconductor nanocrystals as fluorescent biological labels", science 281, 1998, 2013.

[14] D. Gerion, F. Pinaud, S.C. Williams, W.J. Parak, D. Zanchet, S. Weiss, A.P. Alivisatos, "Synthesis and properties of biocompatible water-soluble silica-coated CdSe/ZnS semiconductor quantum dots", J. Phy Chem B 105, 2001, 8861.

[15] W.C.W. Chan, S. Nie, "Quantum dot bioconjugates for ultrasensitive nonisotopic detection", Science 281, 1998, 2016.

[16] L. Ye, K. Yong, L. Liu, I. Roy, R. Hu, J. Zhu, H. Cai, "A pilot study in non-human primates shows no adverse response to intravenous injection of quantum dots", Nature Nanotechnology 7, 2012, 453.

[17] Y. Su, F. Peng, Z. Jiang, Y. Zhong, Y. Lu, X. Jiang, Q. Huang, C. Fan, S. Lee, Y. He, "In vivo distribution, pharmacokinetics, and toxicity of aqueous synthesized cadmium-containing quantum dots", Biomaterials 32, 2011, 5855.

[18] A.M. Derfus, W.C.W. Chan, S.N. Bhatia, "Probing the cytotoxicity of semiconductor quantum dots", Nano letters 4, 2004, 11.

[19] D.R. Larson, W. R. Zipfel, R.M. Williams, S.W. Clark, M.P. Bruchez, F.W. Wise, W.W. Webb, "Water-soluble quantum dots for multiphoton fluorescence imaging in vivo", Science 300, 2003, 1434.

[20] S. Kim, Y.T. Lim, E.G. Soltesz, A.M. De Grand, J. Lee, A.Nakayama, J.A. Parker, "Near-infrared fluorescent type II quantum dots for sentinel lymph node mapping", Nature biotechnology 22, 2004, 93.

[21] J.A. Kloepfer, R. E. Mielke, M. S. Wong, K. H. Nealson, G. Stucky, J. L. Nadeau, "Quantum dots as strain-and metabolism-specific microbiological labels", Applied and environmental microbiology 69, 2003, 4205.

[22] L. Zhu, S. Ang, W. Liu, "Quantum dots as a novel immunofluorescent detection system for Cryptosporidium parvum and Giardia lamblia", Applied and environmental microbiology 70, 2004, 597.

[23] J.K. Jaiswal, S.M. Simon, "Optical monitoring of single cells using quantum dots", Quantum Dots: Applications in Biology, 2007, 93.

[24] Y.T. Lim, S. Kim, A. Nakayama, N.E. Stott, M.G. Bawendi, J.V. Frangioni, “Selection of quantum dot wavelengths for biomedical assays and imaging”, Molecular imaging 2, 2003, 50.

[25] E.R. Goldman, A.R. Clapp, G.P. Anderson, H.T. Uyeda, J.M. Mauro, I.L. Medintz, H. Mattoussi, “Multiplexed toxin analysis using four colors of quantum dot fluororeagents”, Analytical Chemistry 76, 2004, 684.

Chapter 4

Characterization techniques of CdY nanoparticles

In this research work, the CdY NPs were characterized using High Resolution Transmission Electron Microscopy (HRTEM), Energy Dispersive x-ray Spectroscopy (EDS), scanning electron microscopy (SEM), X-ray Diffraction (XRD), Photoluminescence spectroscopy (PL) and UV- visible (UV-vis). This chapter describe the characterization techniques in length including how they operate and some key features required for each of the equipment in this chapter.

4.1 Energy Dispersive X-ray Spectroscopy (EDS)

The qualitative analysis (surface chemical or elemental composition) of the as-synthesized nanopowders prepared in this research study was dogged by EDS spectroscopy. EDS or EDX is a chemical microanalysis technique used in conjunction with HRTEM or SEM. X-rays emitted from the sample during bombardment by an electron beam is detected by the EDS technique and sorts out energies of the X-ray for individual elements. Features or phases as small as 1 μm or less can be analysed [1].

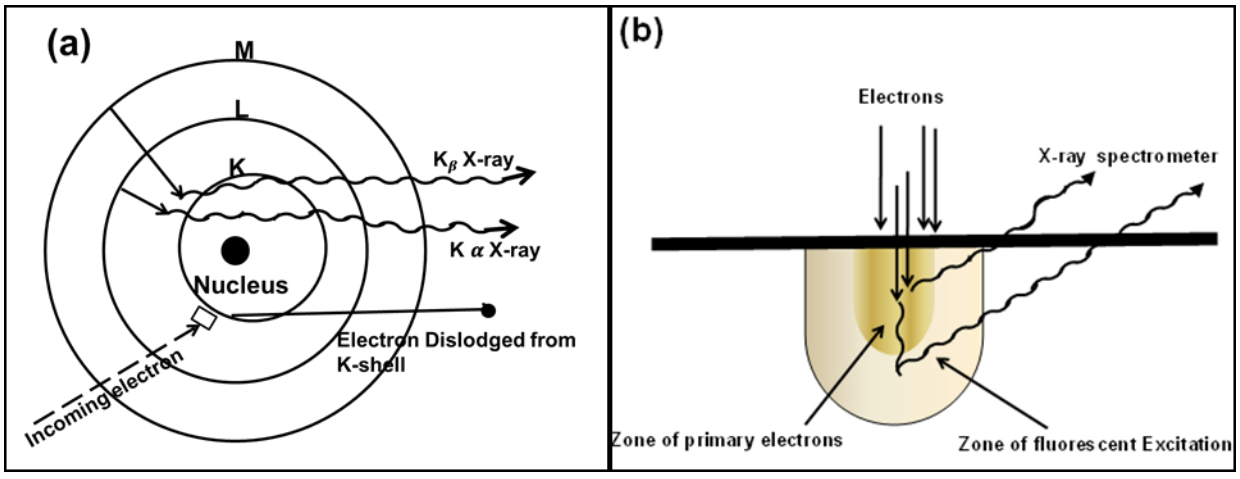

Figure 4.1 (a) and (b): Characteristic x-ray radiation [2]

The intensity distribution and energy of the signal generated by a focused electron beam impinging on the sample is used to obtain information about the chemical composition of the sample. Electron gun is used as the source of the electron in the high resolution transmission microscope or scanning electron microscope. The incident beam of electrons interacts with core electrons of the sample's atoms transferring sufficient energy to it, thereby ejecting it from the target atom. This results in the creation of a hole within the atom's electronic structure. An electron from an outer, higher energy shell then occupies the hole releasing excess energy in the form of an X-ray photon. As a result of electronic transitions which occur between the outer and inner core levels a characteristic X-ray is emitted when the ionized atom 'relaxes' to a lower energy state by the transition of an outer-shell electron to the vacancy in the core shell which provide a quantitative and qualitative elemental composition of the sample [3]. Due to a well-defined nature of the various atomic energy levels, it is clear that the energies and associated wavelengths of the set of X-rays will have characteristic values for each of the atomic species present in a sample [4] as shown in Fig. 4.1 (a) and (b).

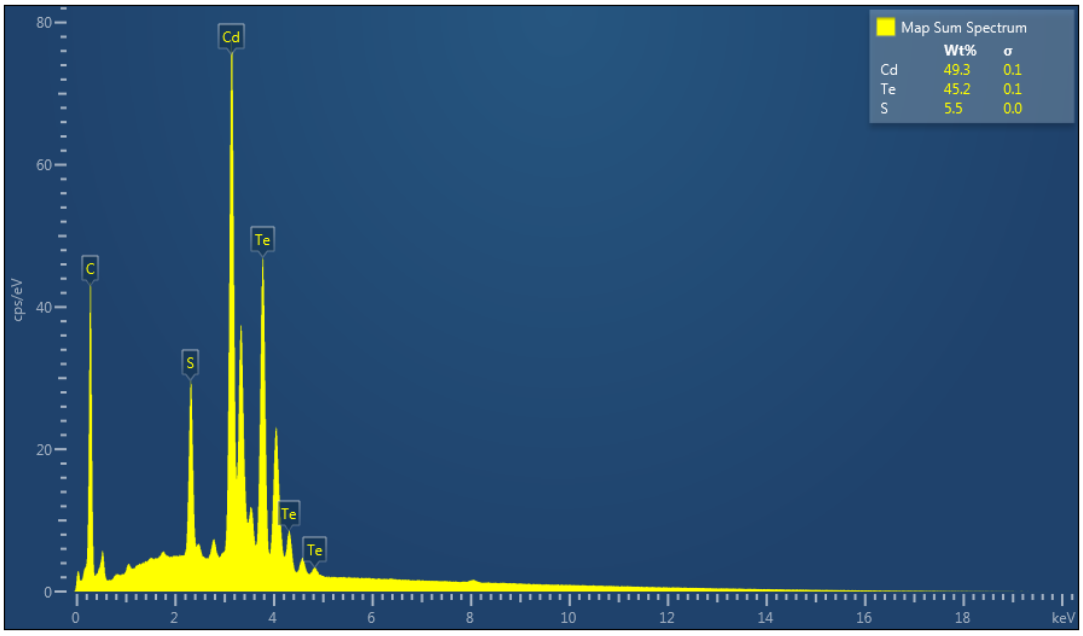

Figure 4.1(c): Example of an EDS spectrum of CdTe.

A characteristic X-ray is usually emitted when the ionized atom 'relaxes' to a lower energy state by the transition of an outer-shell electron to the vacancy in the core shell. The X-ray is called characteristic because its energy equals the energy difference between the two levels involved in the transition and this difference is characteristic of the material.

From the output of an EDS analysis we obtain an EDS spectrum, (Fig 4.1(c)). The EDS spectrum shows the frequency in counts of X-rays received for each energy level. The spectrum normally plots the peaks corresponding to the energy levels for which the most X-rays have been received. Each of these peaks corresponds to a specific atom, and therefore characteristic of a specific element. The intensity of a peak in the spectrum correlates with the concentration of the element in the sample [4].

4.2 X-ray Diffraction (XRD)

X-ray scattering techniques reveal information about the crystallographic structure of nanomaterials and thin films. These techniques are based on observing the scattered intensity of an X-ray beam hitting a sample as a function of incident and scattered angle, polarization, and wavelength or energy. Powder X-ray diffraction (PXRD) is a technique used to characterize the crystallographic structure, crystallite size (grain size), and preferred orientation in polycrystalline, thin films or powdered solid samples.

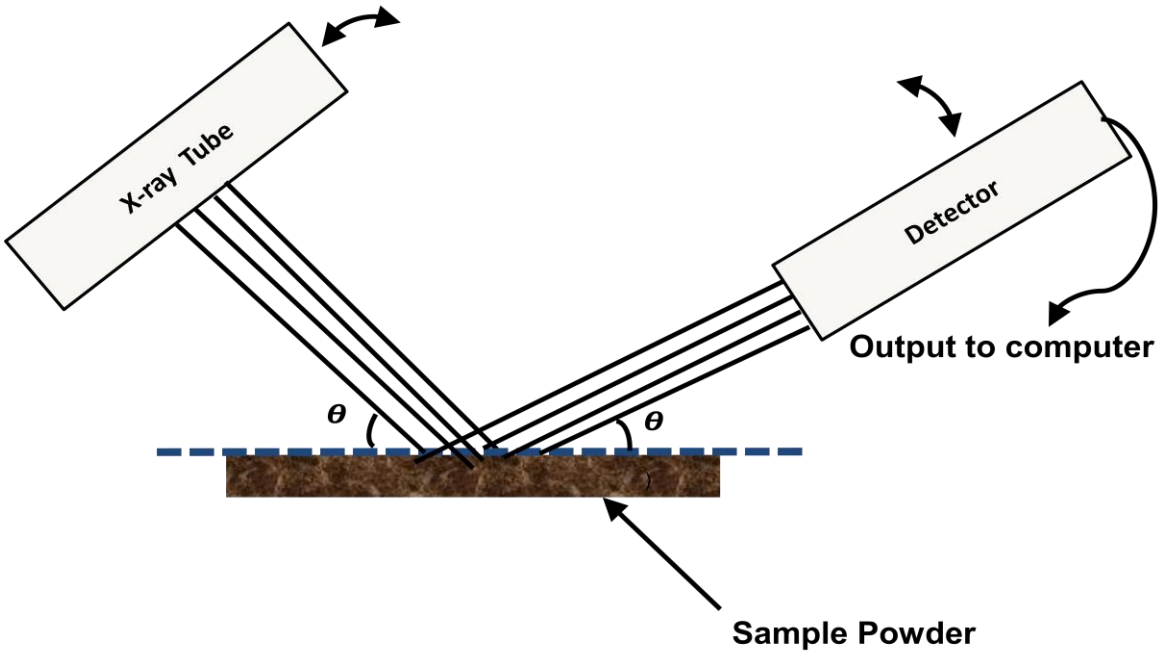

Figure 4.2(a): An X-ray powder diffractometer [7].

Powder diffraction is commonly used to identify unknown substances. XRD is a crystallographic technique used for identifying and quantifying various crystalline phases present in solid materials and powders. It is a commonly known technique for giving the most definitive crystal structures, interatomic spacing and bond angles. The interference of monochromatic X-rays are produced by a cathode ray tube, filtered to produce

monochromatic radiation collimated to concentrate by heating a filament to produce electrons toward a target by applying a voltage, and bombarding the target material with electrons.

A proportion of X-rays are diffracted to produce a pattern. From such a pattern the crystal phases can be identified by comparison to those of internationally recognized databases (such as International Centre of Diffraction Data (ICDD) or the Joint committee on powder diffraction standards (JCPDS)) that contain reference patterns [5]. It is also used for phase identification, determination of grain size, composition of solid solution, lattice constants, and degree of crystallinity in a mixture of amorphous and crystalline substances [6]. A sample is said to be crystalline if the atoms are arranged in such a way that their lattice positions are exactly periodic.

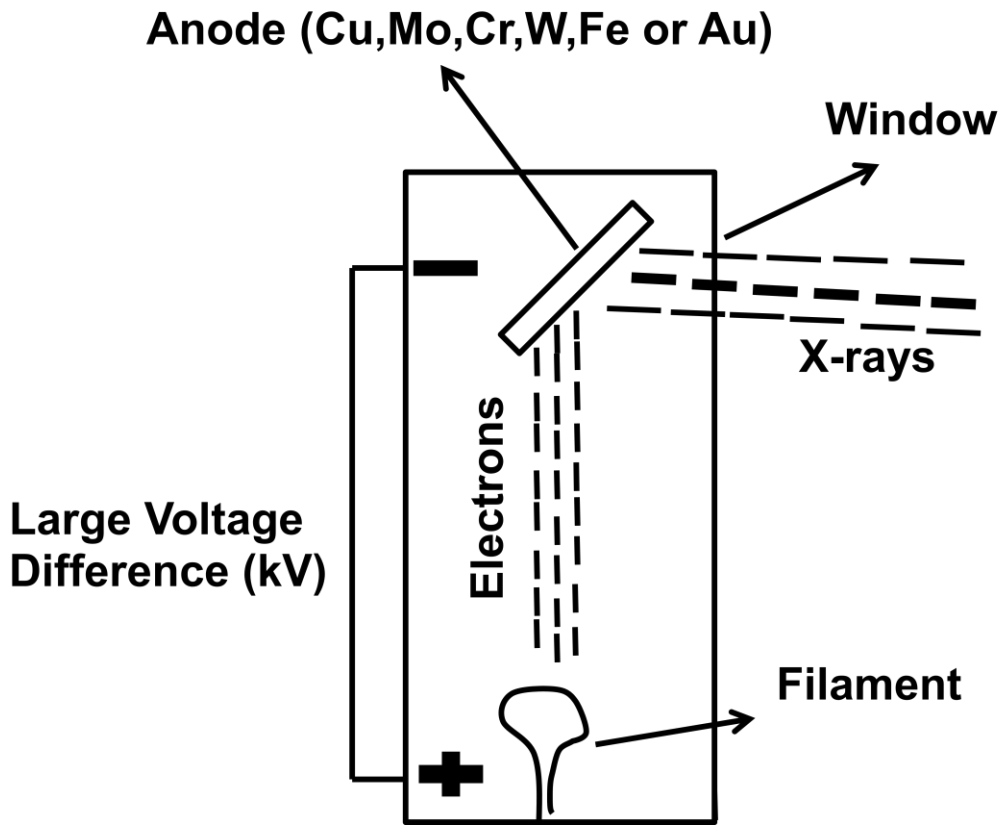

Figure 4.2 (b): Schematic diagram of an X-ray tube [7].

Crystalline materials include ceramics, metals, electronic materials, organics and polymers. The X-ray diffractometer are categorised into two broad classes; single crystals and powder. The powder diffractometer, Figure 4.2(a) is routinely used for phase identification and quantitative phase analysis [10]. Electrical current is run through the tungsten filament,

causing it to glow and emit electrons. A large voltage difference (measured in kilovolts) is placed between the cathode and the anode, causing the electrons to move at high velocity from the filament to the anode target.

Upon striking the atoms in the target, the electrons dislodge inner shell electrons resulting in outer shell electrons having to jump to a lower energy shell to replace the dislodged electrons. These electronic transitions results in the generation of X-rays. The X-rays then move through a window in the X-ray tube (Fig 4.2(b)) producing characteristic X-ray spectra which can be used to provide information on the internal arrangement of atoms in crystals or the structure of internal body parts. These X–ray spectra consist of several components and the most common are Kα and Kβ as shown in Fig 4.2(c) [7].

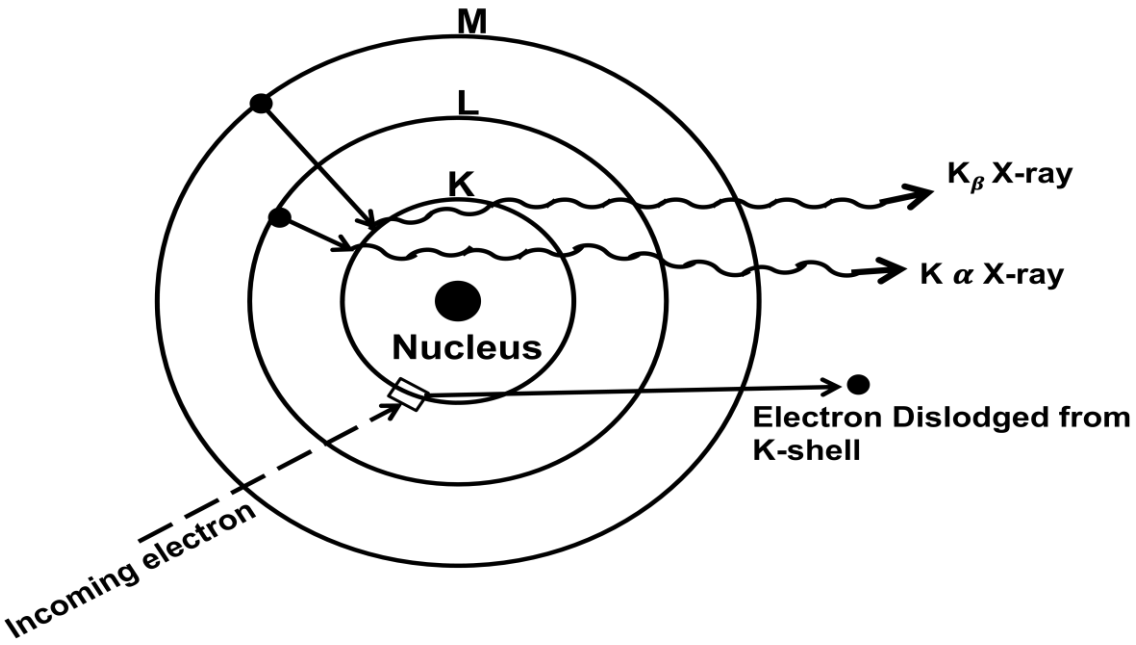

Figure 4.2(c): Characteristic X-ray Radiation [7]

The target materials that are usually used are Cu, Fe, Mo and Cr. Each of these has specific characteristic wavelengths [10] as shown in table 4.1.

Table 4.1: Characteristic wavelengths of target materials [7]

Element	Kα Wavelength (λ) Å
Mo	0.7107
Cu	1.5418
Co	1.7902
Cr	2.2909

In crystallography, the solid to be characterized by XRD has a space lattice with an ordered three - dimensional distribution (cubic, rhombic, etc.) of atoms. These atoms form a series of parallel planes separated by a distance d, which varies according to the nature of the material. For any crystal, planes have their own specific d-spacing. When a monochromatic X-ray beam with wavelength **λ** is irradiated onto a crystalline material with spacing d, at an angle θ, diffraction occurs only when the distance travelled by the rays reflected from successive planes differs by an integer number n of wavelengths to produce constructive interference. Such constructive interference patterns only occur when incident angles fulfil the Bragg's condition such that:

$$n\lambda = 2d \sin\theta \qquad (2)$$

By varying the angle θ, the Bragg's Law condition is satisfied for different d-spacing in polycrystalline materials. Plotting the angular positions versus intensities produces a diffraction pattern, which is characteristic of the sample. When a mixture of different phases is present, the resultant diffractogram is a superposition of the individual patterns [8].

In a typical XRD pattern, the diffracted intensities are plotted versus the detector angle 2θ. Each peak is then assigned a label indicating the spacing of a crystal plane. Bragg's law states the condition for sharp diffraction peaks arising from crystals which are perfectly ordered. Actual diffraction peaks have a finite width resulting from imperfections, either the irradiation source or the sample. A useful phenomenon is that as crystallite dimensions enter the scale the peaks broaden with decreasing crystal size. It is known that the widths of the diffraction peaks allow the determination of crystallite size. Practically, the size of crystallites smaller than 1000 Å can be determined using variants of the Scherer's equation derived from Bragg's law:

$$\boldsymbol{D = \frac{K\lambda}{\beta \cos \theta}} \qquad (3)$$

Where $\boldsymbol{D}$ is the thickness of the crystal, K a constant that depends on the crystallite shape, $\boldsymbol{\lambda}$ is the X-ray wavelength (1.54056 Å), $\boldsymbol{\beta}$ is the full width at half maximum of the broadened peak and $\boldsymbol{\theta}$ is Bragg's diffraction angle. If a Gaussian function is used to describe the broadened peak, then the constant K is equal to 0.89 [9]. XRD has many practical uses for technology enabled sensing applications. Not only does it allow for different phases to be identified, it can also be used to monitor the growth and formation of nanosized crystallites by examining the broadening of peaks in the XRD pattern. This is particularly important for studying sensing materials whose performance depends on the crystal particle size. It is also valuable for determining the distribution of crystals on the surface of a sensing layer [9].

Figure 4.2(d): Bruker D8 Advanced powder Diffractometer

4.3 Photoluminescence Spectroscopy

Luminescence refers to the emission of light by a material through any process other than blackbody radiation [11]. Photoluminescence is luminescence by which electromagnetic radiation, i.e. photons, are used to excite a material, usually by use of ultraviolet light.

Excitation occurs when light is directed onto a sample and it gets absorbed and imparts excess energy into the material. This excess energy can be released by the sample through the emissions of light [12], a process called luminescence. When the luminescence is accompanied by photo-excitation it is called photoluminescence (Fig 4.3 (a)). It is non-destructive because it is based on pure optical processes, no sample preparation is required and it is highly sensitive. Different types of samples (powder, liquid or bulk semiconducting material) can be characterized. PL is a convenient technique requiring a suitable source of optical excitation, a monochromator and a suitable detector for the emitted light. PL measurements are performed under continuous beam excitation conditions commonly known as continuous wave or steady state PL [13]. The sample is optically excited with laser energy greater than its band gap, Fig. 4.3(a). The incident photons are absorbed under creation of electron-hole pairs in the sample. After a short time the electrons eventually recombine with the holes, to emit photons, and light or luminescence will emerge from the sample. The energy of the emitted photons reflects the energy carrier in the sample. The emitted luminescence is collected, and intensity is recorded as a function of the emitted photon energy or wavelength, to produce a PL spectrum.

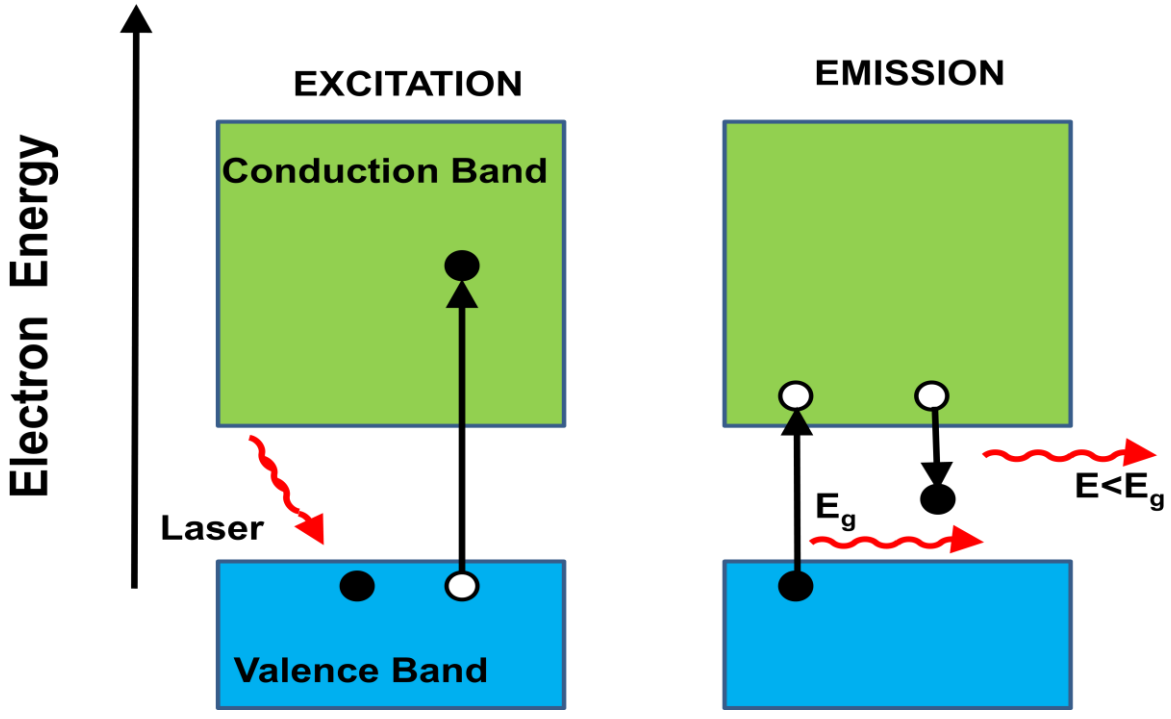

Figure 4.3(a): Excitation and Emission processes

The spectral distribution and time dependence of the emission are related to electronic transition probabilities within the sample, and can be used to provide qualitative and,

sometimes, quantitative information about chemical composition, structure, impurities, kinetic process and energy transfer. Sensitivity is one of the strengths of the PL technique, allowing very small quantities (Nanograms) or low concentrations (parts-per-trillion) of material to be analysed. Precise quantitative concentration determinations are difficult unless conditions can be carefully controlled, and many applications of PL are primarily qualitative. In PL, a material gains energy by absorbing photon at some wavelength by promoting an electron from a low to a higher energy level. This may be described as making a transition from the ground state to an excited state of an atom or molecule, or from the valence band to the conduction band of a semiconductor crystal or polymer (electron-hole creation). The system then undergoes a non-radiative internal relaxation involving interaction with crystalline or molecular vibrational and rotational modes, and the excited electron moves to a more stable excited level, such as the bottom of the conduction band or the lowest vibrational molecular state. After a characteristic lifetime in the excited state, electron will return to the ground state.

Figure 4.3(b): Cary Eclipse fluorescence spectrophotometer

4.4 Ultraviolet-Visible (UV-vis) absorption Spectroscopy

UV-vis absorption spectroscopy is the measurement of the attenuation of a beam of light after it passes through a sample or after reflection from a sample surface. Ultraviolet and visible

light are energetic enough to promote outer electrons to higher energy levels. UV-vis spectroscopy is usually applied to molecules or inorganic complexes in solution. Since the ultraviolet (UV) region scanned is normally from 200 to 400 nm, and the 12 visible portions are from 400 to 800 nm, UV-vis spectroscopy is useful to characterize the absorption, transmission, and reflectivity of a variety of technologically important materials, such as pigments, coatings, windows, and filters. It measures the intensity of light passing through a sample (I), and compares it to the intensity of light before it passes through the sample (I_o). The ratio $\frac{I}{I_o}$ is called the transmittance, and is usually expressed as a percentage (%T). The absorbance, A, is based on the transmittance [14]:

$$A = -\log\frac{T}{100} \quad (4)$$

The basic parts of a spectrophotometer are a light source, a holder for the sample, a diffraction grating or monochromator to separate the different wavelengths of light, and a detector. A spectrophotometer can be either single beam or double beam. In a single beam instrument all of the light passes through the sample cell. It must be measured by removing the sample. In a double-beam instrument, the light is split into two beams before it reaches the sample. One beam is used as the reference; the other beam passes through the sample. Some double-beam instruments have two detectors (photodiodes), and the sample and reference beam are measured at the same time, as shown in Fig 4.4(a).

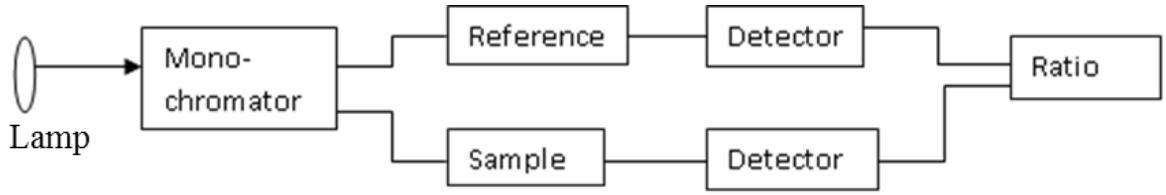

Figure 4.4(a): The schematic diagram of a double-beam UV-vis spectrophotometer [15].

Samples for UV-vis spectrophotometer are most often liquids, although the absorbance of gases and even of solids can also be measured. Samples are typically placed in a transparent cell, known as a cuvette. Cuvettes are typically rectangular in shape, commonly with an internal width of 1 cm. The type of sample container used must allow radiation to pass through the spectral region of interest. The most widely applicable cuvettes are made of high quality fused silica or quartz glass because these are transparent throughout the UV, visible and near infrared regions. Glass and plastic cuvettes are also common, although glass and most plastics absorb in the UV, which limits their usefulness to visible wavelengths [16]. The Spectroscopy used in this study is UV-vis spectrophotometer Lambda 950 (PerkinElmer).

Figure 4.4(b): UV-vis spectrophotometer Lambda 950 (PerkinElmer).

4.5 High Resolution Transmission Electron Microscopy

High-resolution transmission electron microscopy (HRTEM) or (HREM) is an imaging mode of the transmission electron microscope (TEM) that allows for direct imaging of the atomic structure of the sample. It is a powerful tool to study properties of materials on the atomic scale, such as semiconductors, metals, nanoparticles and sp^2-bonded carbon (e.g. graphene, C nanotubes). HRTEM is often also used to refer to high resolution scanning TEM (STEM), mostly in high angle annular dark field mode. For disambiguation, the technique is also often referred to as phase contrast TEM. At present, the highest point resolution realised in phase contrast TEM is around 0.5 angstroms (0.050 nm). At these small scales, individual atoms of a crystal and its defects can be resolved. For 3-dimensional crystals, it may be necessary to combine several views, taken from different angles, into a 3D map. This technique is called electron crystallography [17].

Transmission electron microscopy is an irreplaceable tool to characterize the structure of nanocrystals. Lattice image contrast and Z contrast provide complimentary information. Lattice imaging probes the crystalline core of particles with planes oriented perpendicular to the electron beam; Z contrast refers to the diffuse scattering of the electron beam being proportional to the atomic number (Z) of the element, and Z contrast provides contrast in the disordered/disoriented regions.

TEM is used on thin sections of material to determine the distribution of atoms, size and shape of nano- and micron-sized structures. In nanotechnology TEM is specifically used to characterize the structure, morphology, and composition of nanoparticles and other nanoscale materials. In addition, back-scattered X-ray (EDX) is used to map the position of elements in

the sample. Through these methods, one can reconstruct an atomic map of the imaged sample. HRTEM, high resolution imaging capability, it is an invaluable tool to study nanoscale properties of crystalline material such as semiconductors and metals. HRTEM has been widely and effectively used for analyzing crystal structures and lattice imperfections in various kinds of advanced materials on an atomic scale. Some of the applications include: particle size and shape analysis, particle size distribution, determination of crystallographic phases and elemental mapping [17, 18].

Figure 4.5: An image of a high resolution transmission electron microscope. [17]

References

[1] Description of EDS Technique http://mee-inc.com/index.html. [Accessed April 2016].

[2] Energy Dispersive X-ray Spectroscopy (EDS/EDX), [online].Available from http://www.thermo.com/com/cda/technology/detail/1,,12700,00.html. [Accessed May 2017].

[3] B.G. Yacobi, D. B. Holt, L.L. Kazmerski, "Microanalysis of solids", New York Plenum Press, 1994.

[4] EDS online. Available from http://ion.eas.asu.edu/descript_eds.htm. [Accessed 17 May 2017].

[5] B.E. Warren, "X-ray Diffraction", Addison-Wesley Publishing Company, Inc, USA, 1969.

[6] D.W. Groot, "Luminescence decay and related phenomena." Physica, 1939, 275IN1289-288.

[7] Prof. Stephen A. Nelson, "lecturer material", Tulane University 2010, 46.

[8] B.D. Cullity and S. R. Stock, "Elements of X-Ray Diffraction", Addison Wesley Pub. Co. Reading, USA 2001.

[9] H. Lipson and H. Steeple. "Interpretation of X-Ray Powder Diffraction Patterns Chap. 9 Macmillan", 1970, 262.

[10] F.A. Settle, "Handbook of Instrumental Techniques for Analytical Chemistry", Prentice Hall PTR, USA, 339.

[11] P.K. Chu, C. R. Brundle, C. A. Evans Jr, and S. Wilson. "Encyclopedia of Materials Characterization", 1992, 373.

[12] A.R. Barron, "Physical methods in chemistry and nano science", Rice University, Houston, Texas: C O N NEX IO N S, 2012, 295.

[13] PL [0nline], Available from http://www.purdue.edu/REM/rs/sem.htm 2008. [Accessed March 2017]

[14] UV-visspectroscopy http://www.cem.msu.edu/~reusch/VirtualText/Spectrpy/UV-Vis/uvspec.htm. m≠uv. [Accessed March 2017]

[15] UV-Vis Absorption Spectroscopy [online] http://www.files.chem.vt.edu/chem-ed/spec/uv-vis/uv-vis.html. [Accessed March 2017].

[16] D.A. Scoog, F.J. Holler, and S.R. Crouch. "Principles of instrumental analysis (Thomson Brooks/Cole, Bellmont, CA)", 2007.

[17] HRTEM [0nline], Available from http://www.purdue.edu/REM/rs/sem.htm. 2008. [Accessed August 2015]

[18] http://www.vcbio.science.ru.nl/en/fesem/info/principe/. [Accessed 12 May 2016].

Chapter 5

High luminescent L-cysteine capped CdTe quantum dots prepared at different reaction times [1]

5.1 Introduction

As new type of fluorescence materials, quantum dots (QDs) have attracted great scientific interests due to their unique properties and advantages over traditional organic fluorophores [1]. They possess unique optical and chemical characteristics which are useful for industrial, biological and analytical chemistry-related research. These properties include high photoluminescence (PL) intensity, narrow emission spectra or broad excitation, reasonable photochemical stability, controllable spectroscopic properties, photochemical stability, high quantum yields, and the ability to provide specific color fluorescence with a specific single excitation [2-4]. For biological imaging applications, a surface coating has been widely used to prevent QD oxidation and thereby reduce their possible cytotoxicity. The CdTe nanocrystals of different sizes have tunable emission from green to red due to quantum confinement and have been substantially studied in industrial and biomedical applications such as light-emitting devices (LEDs), photonic crystals, nonlinear optical devices, biological labels and neuroplastic cells following conjugation with some bio-active moieties [5].

The ability to synthesize CdTe nanocrystals with controlled shapes, compositions, and structures would enable a variety of size-dependent physical and optical properties to be explored. There have been two successful routes reported for the synthesis of CdTe nanocrystals which include synthesis in the organic phase [6, 7] and aqueous synthesis [8, 9] of thiol-capped CdTe nanocrystals [10, 11]. In most of the aqueous methodologies where NaHTe and H_2Te were used as the Te sources, they needed a pre-treatment to synthesize the unstable Te precursors. These, however, need equipping the chamber with the Schlenk line (which is expensive) and use of inert atmosphere. There have been other synthetic methods

reported for the preparation of monodisperse CdX (X = S, Se, Te) nanocrystals [5]. Typically, most of these preparation techniques involve the use of coordinating solvents like trioctylphosphine oxide/trioctylphosphine (TOPO/TOP) which act as stabilizers thus preventing their agglomeration. These organic solvents, however, contain hydrophobic molecules which causes the resulting QDs to be insoluble in water. For the QDs to be used for biological applications, these nanocrystals need to be transferred to aqueous solutions using various routine methods, such as ligand exchange, surface silanization, embedding in a polymer shell or incorporation in micelles [12]. Other researchers proposed that this insolubility problem could be solved by embedding the QDs into a shell or stable surfactant layer [13]. The material properties of the CdTe QDs are influenced by multiple factors derived from both intrinsic physico-chemical properties and environmental conditions that have contributed to the toxicity of the as-prepared QDs [14]. If this toxicity problem is addressed, the resulting QDs can be used as fluorescent probes for biological imaging, to monitor targeted drug delivery. Also, the elongated QDs like nanorods are known to lack strong polarization of the emitted photons [15].

There are very few reports on CdTe near infrared emitting nanocrystals in the biological field. Here in reports the synthesis of L-cysteine capped CdTe QDs using potassium telluride as stable tellurium source while sodium borohydride was used as a reductant and antioxidant. L-cysteine is found in human body and therefore the resulting QDs will be highly stable with minimum toxicity. The aim of this work is to produce near-infrared (NIR) emitting QDs because they possess many superior properties, for instance, NIR light traveling in biological tissues is weakened very little due to the relatively low absorbance of NIR photons by biological tissues. This means that NIR photons can travel deep into biological tissues, which is useful for biological detection and imaging [16]. In trying to curb the discussed detriments, our method presents a simple way of preparing spherical and highly stable L-cysteine capped CdTe QDs that are soluble in water without any further ligand exchange which has not been reported so far to the best of our knowledge. Most importantly the QDs produced using this simple and less expensive methods are stable and highly crystalline.

5.2 Experimental

5.2.1 Synthesis

The starting chemicals used were cadmium acetate dihydrate ($Cd(CH_3COO)_2 . 2H_2O$) (> 99%), as the source of cadmium ions, potassium tellurite (K_2TeO_3) (> 90%) which provided

tellurium ions L-cysteine (> 98%) as a capping agent and sodium borohydride which was used as reducing agent. All the chemicals used were of analytical grade. Synthesis method was adapted from reference [17]. Typically, the CdTe QDs were prepared by mixing the appropriate amount of cadmium acetate and L-cysteine in a beaker. The pH of the solution was adjusted to 11 by an addition of sodium hydroxide. After which, 50 ml of dissolved 0.2 mmol K_2TeO_3 was added to obtain a final volume of 100 ml. After stirring for a while, an appropriate amount of sodium borohydride was added to the mixture. The mixture was transferred to a three-necked flask and refluxed at 100 ^oC in open air for different reaction times. Cd: L-Cyst: Te: NaBH4 molar ratios were kept constant at 1:1:0.5:10.

5.2.2 Characterization

Characterization of the optical properties, particle diameter distribution, and the crystal structure of the prepared QDs were done by various techniques, including use of high-resolution transmission microscope (HRTEM), powder X-ray diffractometer (XRD), scanning electron microscope (SEM), Electron dispersive spectroscopy (EDS), ultra-violet and visible (UV–Vis) reflection and photoluminescence (PL) spectra for the CdTe QDs. All the measurements were taken at room temperature. PL spectra were taken at the excitation wavelength $\lambda = 400$ nm.

5.3 Results and Discussion

5.3.1. Structural and Compositional analysis

5.3.1.1 SEM images

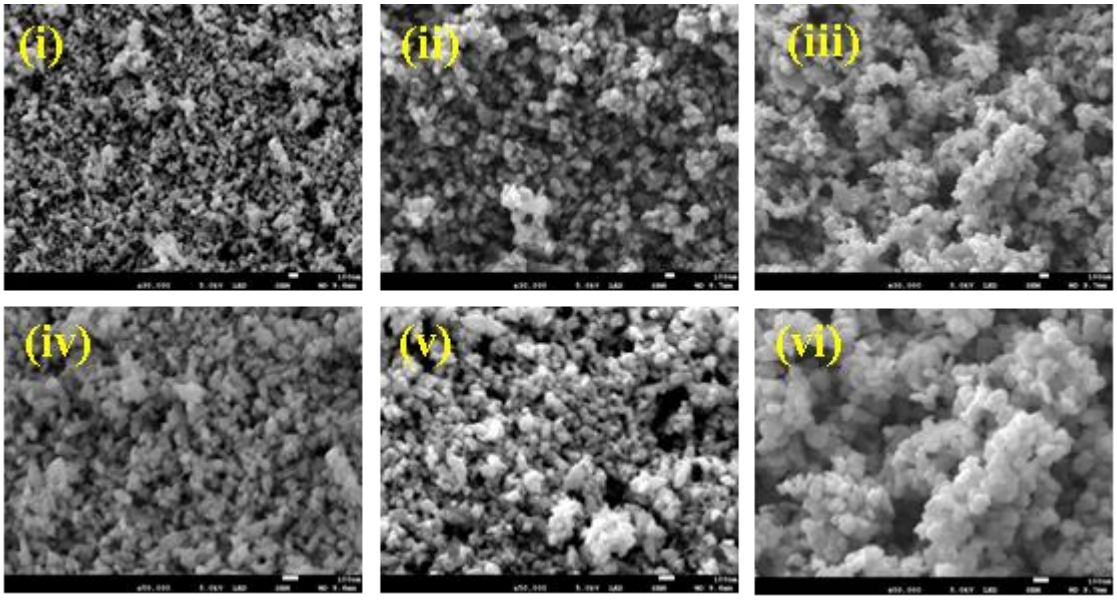

Figure 5.1(a): Representative SEM micrographs of CdTe samples ((i) and (ii)) – 60 min, ((iii) and (iv)) – 120 min and ((v) and (vi)) - 180 min taken at different magnification.

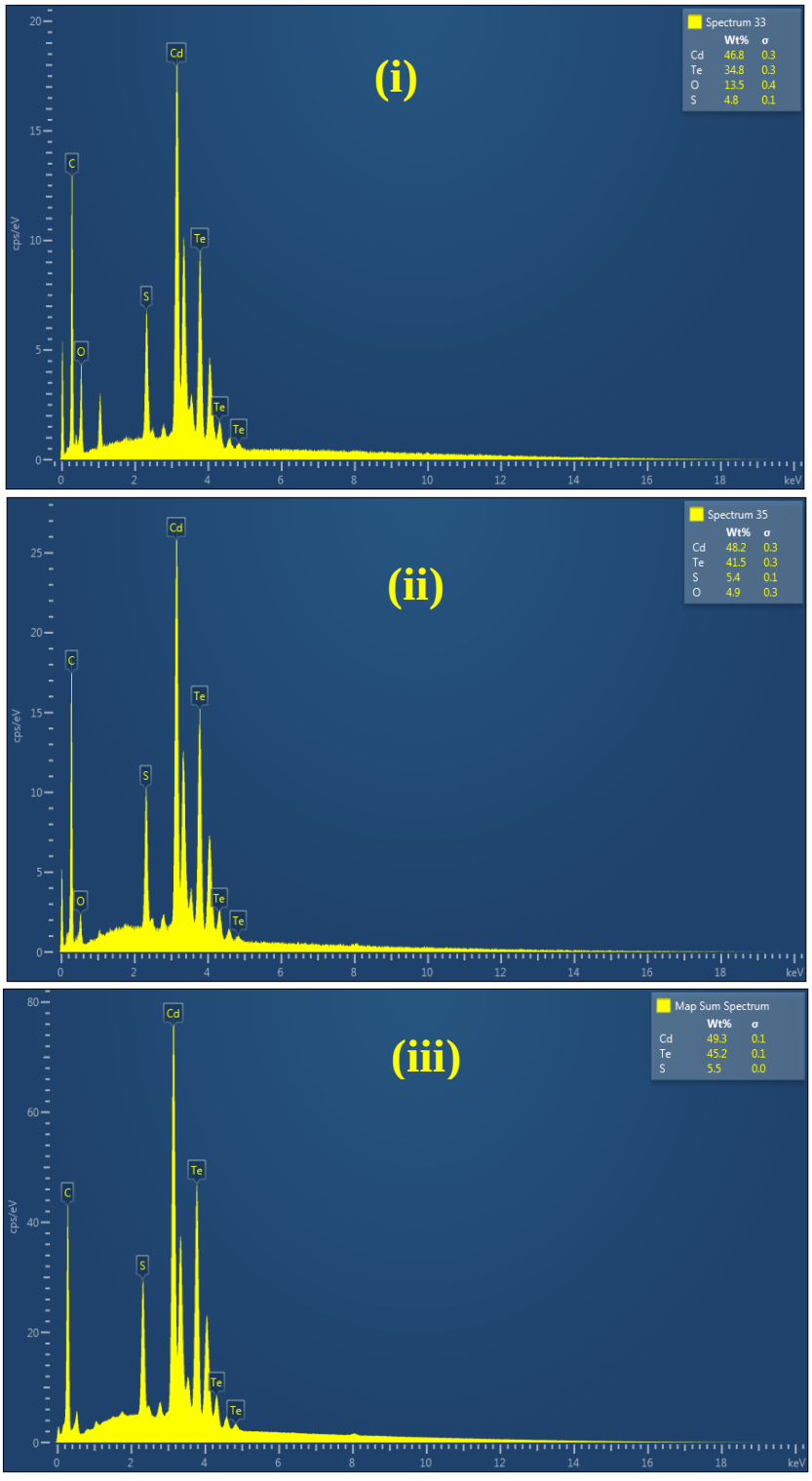

Figure 5.1(b): Representative EDS spectra of CdTe samples taken at (i) - 60, (ii) - 120 and (iii) - 180 min of reaction time.

Fig. 5.1(a) shows the representative SEM images of the CdTe QDs prepared at different reaction times. The variation of CdTe QDs morphology due to change in reaction time was

evident from the images. CdTe QDs possess uniform surface morphology and display spherical shapes which agglomerate at a longer synthesis time. Particle sizes increased with an increase in reaction time. Elemental analysis of the as-prepared CdTe QDs was done using the EDS. From Fig. 5.1(b) it is clear that the expected Cd and Te elements were present. At shorter synthesis time, S and O elements were observed being an impurity which could not be eliminated completely in the sample. Longer growth time helped in eliminating some of these impurities as confirmed by decrease in O atomic%. C element is also present which was from the carbon tape used to mount the sample. However, the S and O percentages are small and therefore they are considered as trace impurities in the CdTe samples prepared. The atomic ratio of the Cd:Te elements analysed increased with growth time and are in close agreement with the volumetric ratio of the elemental chemical precursor solutions during synthesis. This shows that all the samples have a stoichiometric composition.

5.3.1.2 HRTEM Analysis

Fig. 5.2(a) display representative HRTEM micrographs containing insets of selected area electron diffraction patterns (SAED) and particle size distribution histogram obtained from HRTEM micrographs of the CdTe QDs prepared at (i) - 60 min, (ii) - 120 min and (iii) - 180 min. Changes in shape and size can be observed as the reaction progresses to longer time. Longer reaction time produces QDs with larger particle diameter (6.40 nm, 6.81 nm and 7.81 nm for 60 min, 120 min and 180 min respectively). The morphology studies confirmed spherical and monodispersed CdTe QDs as observed from SEM images. It was also evident from the SAED rings that the structural changes in CdTe QDs were not many when subjected to different reaction times.

Images i, ii and iii in Fig. 5.2 (b) were used to estimate the particle diameters of the as obtained CdTe QDs. The micrographs (iv, v and iv) exhibit clear lattice fringes which are indication of good crystallinity of the sample. Several particles were considered in estimating its diameters. A size distribution histogram was then plotted and a Gaussian fit drawn as shown in Fig. 5.2(a).

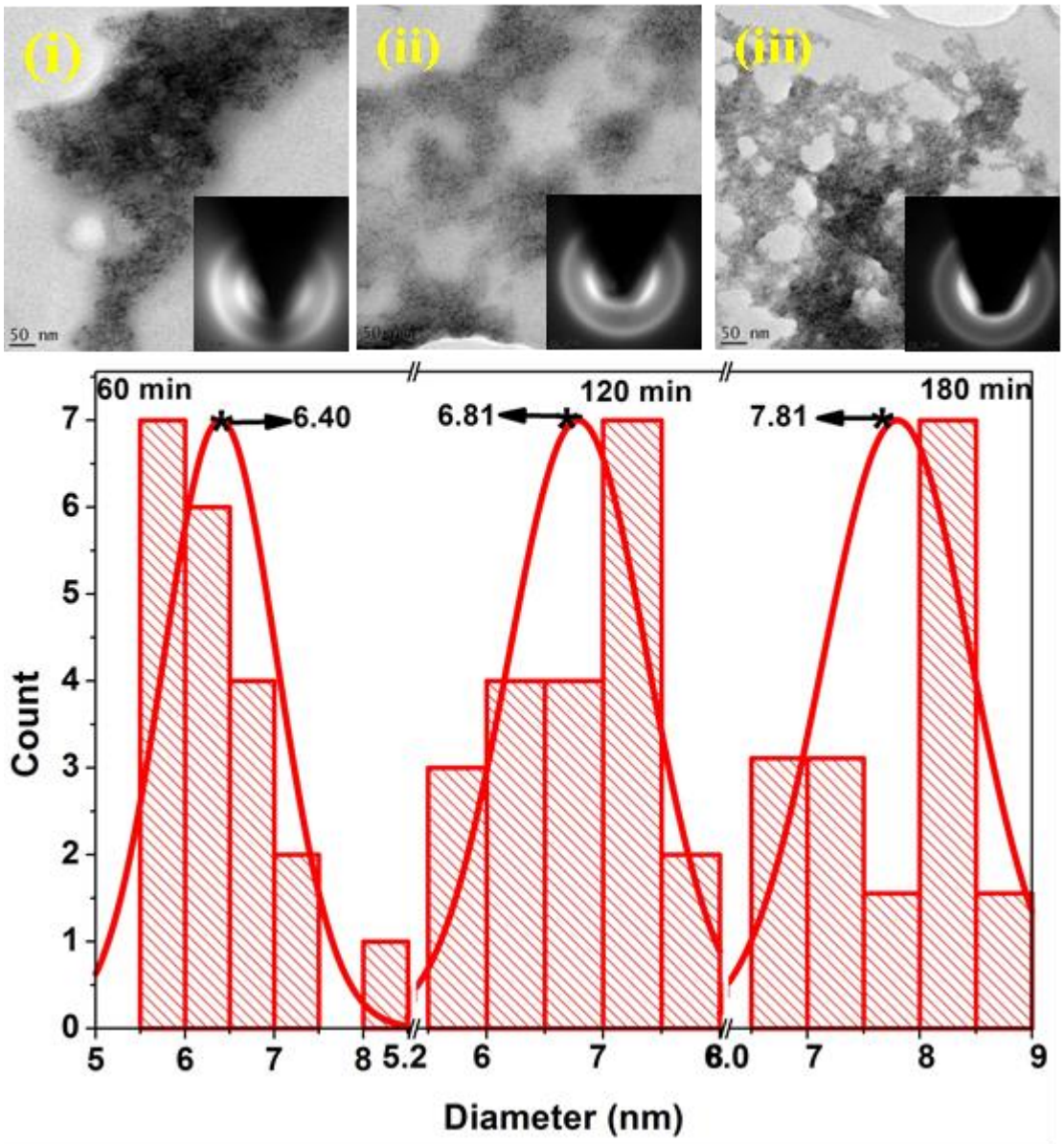

Figure 5.2(a): TEM micrographs (with SAED pattern inset) and particle size distribution histogram obtained from HRTEM micrographs of CdTe QDs prepared at reaction times (i) -60, (ii) -120 and (iii) -180 min

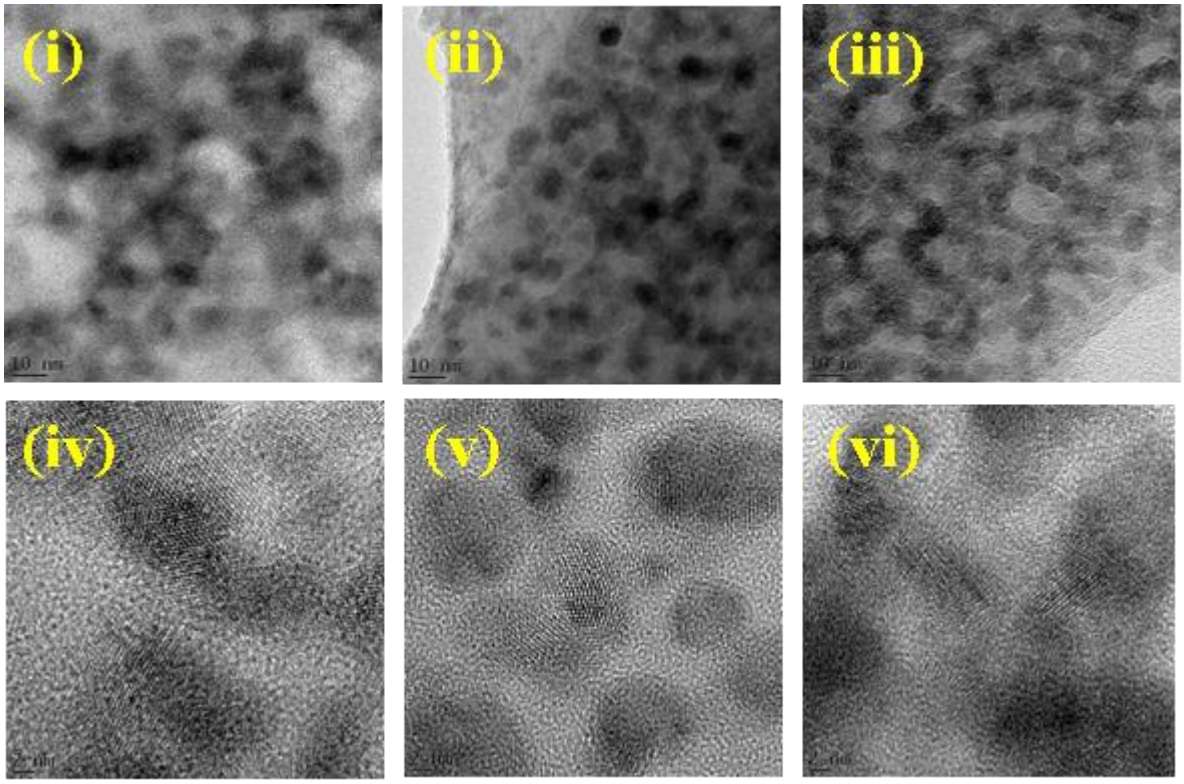

Figure 5.2(b): HRTEM micrographs of CdTe QDs prepared at 60 min - (i) & (iv), 120 min - (ii) & (v) and 180 min - (iii) & (vi) of reaction time.

5.3.1.3 XRD Analysis

The XRD pattern of as obtained CdTe QDs is shown in Fig 5.3(a).The patterns display polycrystalline nature of the sample. The XRD peaks dominantly match well with JCPDS file no.75-2086 exhibiting face-centered cubic structure. The estimated lattice parameters a=b=c were 6.41,6.45,6.43 and 6.38 Å for 15, 30, 45 and 60 min of reaction time which are in close agreement with that from the standard JCPDS file. It was observed that at 60 min CdTe QDs crystal structure was fully formed with minimal impurity. There were no significant changes in the structure observed from the pattern as the reaction progressed to a longer reaction time as was also confirmed by SAED diffraction rings obtained from HRTEM measurement. The peaks marked with asterisks (*) are impurities from unreacted tellurium or could be due to the formation of impurity metal oxide in the sample. Te presents a degree of oxidation +4 if bound with oxygen and -2 with cadmium and suggests a compositional mixture of several $Cd_xTe_yO_z$ compounds [18, 19] which explains the presence of different CdTe phases present in one sample.

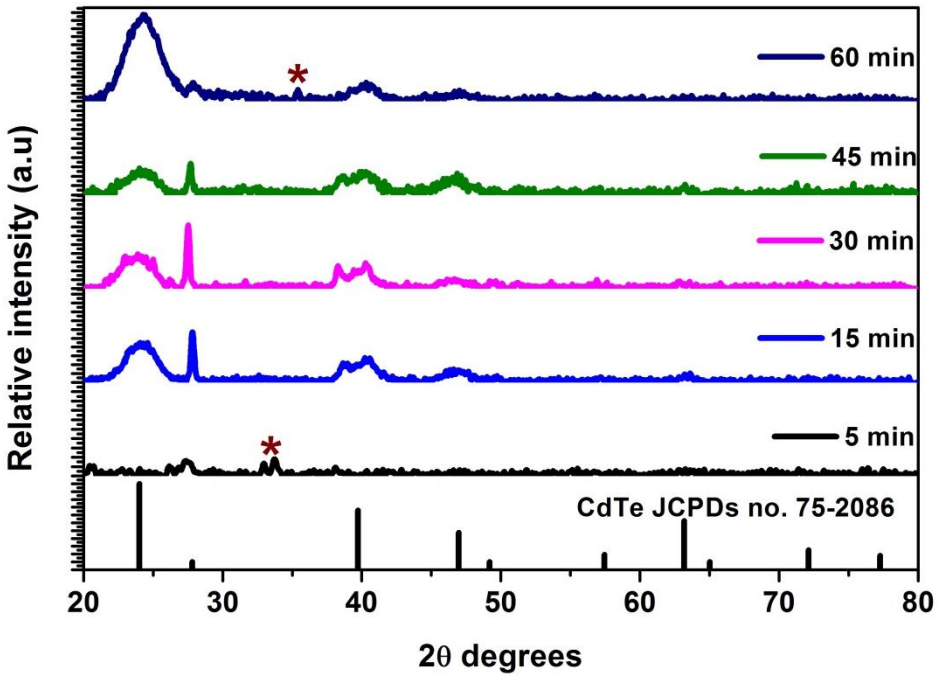

Figure 5.3(a): Representative XRD pattern for CdTe QDs prepared at different reaction times.

The crystallite sizes of the as-prepared CdTe QDs were approximated using Debye–Scherrer formula [20].

$$D = \frac{0.9\,\lambda}{\beta\,\cos\theta_B} \qquad (5)$$

where D is the crystallite diameter, λ is the wavelength of CuKα radiation (1.5406 Å), θ is the Bragg's diffraction angle, and β is the broadening of the diffraction line full width at half maximum (FWHM). It is well known that the Debye-Scherrer formula is a good approximation for a spherical crystal where the size is inversely proportional to the full width at half maximum. Precisely, the value of full width at half maximum depends on the length over which the periodicity of the crystal is complete. Using Scherrer formula for (111) plane of the dominant phase, the average crystallite size of the as-prepared CdTe QDs were 3.54, 4.10, 4.60 and 6.12 nm for 15, 30, 45 and 60 min reaction time. These values were closer to those obtained from the HRTEM measurement value. The discrepancy could be due to the fact that HRTEM estimates the particle size while XRD estimates the crystallite size of the QDs.

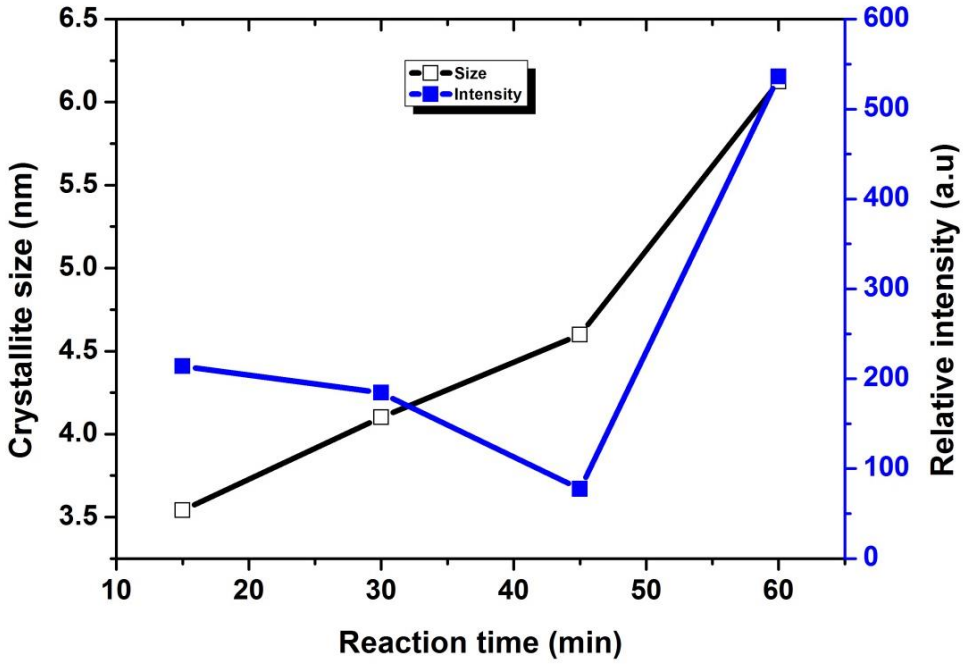

Figure 5.3(b): a graph showing changes in crystallite sizes and relative peak intensities of CdTe QDs obtained from XRD pattern with respect to reaction time.

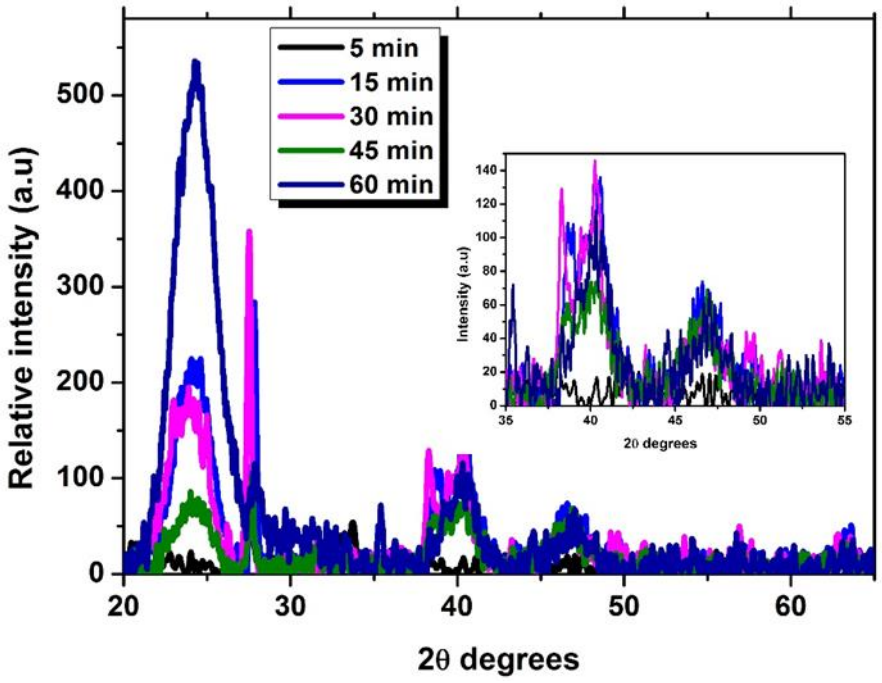

Figure 5.3(c): A merged and a magnified (2$\boldsymbol{\theta}$ = 35 to 55 degrees) CdTe QDs XRD pattern for different reaction times

Fig. 5.3(b) displays changes in crystallite size and peak intensity with reaction time. It shows that highest peak intensity was obtained at 60 minutes of reaction time indicating enhanced crystallinity of the sample. Reduction of peak intensity at shorter reaction time could most likely be due to the oxidation of the stabilizer molecules which probably caused the

ineffective passivation of nanocrystal surface defects [21]. Crystallite sizes of as-prepared CdTe QDs showed a direct relation with reaction time.

Fig. 5.3(c) displays a merged and a magnified XRD pattern from 35 to 55 degrees for various reaction times. Diffraction peaks shift to lower angles as reaction time increased from 10 to 30 minutes but a shift to higher diffraction angle at 45 min was observed. There was also narrowing of diffraction peaks observed due to increase in particle sizes as confirmed by HRTEM analysis. The shift in diffraction peaks was accompanied by variation of lattice parameters with change in reaction time. The shift in diffraction peaks to higher angle is due to decrease in the lattice parameters attributed to lattice contraction caused by impurity defects (oxygen) present in the crystal lattice as observed in the EDS analysis. The average lattice constant (a_{hkl}) for the CdTe cubic structure was calculated using Equation (Eq.) (6) where the inter-planar spacing d_{hkl} was estimated from Bragg's law (Eq. 7) for plane (111) and (311).

$$a_{hkl} = d_{hkl}\sqrt{h^2 + k^2 + l^2} \quad (6)$$

$$d_{hkl} = \frac{\lambda}{2\sin\theta_{hkl}} \quad (7)$$

5.3.2 Photoluminescence Analysis

Room temperature PL spectra excited at 400 nm of CdTe QDs prepared at various reaction times are shown in Fig. 5.4(a). With protracted reaction time, the emission band was shifted to longer wavelength. The PL emission bands red shifted from 517-558 nm for 5-180 min of reaction time. There was also an observation of change in peak intensities as reaction time progressed to longer time. For reaction time longer than 60 min, there were some black depositions in the solution, which may have been caused by the oxidization and aggregation of CdTe QDs. As reaction time increased, Ostwald ripening occurred, during which large particles grew by means of sacrificing small ones [22]. Therefore, reducing the total number of particles while increasing the average particle size and broadening the size distribution of particles (Fig. 5.4(e)). All the samples possessed good symmetric PL spectra with no tail at longer or shorter wavelength. Fig. 5.4(b) displays analysis of the changes in PL peak intensity and the peak position with respect to reaction time. It is clear from the graph that reaction time has great influence on the luminescence of CdTe QDs prepared by this method. The intensity of the PL emission spectra increased until 120 min when it starts to decrease.

Reduction of the PL peak intensity at longer reaction time could be due to oxidation and decomposition of the stabilizer causing defects in the sample hence reduction in the peak intensity.

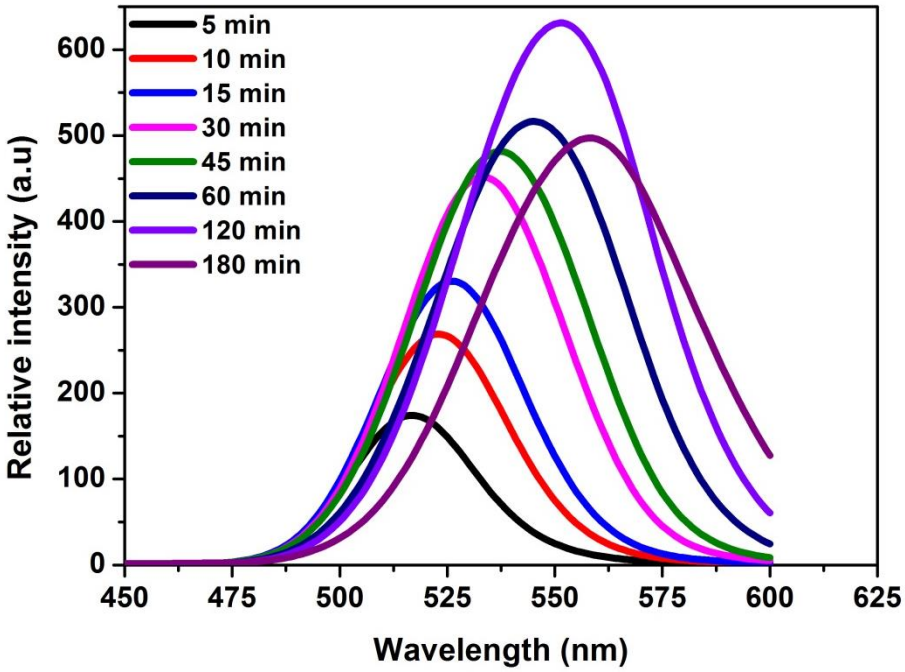

Figure 5.4(a): PL emission spectra of CdTe QDs prepared at various reaction times.

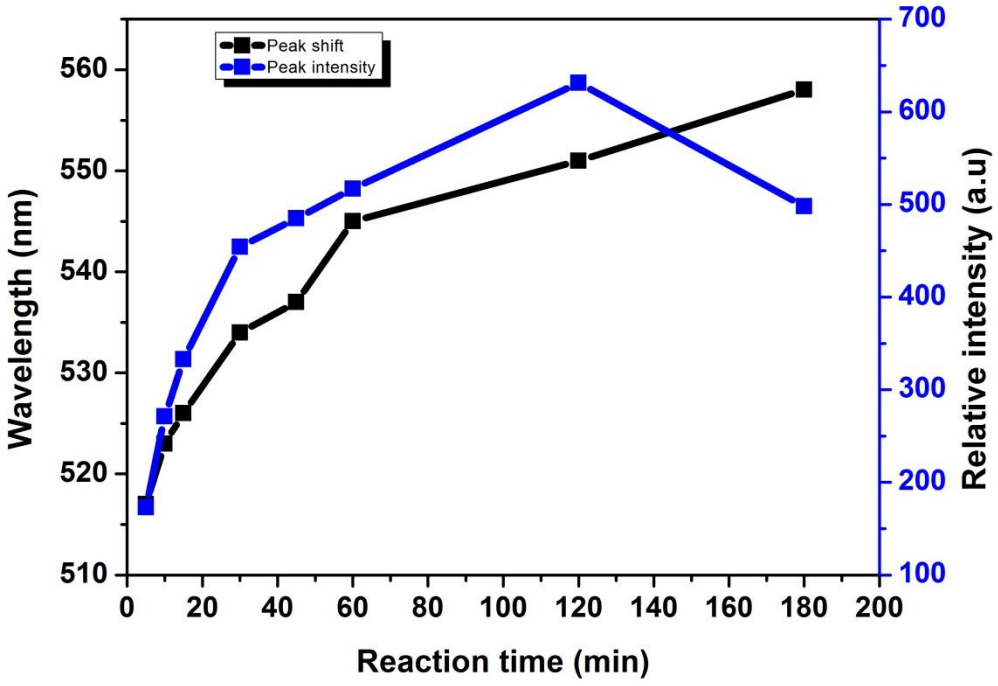

Figure 5.4(b): Variation of peak position and intensity with respect to reaction time.

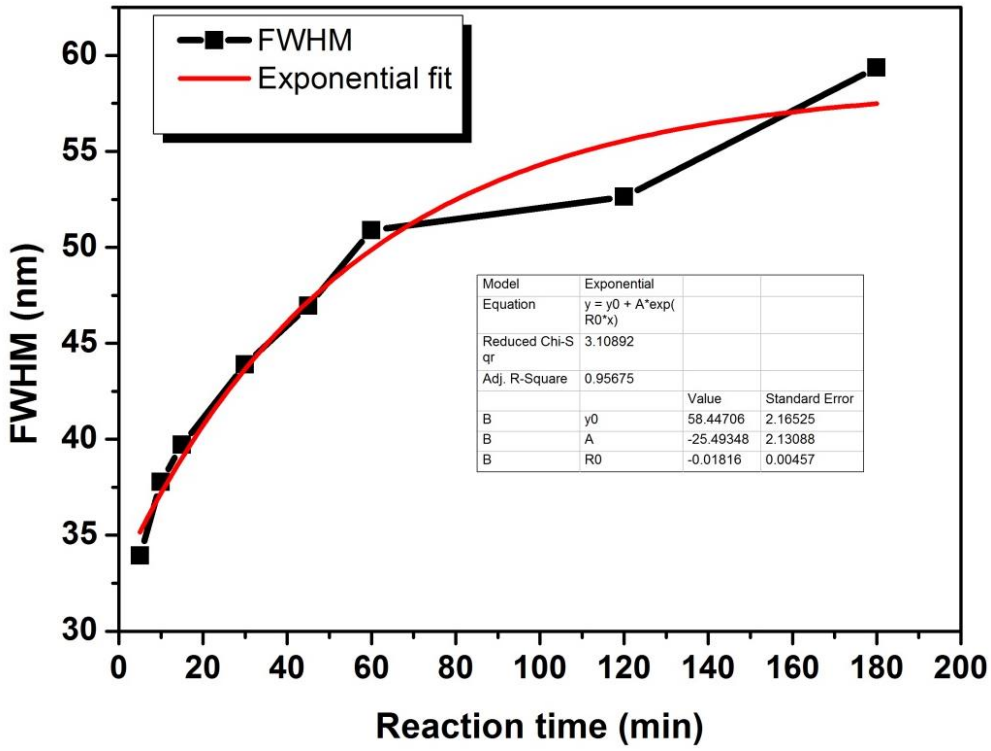

Figure 5.4(c): Exponential curve fit for FWHM data points of as-prepared CdTe QDs.

Evolution of the PL FWHM shown in Fig. 5.4(c) increased exponentially with reaction time from 33.94-59.35 nm for 5-180 min indicating narrow size distribution of the as-obtained CdTe QDs. It was also observed that excitation wavelength had slight effect on the emission spectra. When excited at wavelength lower than 350 nm there was barely any emission observed for the as-prepared samples. However, excitation wavelength of 400 nm gave the most intense emmission spectra as compared to 350 and 400 nm as it is observed in Fig. 5.4 (d). There was a very small shift in position of the emission band (544.1, 544.9 and 546.2 for 350, 400 and 450 excitation wavelength). Fig. 5.4(e) displays a proposed schematic diagram for variation of band gap energies for different samples prepared at various reaction times. All samples were excited at wavelength of 400 nm and displayed a red shift in emission with increase in reaction time accompanied by a decrease in the band gap energies estimated from the absorbance spectra as shown in Fig. 5.4(e).

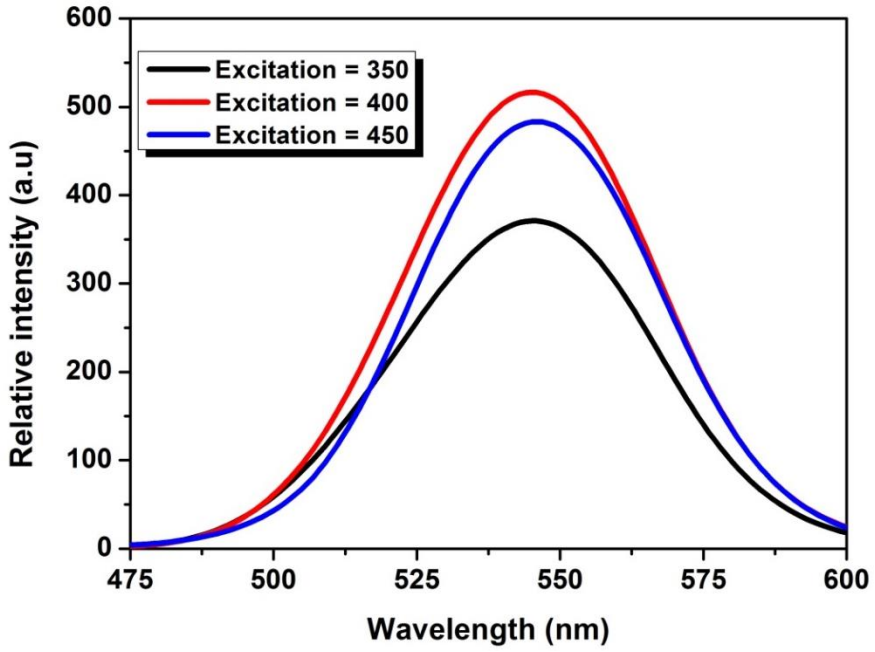

Figure 5.4(d): Changes in Peak width (nm) of CdTe nanoparticles with respect to synthesis time.

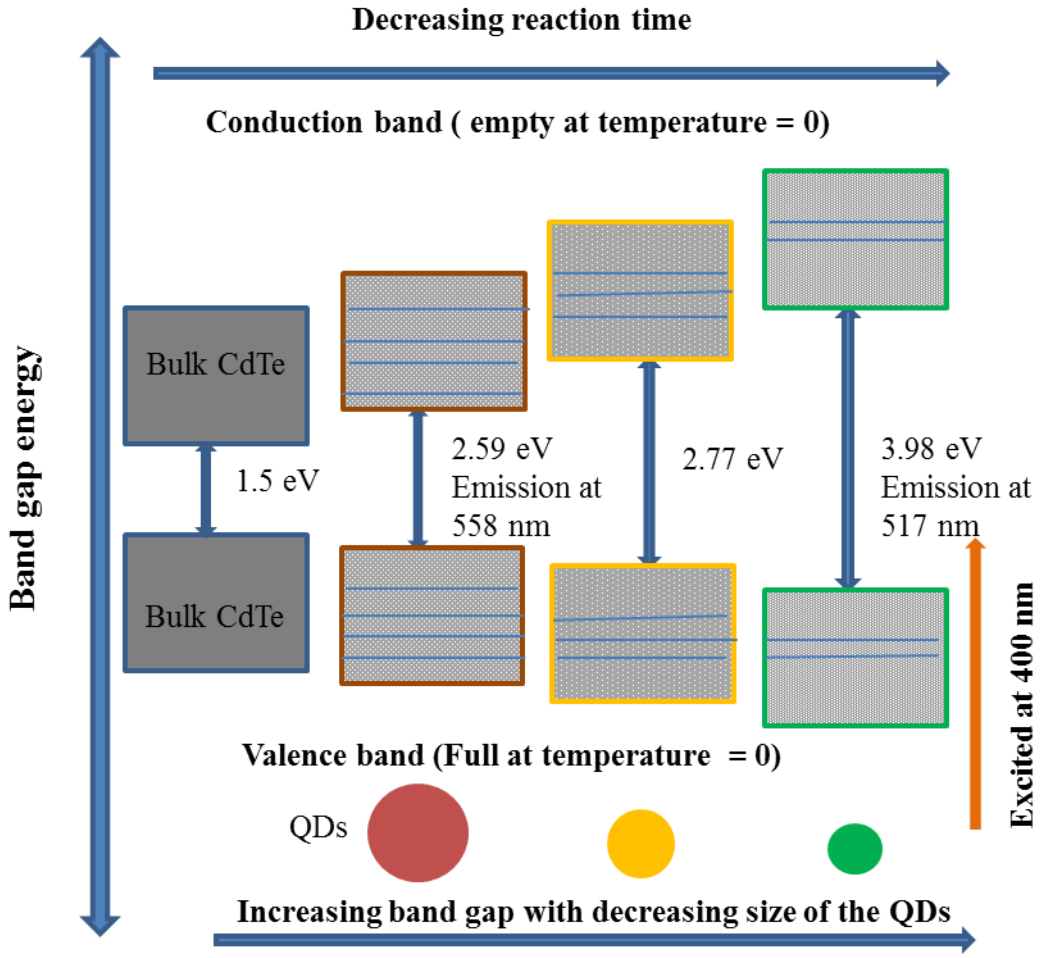

Figure 5.4(e): Changes in Peak width (nm) of CdTe nanoparticles with respect to synthesis time.

5.3.3 Ultra-violet visible analysis

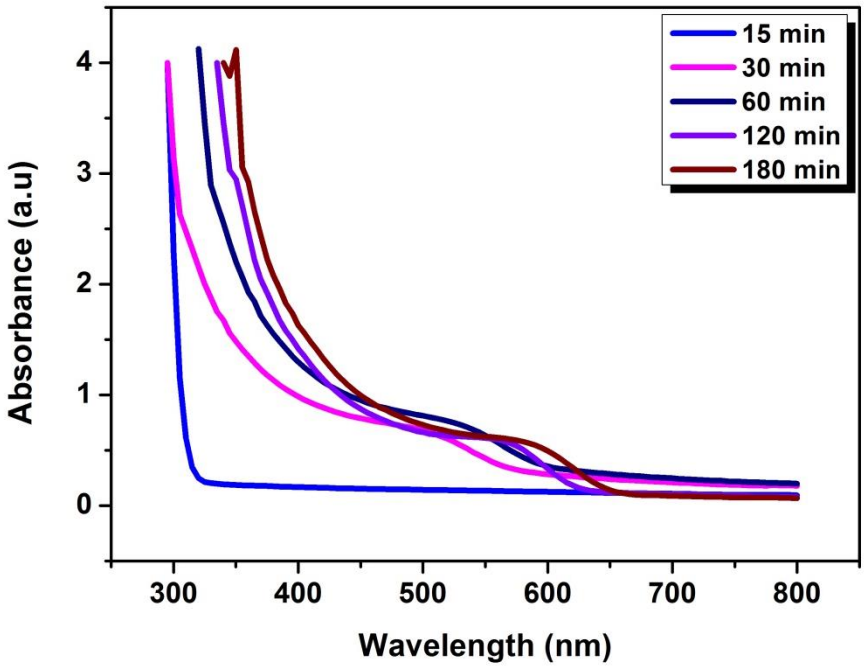

Figure 5.5(a): absorption spectra of CdTe QDs prepared at various reaction times

Typical absorption spectra of CdTe QDs obtained with different reaction times were given in Fig. 5.5(a). Quantum confinement effects would change the band gaps of QDs with the variation of particle sizes and further influence the absorption wavelength of the samples [23, 24]. From the graph (Fig. 5.5(a)), it is observed that the absorption edges shift to longer wavelength and also the slope decreases with prolonged growth time. The observed redshifts of the absorption edges indicated the growth of CdTe QDs during the synthesis. Stokes shift of the CdTe QDs is defined as the energy difference between the first absorption peak and the PL emission peak [25]. The first absorption peak generally follows the crystal size distribution while the position of the luminescence line for non-resonant excitation is determined by the largest crystals within this distribution. This causes a Stokes shift because the energy of the band-edge transitions in larger crystals is less than in smaller ones [26]. The Stokes shift for the as-prepared CdTe QDs became narrower with the growth of the QDs. This trend is similar to that reported by Kuno et.al. [27].The observed Stokes shift decreased from 53-24 nm for 30-180 min reaction time respectively. This can be explained by the fact that nucleation occurs fast during the early stages of reaction and the particles have high surface area, this would lead to a frequent electron-hole-exchange interaction making the excited-state electron to lose its energy easily and resulting in a broader stokes shift [28].

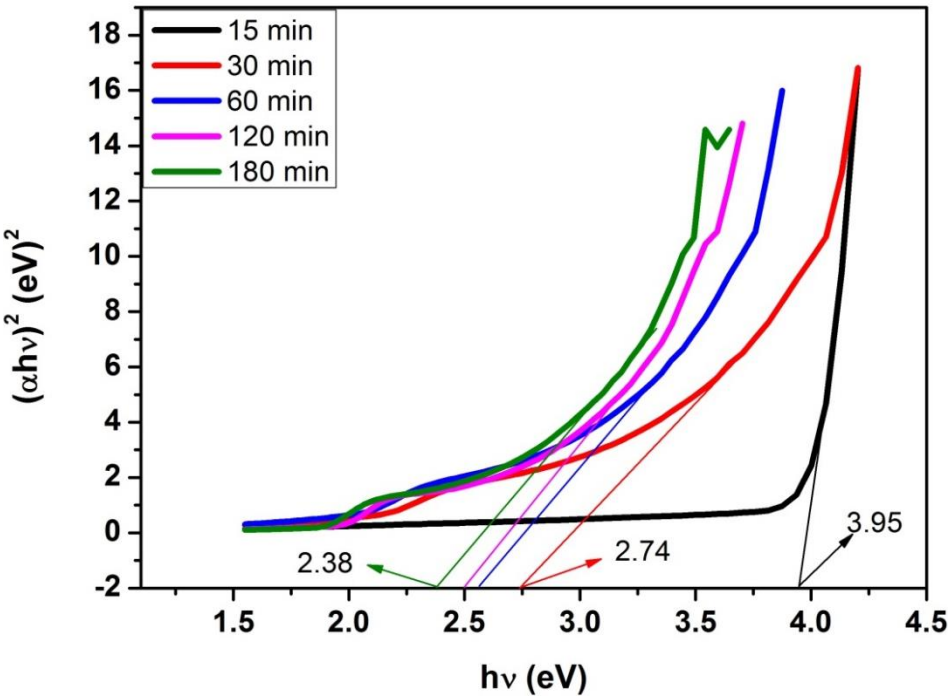

Figure 5.5(b): Tauc plot $(\alpha h\nu)^2$ v/s hν to determine the band gap energy of CdTe QDs prepared at various reaction times.

The value of the optical band gap was calculated using the fundamental absorption which corresponds to electron excitation from the valence band to the conduction band. The absorption coefficient (α) and incident photon energy (hν) are related by the Eq. (5). The variation in optical density with wavelength was analysed to find out the optical energy band gap using the Tauc relation [29];

$$\alpha = (hv - Eg)^n A/\, hv \qquad (8)$$

where A is a constant (free of photon energy) directly related to the optical absorbance, Eg is the band gap of the material and exponent n is the parameter which characterizes the transition process involved. The parameter n has the value of 1/2 for direct allowed transition and 2 for indirectly allowed transition. In order to determine the band gap energies of the as-prepared CdTe QDs, the linear portion of the graph was extrapolated to meet the energy axis from the Tauc's plot between $(\alpha h\nu)^2$ versus energy (hν) (Fig. 5.5(b)). The band gap values had an inverse relation with the reaction time and were in the range between 3.98 and 2.59 eV for reaction time 15-180 min. The observed blue shift in the band gap of CdTe QDs with increase in reaction time can be correlated to the well-known Burtein-Moss effect [30]. Also, the variation in the bandgap of CdTe QDs is mainly due to change in localized density of states and structural modification which arises due to the formation of more interstitial Cd+ ions in the CdTe lattice [31].

5.3.4 Growth mechanism of the CdTe QDs

Formation of QDs can be divided into three stages: nucleation, growth, and ripening [32]. At shorter reaction time, the concentration of the monomer precursors is still high and this promotes the formation of many nuclei of almost the same sizes. This stage is followed by the QDs' growth by monomer consumption and finally, as the monomer is depleted from the precursor solutions the particles will continue to increase in size by ripening process where the larger particles grow at the expense of the smaller ones. These three stages are governed by certain growth mechanisms that occur during the formation process. These mechanisms include diffusion and aggregation [33]. Each of the growth mechanisms can occur independently or both can occur simultaneously during the formation of the QDs. During the growth of CdTe QDs both diffusion and aggregation might have occurred simultaneously. At early stage (nucleation) (Fig. 5.6 (A)) where the concentration of monomers is high, diffusion plays an important role in the formation of the QDs to a certain critical size when it will start to grow by aggregation (Fig. 5.6 (B and C) to form larger particles sizes Fig. 5.6(D).

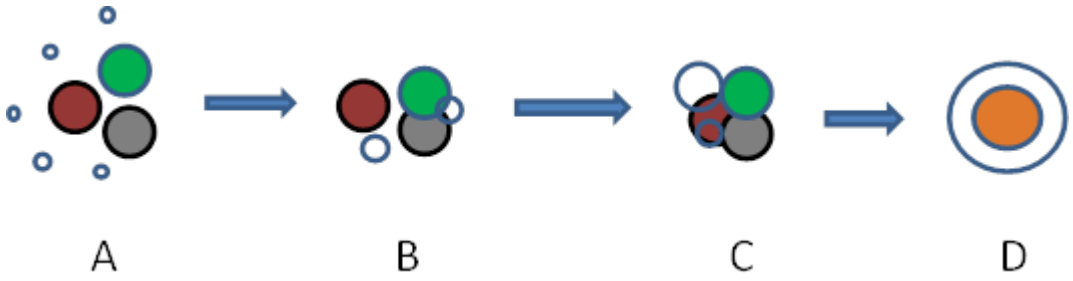

Figure 5.6: Schematic diagrams for the growth mechanism of the as-prepared CdTe QDs.

Aggregation is initiated by the general decrease of the stabilizer concentration, which results in the shift of the dynamic equilibrium between nanoparticles bonded and free stabilizer toward its dissolved state [33]. At longer reaction time the stabilizer molecules are depleted or may have undergone decomposition hence paving way for aggregation to occur as observed in the SEM images. The PL FWHM and UV-Vis absorption bands were observed to broaden with increase in reaction time which indicates to Ostwald ripening process. The PL peaks and UV-Vis absorption bands were also observed to shift to longer wavelength which is another indication of aggregation of the as-prepared CdTe QDs. The Ostwald ripening process occurred at longer duration of synthesis because the monomer concentration had been decreased as predicted by Gibbs-Thomson relation [34].

Conclusion

In summary, a facile synthetic route for the preparation of highly luminescent water-soluble CdTe QDs was done successfully using L-cysteine as capping agent and sodium borohydride as reducing agent. Room temperature PL indicated red shift of the emission wavelength with reaction time and narrow line width at half maximum. The XRD and EDS analyses clearly indicate that highly pure CdTe QDs was formed in the above method. EDS' analysis confirmed that the prepared material had a high purity and the presence of elements like O and S in trace level. Crystallite sizes estimated from XRD increased with reaction times which were in accord with the HRTEM measurement. Clear lattice fringes from HRTEM confirmed good crystallinity of the as prepared samples. SEM images of CdTe QDs displayed spherical morphology of the QDs as observed in the HRTEM micrographs. The band gap of CdTe QDs was decreased by an increase in reaction time and the absorption maximum was also shifted to higher wavelengths. The as obtained CdTe QDs were highly luminescent, which make them useful for applications in biological field.

References

[1] W.R. Algar, K. Susumu, J.B. Delehanty, I.L. Medintz, "Semiconductor quantum dots in bioanalysis: crossing the valley of death", Anal. Chem. 2011, 83, 8826.

[2] M. Gao, C. Lesser, S. Kirstein, H. Mçhwald, A.L. Rogach, H.Weller, "Electroluminescence of different colors from polycation/CdTe nanocrystal self-assembled films", J. Appl. Phys. 2000, 87, 2297.

[3] N.N. Mamedova, N. A. Kotov, A.L. Rogach, J. Studer, "Albumin− CdTe nanoparticle bioconjugates: preparation, structure, and interunit energy transfer with antenna effect", Nano Lett. 2001, 1, 281.

[4] J.M. Perez-Donoso, J.P. Monras, D. Bravo, A. Aguirre, A.F. Quest, I.O. Osorio-Roman, R.F. Aroca, T.G. Chasteen, C.C. Vasquez, "Biomimetic, mild chemical synthesis of CdTe-GSH quantum dots with improved biocompatibility", PloS one, 2012, 7, 30741.

[5] C.B. Murray, D. J. Norris, M. G. Bawendi, "Synthesis and characterization of nearly monodisperse CdE (E= sulfur, selenium, tellurium) semiconductor nanocrystallites", J. Am. Chem. Soc. 1993, 115, 8706.

[6] Z. A. Peng, X. Peng, "Formation of high-quality CdTe, CdSe, and CdS nanocrystals using CdO as precursor", J. Am. Chem. Soc. 2001, 123, 183.

[7] D.V. Talapin, S. Haubold, A. L. Rogach, A. Kornowski, M. Haase, H. Weller, "A novel organometallic synthesis of highly luminescent CdTe nanocrystals", J. Phys. Chem. B, 2001, 105, 2260.

[8] W.W. Yu, Y.A. Wang, X. Peng, "Formation and stability of size-, shape-, and structure-controlled CdTe nanocrystals: ligand effects on monomers and nanocrystals", Chem. Mater. 2003, 15, 4300.

[9] N. Gaponik, D.V. Talapin, A.L. Rogach, K. Hoppe, E.V. Shevchenko, A. Kornowski, A. EychmJller, H. Weller, "Thiol-capping of CdTe nanocrystals: an alternative to organometallic synthetic routes", J. Phys. Chem. B, 2002, 106, 7177.

[10] A.L. Rogach, L. Katsikas, A. Kornowski, D. Su, A. EychmJller, H. Weller, Ber. Bunsenges. "Synthesis and characterization of thiol-stabilized CdTe nanocrystals", Phys. Chem., 1996, 100, 1772.

[11] H. Zhang, L. Wang, H. Xiong, L. Hu, B. Yang, W. Li, "Hydrothermal Synthesis for High-Quality CdTe Nanocrystals", Adv. Mater., 2003, 15, 1712.

[12] A.M. Smith, G. Ruan, M.N. Rhyner, S. Nie, "Engineering luminescent quantum dots for in vivo molecular and cellular imaging", Ann. Biomed. Eng 2006, 34, 3.

[13] J. Drbohlavova, V. Adam, R. Kizek, J. Hubalek, "Quantum dots characterization, preparation and usage in biological systems", Int. J. of mol sc, 2009, 10, 656.

[14] R.A Hardman, toxicologic review of quantum dots: Health Perspect. 2006, 114, 165.

[15] J.T. Hu, L.S. Li, W.D. Yang, L. Manna, L.W. Wang, A.P. Alivisatos, "Linearly polarized emission from colloidal semiconductor quantum rods", Science 2001, 292, 2060.

[16] P. Yang, M. Ando, T. Taguchi, N. Murase, "Highly luminescent CdSe/CdxZn1–xS quantum dots with narrow spectrum and widely tunable wavelength", J .Phys. Chem. C, 2011, 115, 14455.

[17] S. Kiprotich, B.F. Dejene, J. Ungula, M.O. Onani, "The influence of reaction times on structural, optical and luminescence properties of cadmium telluride nanoparticles prepared by wet-chemical process", Phys.B, 2016, 480, 125.

[18] M.Y. El Azhari, M. Azizan, A. Bennouna, A. Outzourhit, E. L. Ameziane, M. Brunel., "Preparation and characterization of CdTeO 3 thin films", Thin Solid Films 2000, 366, 82.

[19] R. Ramírez-Bon, F.J. Espinoza-Beltrán, H. Arizpe-Chávez, O. Zelaya-Angel, F. Sánchez-Sinencio, "Structural and optical studies in a-CdTe: O annealed films", J. appl. Phy. 1996, 79, 7682.

[20] B.D. Cullity, "Elements of X-ray Diffraction", A.W.P.C. Inc., Massachusetts, 1967.

[21] I.M. Lifshitz, V.V. Slyozov, "The kinetics of precipitation from supersaturated solid solutions", J. Phys. Chem. Solids, 1961, 19, 35.

[22] D. Mutavdzic, J.M. Xu, G. Thakur, R. Triulzi, S. Kasas, M. Jeremi, R. Leblanc, K. Radoti "Determination of the size of quantum dots by fluorescence spectroscopy.", Analyst, 2011, 136, 2391.

[23] W.W. Yu, L. Qu, W. Guo, X. Peng. "Experimental determination of the extinction coefficient of CdTe, CdSe, and CdS nanocrystals", J. Chemistry of Materials, 2003, 15, 2854.

[24] A.P. Alivisatos, "Perspectives on the physical chemistry of semiconductor nanocrystals", J. Science, 1996, 271, 933.

[25] X. Chen, A.C.S. Samia, Y. Lou, C.J. Burda, "Shape control of CdSe nanocrystals", J. Am. Chem. Soc., 2005, 12, 4372.

[26] A.L. Efros, M. Rosen, M. Kuno, M. Nirmal, D.J. Norris, M. Bawendi. "Band-edge exciton in quantum dots of semiconductors with a degenerate valence band: Dark and bright exciton states", Physical Review B, 1996, 54, 4843.

[27] M. Kuno, J.K. Lee, B.O. Dabbousi, F.V. Mikulec, M.G. Bawendi, "The band edge luminescence of surface modified CdSe nanocrystallites: Probing the luminescing state", J. Chem. Phys., 1997, 106, 9869.

[28] J. Perez-Conde, A.K. Bhattacharjee, M. Chamarro, P. Lavallard, V.D. Petrikov, A. A. Lipovskii, "Photoluminescence Stokes shift and exciton fine structure in CdTe nanocrystals", Physical Review B, 2001, 11, 113303.

[29] J. Tauc, Plenum Press, "Optical properties of amorphous semiconductors", New York, 1974, 159

[30] R. Kumaravel, S. Bhuvaneswari, K. Ramamurthi, V. Krishnakumar, "Structural, optical and electrical properties of molybdenum-doped cadmium oxide thin films prepared by spray pyrolysis method", Appl. Phys. A, 2012, 109, 579.

[31] K. Usharani, N. Raja, N. Manjula, V.S. Nagarethinam, A.R. Balu, "Characteristic Analysis on the Suitability of CdO Thin Films Towards Optical Device Applications-Substrate Temperature Effect", Int. J. Thin. Film Sci. Tech., 2015, 4, 89.

[32] Z.Y. Tang, N.A. Kotov, M. Giersig, "Spontaneous organization of single CdTe nanoparticles into luminescent nanowires", Science 2002, 297, 237.

[33] P. Dagtepe, V. Chikan, J. Jasinski, V.J. Leppert. "Quantized growth of CdTe quantum dots; observation of magic-sized CdTe quantum dots", J. of Phy. Chem. C 2007, 111, 14977.

[34] B.D. Dickerson, "Organometallic synthesis kinetics of CdSe quantum dots" PhD diss., Virginia Tech, 2005.

Chapter 6

Effect of growth temperature on the structural, optical and luminescence properties of cadmium telluride nanoparticles

6.1 Introduction

In the past few decades, exploring novel materials based on semiconductor nanoparticles (NPs) has become one of the most attractive areas of research [1-4]. Studies have been dedicated to the fabrication and characterization of chalcogenide compounds. Cadmium telluride (CdTe) being among these group II-VI compounds, is known to be a good and promising material for the fabrication of various fascinating applications such as optoelectronic devices, biomedical imaging device, ,nanosensors, photoelectrochemical, electron-beam pumped lasers, solar cells , electroluminescent devices, light emitting diodes etc. [5-10].

As biological labels, particularly, much attention have been devoted to these semiconductor NPs due to their superior properties like small tunable size, emission tenability, superior photostability, and extended photoluminescence (PL) decay times when compared with organic dyes [11-13]. CdTe is reported to possess a radioactive recombination of high efficiency, high photosensitivity, high absorption coefficient and direct band gap which correspond to the wide wavelength spectrum from ultraviolet to infrared regions and displaying quantum size effects [14, 15]. The NPs' size and size distribution strongly affect the emission color and its purity [16-19].With better familiarity regarding the growth of NPs, the color of emission and color purity can be controlled to a certain extent so far. When the NPs surface structures are controlled, good PL properties can be obtained which can be used freely for the desired application.

The two main existing general approaches for the preparation of NPs are organometallic synthesis using high-temperature precursors [20] and the synthesis in aqueous phase using thiols [21] as capping agents. The most established organometallic synthesis approaches to make crystalline colloidal II-VI NPs [22] is the decomposition of the precursors in high boiling point coordinating solvents such as trioctylphosphine and trioctylphosphine oxide (TOP-TOPO). The CdTe NPs are the constituents which provide the relatively high PL quantum yields with a reported room temperature value of 65% prepared from organometallic route. However, hindrances of these NPs in many potential applications are the PL instability in air [23]. Aqueous technique for the preparation of CdTe can be a good alternative to trioctylphosphine oxide (TOPO)-capped particles because the synthetic routes are less expensive, arguably easier to perform and more stable NPs are produced which display higher quantum yields than the organometallic counterparts.

We herein report on a method for preparing CdTe nanocrystals of different sizes which is cost effective because no inert atmosphere is required (which is expensive to set up) and produces NPs with enhanced stability. The effects of different growth temperatures on the material properties of CdTe NPs are studied in order to investigate the suitability of the NPs in various applications.

6.2. Experimental

6.2.1 Synthesis

The materials used were cadmium acetate dihydrate (Cd $(CH_3COO)_2$. $2H_2O$) (> 99%), to provide cadmium ions, potassium tellurite (K_2TeO_3) (> 90%) which was the source of tellurium ions, L-cysteine (> 98%) as a capping agent and sodium borohydride which was used as reducing agent. All the chemicals used were of analytical grade purchased from Aldrich. Synthesis method was adapted from the literature [24]. Typically, the CdTe QDs was prepared by mixing the proper quantities of cadmium acetate and L-cysteine in a glass beaker. The pH of the solution was then adjusted to 11 by an addition of sodium hydroxide. After that, 50 ml of dissolved 0.2 mmol K_2TeO_3 was added to get an ultimate volume of 100 ml. After stirring for a while, an appropriate amount of sodium borohydride was added to the mixture. The mixture was transferred to a three-necked flask and refluxed at different selected growth temperatures of 50, 100, 150 and 200 ^oC in open air. Cd: L-Cyst: Te: $NaBH_4$ molar ratios were kept at 1:1:0.5:10.

6.2.2 Characterization

The crystallographic structure of the CdTe NPs was analyzed using a powder X-ray diffractometer with a Cu-Kα radiation (λα = 1.5406 Å) source. The qualitative elemental compositions of the samples were determined by using an energy dispersive X-ray analysis (EDX) attached to the scanning electron microscope (SEM) equipment. The UV-Vis analysis were measured at room temperature by using a Shimadzu UV/Vis evolution 100 Spectrophotometer within the wavelength range of 200 - 1100 nm while photoluminescence measurement was done using Cary Eclipse spectrophotometer; model LS-55 with a built-in 150 W xenon flash lamp.

6.3 Results and Discussion

6.3.1 Structural and Compositional analysis

6.3.1.1 SEM micrographs

The scanning electron microscopy (SEM) shows the surface topography and composition of a sample. Fig. 6.1 shows the SEM images of CdTe nanocrystals formed at different growth temperatures. At lower temperature, monodispersed CdTe nanocrystals with nearly spherical shape were formed in groups as observed in Fig. 6.1(a). When the temperature was increased to 100 °C, the spherical nanocrystals became uniformly distributed over the entire surface with some rod- like features in them. On further increase in growth temperature to 200 °C agglomerated spherical shape nanocrystals were observed. The observed results show the particle agglomerates, a consequence of Oswald ripening process which is brought by increase in the supply of thermal energy. At 100 °C and 200 °C of growth temperatures, larger particles developed as seen in Fig. 6.1(b) and 1(c). Increasing the growth temperature can result in an increase in the critical particle radius which results in the disappearance of the smaller particles to enhance the growth of the larger ones [25]. When the reaction temperature is increased from 50 to 200 °C, the morphology of the nanocrystals changes which confirms that the growth rate of the NPs is sensitive to temperature. Therefore, varying the growth temperature is one of the key ways to control the size and shape of the NPs. However, a growth temperature of 100 °C was found to produce well dispersed spherical NPs.

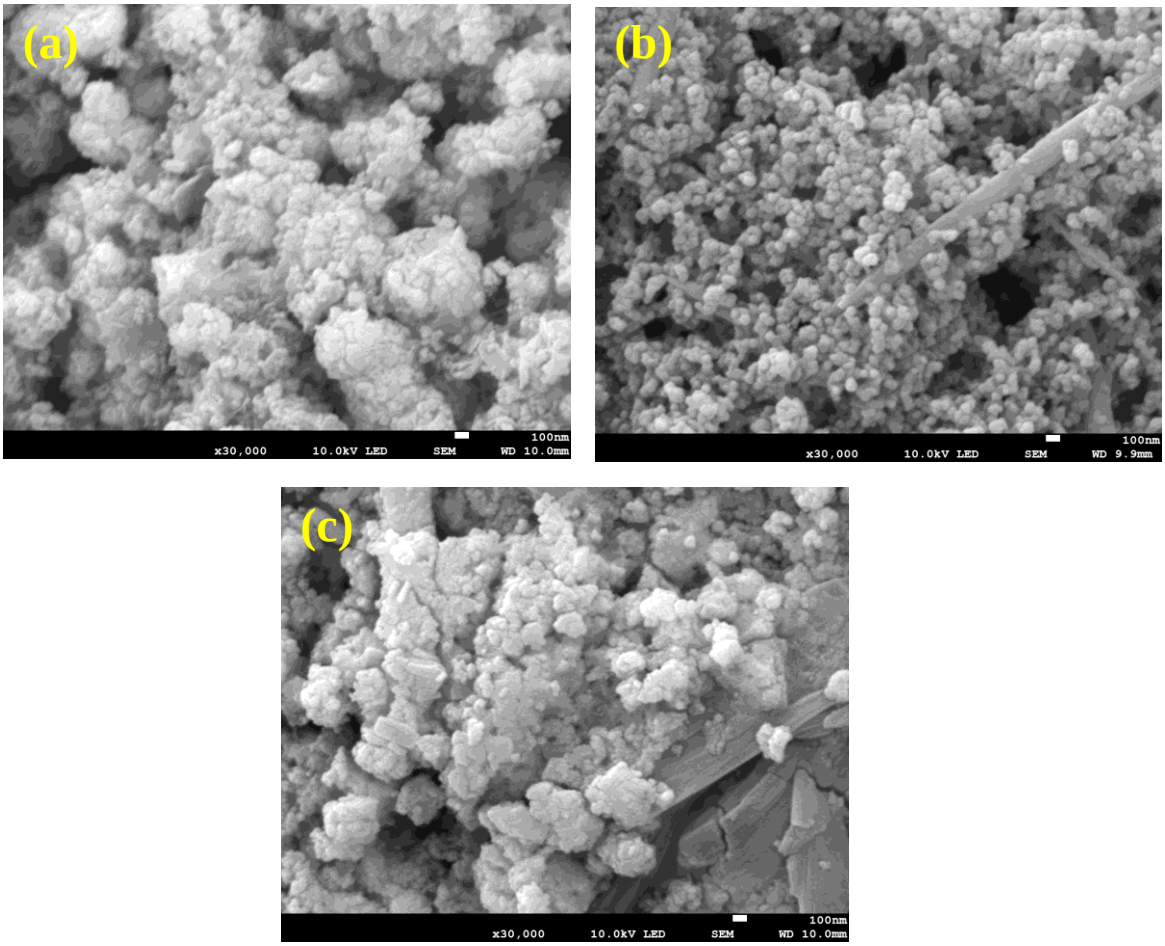

Figure 6.1: SEM micrographs of CdTe samples prepared at different growth temperatures ((a) 50 °C, (b) 100 °C and (c) 200 °C).

6.3.1.2 XRD Analysis

The X-ray diffraction is a unique technique for determining the crystallinity of a material. The XRD patterns of the as-prepared CdTe samples are displayed in Fig. 6.2(a). Three different peaks are observed which shows that the CdTe samples have zinc blende structures which match well with the standard card no. 75-2086 of bulk CdTe. The XRD peaks correspond to Bragg diffraction at (111), (220) and (311) planes of cubic CdTe. The broadened peaks indicate nanocrystalline behavior and infinitely small size of the CdTe NPs. The values of the full-width half maximum (FWHM) of the XRD peaks were found to increase while the sizes of the nanoparticles decrease and vice versa up to a certain growth temperature (Fig. 6.2(b)). The size of the nanoparticles were calculated using the FWHM values of the peak (111) using Debye-Scherer formula [26].The CdTe NPs sizes of all the as-prepared samples were in the range of 2 - 4 nm.

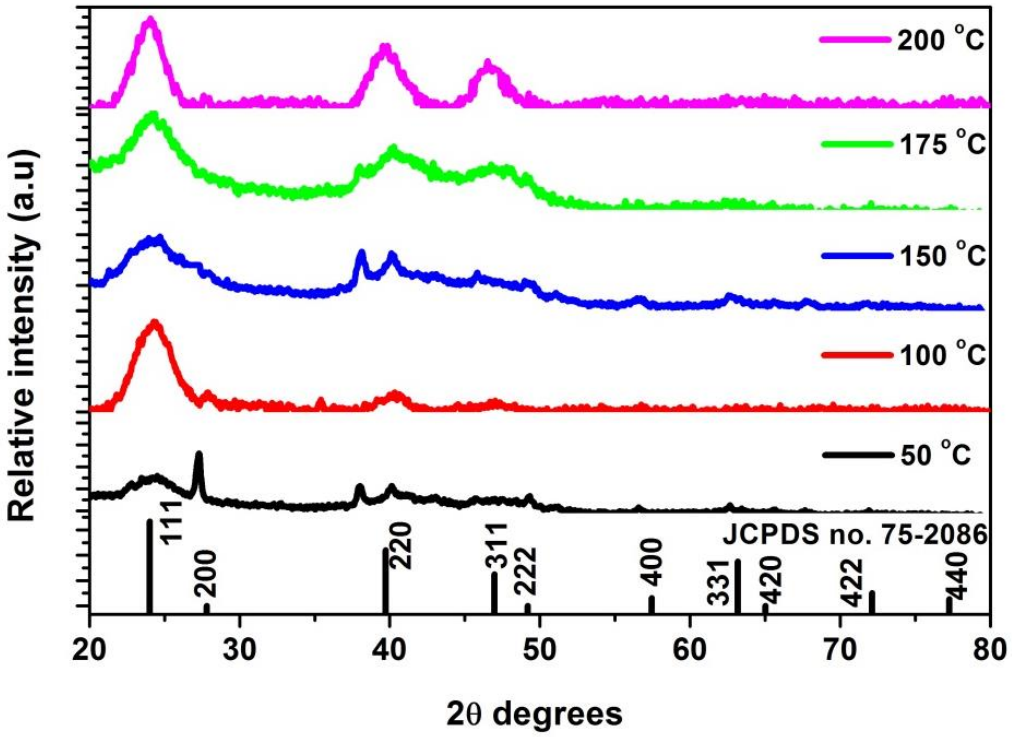

Figure 6.2(a): Representative XRD pattern for CdTe QDs prepared at 200°C with an inset of XRD patterns grown at different growth temperatures.

The calculated average crystallite size values were 2.86, 2.85, 2.74, 2.81 and 3.62 nm for as-prepared CdTe NPs grown at 50, 100, 150, 175 and 200 °C respectively. Thus the particle size was found to depend so much on the reaction temperature. Increase in the crystallite size indicates the diffusion of smaller particles to form larger ones on increasing the growth temperature. Moreover, increase in crystallite size of the CdTe NPs on increasing the growth temperature also indicates to the fact for a stable cubic crystal structure to be formed, a minimum crystallite size is required. From the calculated values (6.35 - 6.43 Å), lattice constant differs from the standard bulk value (6.41 Å) which is an indication that the nanocrystallites may be under some strain. The calculation of strain gives additional information about the structural properties of the CdTe NPs, which can be obtained from the following equation [27];

$$\varepsilon = \frac{\beta \cos\theta}{4} \qquad (9)$$

Where θ is the Bragg's diffraction angle, ε is the strain of the as-prepared CdTe NPs and β is the broadening of the diffraction line (FWHM). It is observed that the strain in the as-prepared CdTe NPs increases from 5.972×10^{-1} to 7.163×10^{-1}, with an increase in the

growth temperature up to 150 °C which then decreases to 5.907×10^{-1}. The increase in strain value is readily ascribed to the increase in defect density or lattice distortion in the CdTe NPs [27].

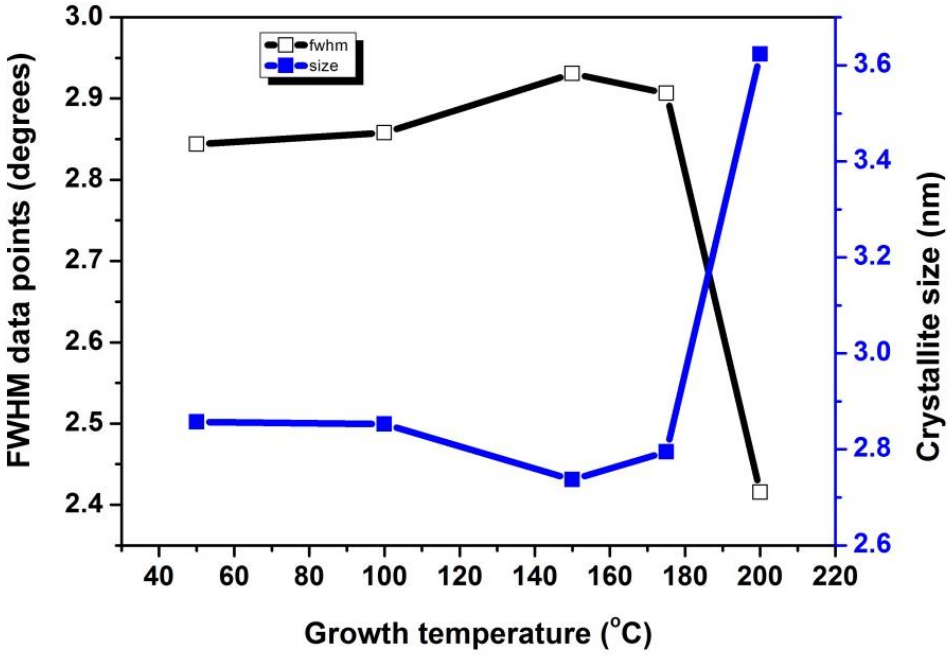

Figure 6.2(b): changes in crystallite sizes and FWHM values of the as-prepared CdTe NPs obtained from XRD pattern peak (111) for different growth temperatures.

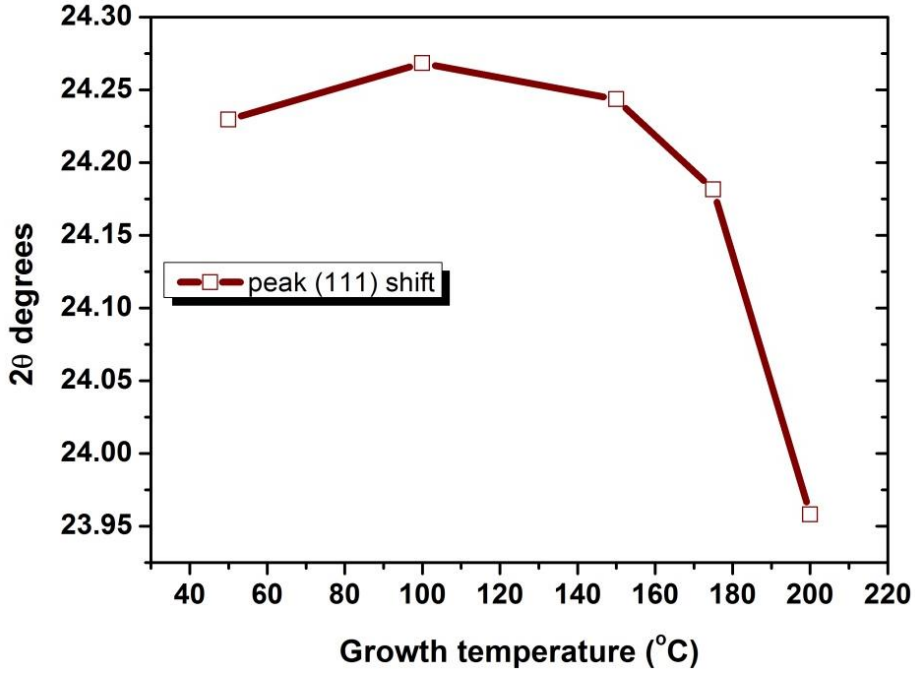

Figure 6.2(c): changes in the peak position of the CdTe NPs XRD peak (111) with growth temperature.

Fig. 6.2(b) displays changes in crystallite size and FWHM values of CdTe NPs with growth temperature. It shows that highest peak intensity was obtained at a growth temperature of 100 °C indicating good crystallinity of the sample. Fig. 6.2(c) depicts changes in XRD peak position for the plane (111) at different growth temperatures. Diffraction peaks generally shift to lower diffraction angle as growth temperature is increased from 50 to 200 °C. The shift in diffraction peaks was accompanied by a variation in the lattice parameters. The shift in diffraction peaks to lower angle is due to increase in the lattice parameters attributed to lattice expansion.

6.3.2 Influence on photoluminescence properties

The optical analysis was studied using spectrophotometer in order to follow the evolution of nanoparticle growth within a solution. The PL spectra of CdTe NPs grown at various growth temperatures displayed in Fig. 6.3(a) show similar PL features. At the nucleation stage after refluxing at 50 °C, there is a weak luminescence observed from the solution. As the solution heats to 200 °C in about 20 min, the color of the solution becomes green and finally red. The emission bands could be as a result of the electron-hole recombination.

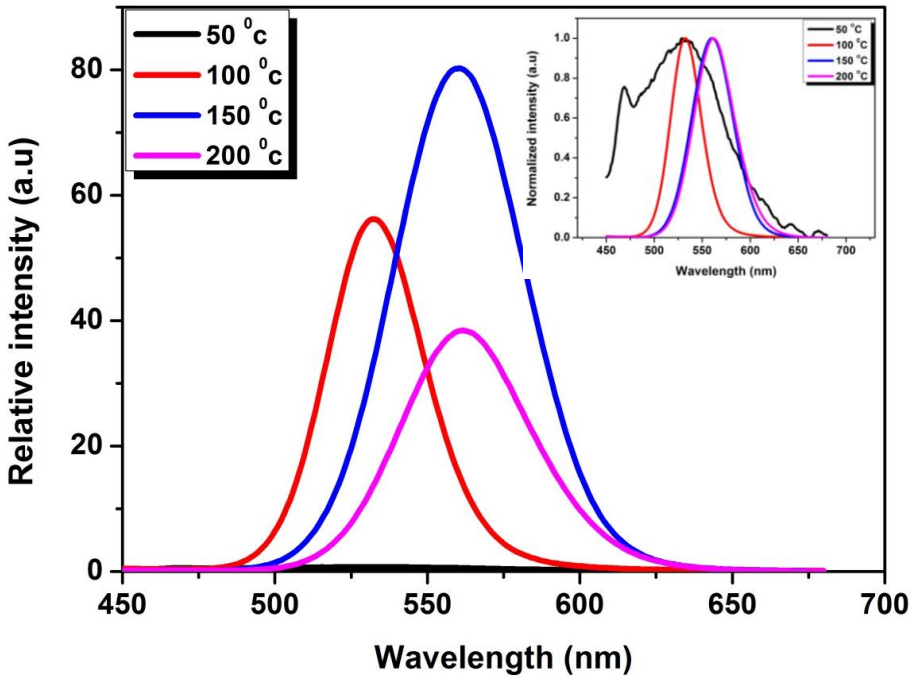

Figure 6.3(a): PL emission spectra of CdTe QDs prepared at different growth temperatures.

Here, it is observed that increase in the growth temperature causes a red shift in the PL emission wavelengths accompanied by variation in the relative intensity. The aliquot with an

emission maximum at 561 nm approached the highest luminescent intensity at 150 °C. The PL intensity increases greatly when the growth temperature is increased to 150 °C but decreased at 200 °C of growth temperature as shown in Fig. 6.3(b). This shows that increasing the growth temperature will enhances the crystal quality of CdTe NPs to a certain extent. Although not quite clear, the temperature dependent PL, is said to be related to the growth rate mechanism which causes changes in the NPs size [28].

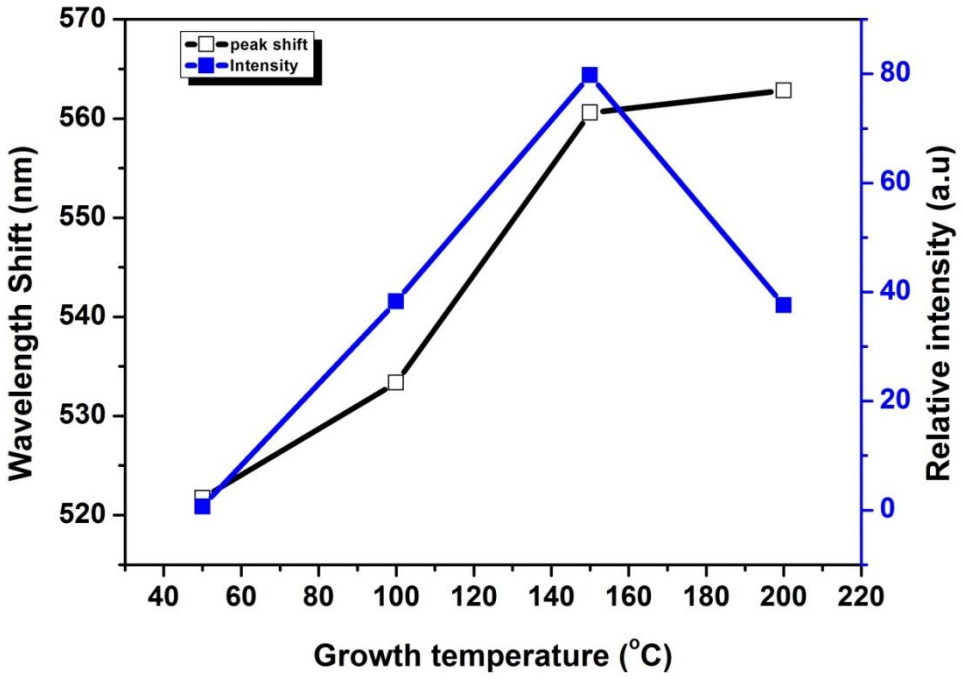

Figure 6.3(b): changes in peak position and intensity with respect to growth temperature.

The bathochromic shift observed in Fig. 6.3 (b) is a characteristic nature for nanostructured semiconductors. The results signify that upon an increase in the reaction temperature, the growth rate of the CdTe NPs is increased. The possible explanation for this behavior could be that high reaction temperatures cause the growth of larger and irregular NPs with abridged crystallinity due to random, rapid nucleation and with the fast growth affecting the ligand structure of the nanocrystal surface [29]. It should be noted that the red shift in emission peaks supports the reported XRD results of an increase in the diameter of the NPs at higher growth temperatures. It was also observed that the red shift in the PL emission wavelength was due to change in the color of emission with variation in the growth temperature. This phenomenon was further confirmed by the CIE color co-ordinates image shown in Fig 6.3(d).

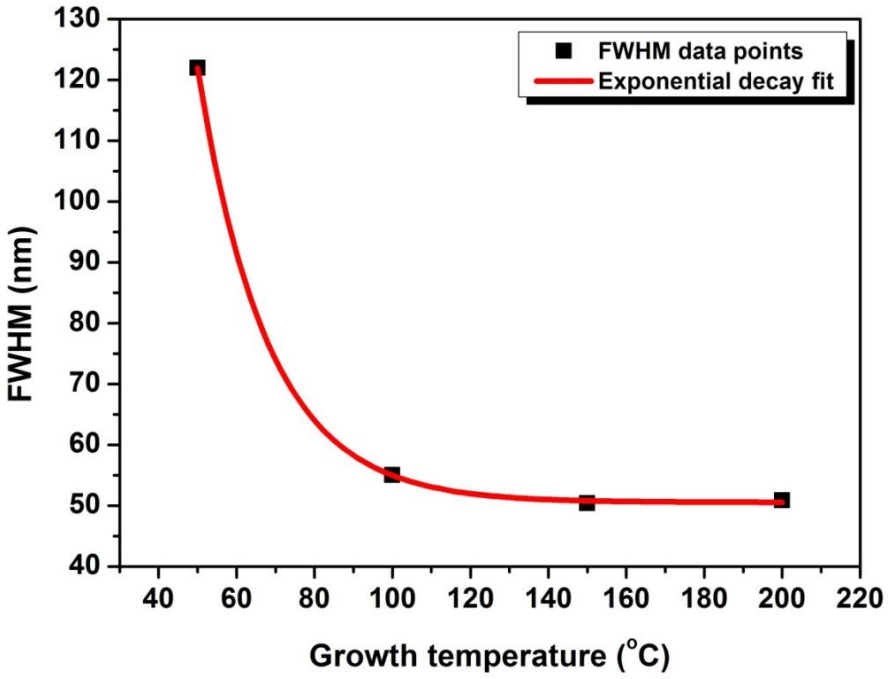

Figure 6.3(c): Exponential curve fit for FWHM data points of as-prepared CdTe QDs at different growth temperatures.

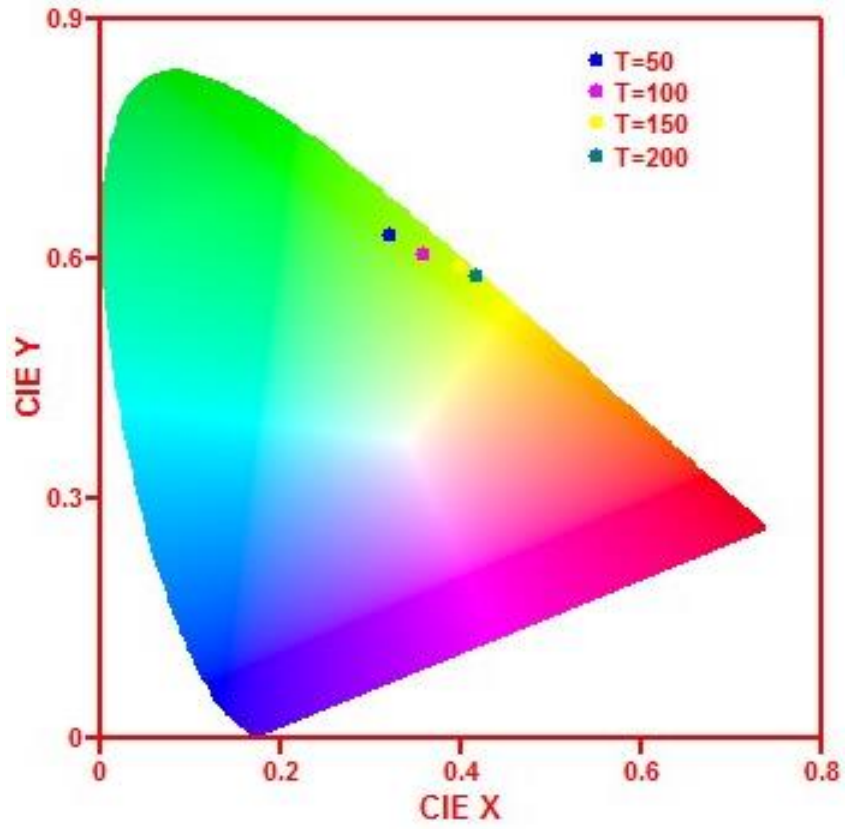

Figure 6.3(d): CIE image obtained from PL emission data of as-prepared CdTe NPs taken at different growth temperatures.

6.3.3 Influence on ultra-violet visible properties

Typical absorption spectra of CdTe NPs obtained with different reaction times were given in Fig. 6.4(a). Quantum confinement effects would change the band gaps of NPs with the variation of particle sizes and hence influence the absorption wavelength of the as-prepared samples [30]. From the graph, it is observed that the absorption edges shift to longer wavelength with prolonged growth time. The observed redshifts of the absorption edges indicated the growth of CdTe NPs during the synthesis hence confirming the PL observation. Absorption band maxima were also observed to shift to longer wavelength for higher growth temperatures. The approximated values of the absorption band maxima were 517, 526, 530 and 332 nm for 50, 100, 150 and 200 ^{o}C of growth temperature respectively. Stokes shift for both green and yellow of the CdTe nanoparticles is known to be larger for the particles made in open air due to strong phonon coupling [31]. The observed Stoke shift was caused by the band-edge transition due to crystal size distribution [32]. The Stoke shifts for the as-prepared CdTe NPs were 4.9, 7.51, 31.52 and 31.82 nm for 50, 100, 150 and 200 ^{o}C.

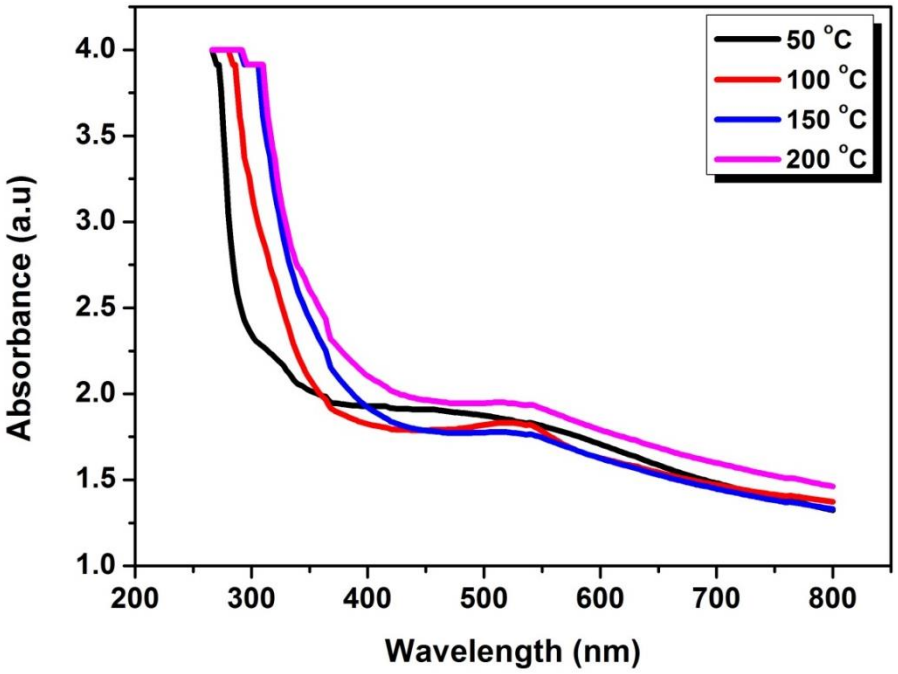

Figure 6.4(a): absorption spectra of CdTe NPs prepared at different growth temperatures.

The increase in the Stoke shift with an increase in growth temperature can be attributed to the idea that nucleation occurs fast at higher growth temperatures and the particles have a high surface area which would lead to a frequent electron-hole-exchange interaction making the

excited-state electron to lose its energy easily resulting in a broader stokes shift [33]. The NPs' sizes could be estimated from the UV–vis absorption spectra using the empirical Eq. (10) [34] where D is the NPs' diameter and λ is the first absorption maximum. The diameters of the CdTe NPs were 2.75, 2.91, 2.97 and 3.00 nm for 50, 100, 150 and 200 ^{o}C growth temperatures respectively which are in close agreement to those acquired from XRD studies.

$$D = (9.8127\times10^{-7})\lambda^3 - (1.7147\times10^{-3})\lambda^2 + (1.0064)\lambda - 194.84 \qquad (10)$$

The absorbance spectra were used to estimate the band gap energies of as-prepared CdTe NPs by using the following Tauc relation for near band-edge optical absorption of semiconductors [35]. The extrpolation of the linear portion of the curve to the X-axis (energy (hν) axis), the intercept gives the value of band gap energy of the as-prepared NPs (Fig. 6.4(b)). CdTe NPs band gap values were 2.67, 2.50, 2.31 and 2.08 eV for 50, 100, 150 and 200 ^{o}C of growth temperature respectively. The band gap values for as-prepared CdTe NPs indicate that as the growth temperature increases, the band gap energy of the NPs decreases. Thus increasing growth temperature increases the size of the NPs hence reducing the optical band gap of the as-prepared NPs.

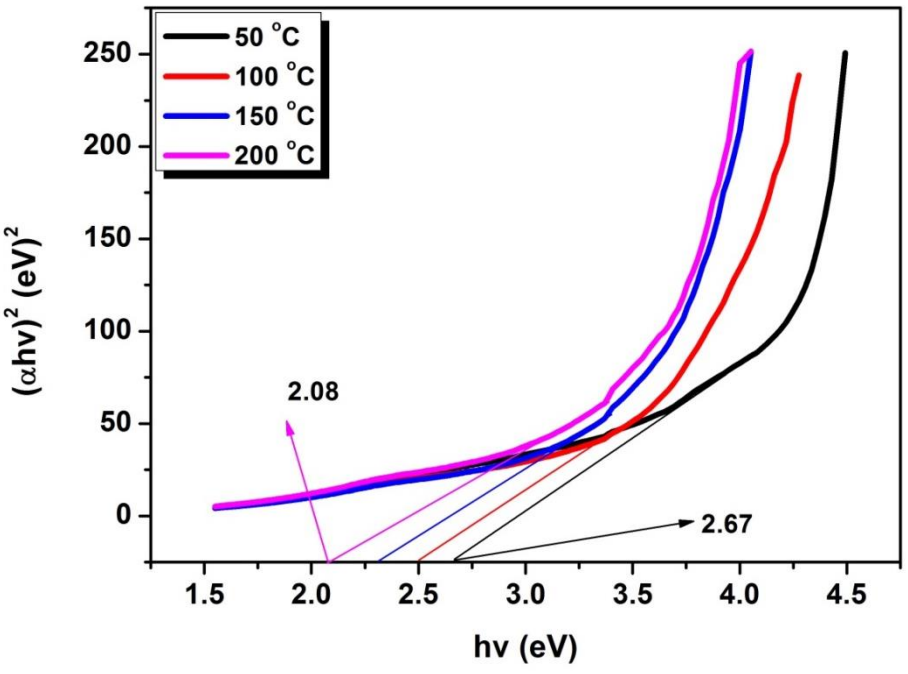

Figure 6.4(b): Tauc plot (Khν) ^{2} v/s hν to determine the band gap energy of CdTe QDs prepared at different growth temperatures.

The Tauc plot of (Ahν) ^{2} versus the photon energy (hυ) for as-prepared CdTe NPs is shown in Fig. 6.4(b). The band gap value of the as-prepared CdTe NPs is shown in Fig. 6.4(b). The observed values are slightly higher than the reported bulk value of 1.5 eV [36]. The shift to

higher optical band gap is reported to be attributed to the infinitely small particle size and the subsequent quantum confinement of electronic states in the NPs [2]. In the as-prepared CdTe NPs sample here in reported, the estimated particle size from XRD measurements was about 3 nm and this clarifies the observed large optical band gaps (Fig. 6.4(b)) in comparison to the bulk value.

Conclusion

The nanoparticles of CdTe were successfully grown by a simple wet chemical route at different growth temperatures. The XRD studies revealed the formation of a cubic phase of CdTe nanocrystalline NPs. The average crystallite sizes of CdTe NPs obtained using the Debye-Scherrer equation was found to be in the range 2 - 3 nm. The SEM analysis on the surface morphology displayed that the micrographs was composed of spherically-shaped NPs. The PL and UV-Vis analysis showed temperature-dependent properties of the as-prepared NPs. The size of the nanoparticles increased with an increase in the reaction temperature hence the growth temperature is yet another important parameter for the synthesis of CdTe NPs.

References

[1] H. Weller, "Colloidal semiconductor Q-particles: chemistry in the transition region between solid state and molecules", Angewandte Chem International Edition in English 32, 1, 1993, 41-53.

[2] A.P. Alivisatos, "Semiconductor Clusters, Nanocrystals, and Quantum Dots materials", Science 271, 5251, 1996, 933.

[3] J.H. Fendler, "Chemical self-assembly for electronic applications", Chem of Materials 13, 10, 2001, 3196-3210.

[4] V.I. Klimov, A.A. Mikhailovsky, S. Xu, A. Malko, J.A. Hollingsworth, C.A. Leatherdale, H.J. Eisler, M.G. Bawendi, "Optical gain and stimulated emission in nanocrystal quantum dots", Science 290, 5490, 2000, 314-317.

[5] N.P. Gaponik, D.V. Talapin, A. L. Rogach, "A light-emitting device based on a CdTe nanocrystal/polyaniline composite", Phy Chem 1, 8, 1999, 1787-1789.

[6] N.P. Gaponik, D.V. Talapin, A.L. Rogach, A. Eychmüller, "Electrochemical synthesis of CdTe nanocrystal/polypyrrole composites for optoelectronic applications", J. Materials Chemistry 10, 9, 2000, 2163-2166.

[7] S.V. Gaponenko, A.M. Kapitonov, V.N. Bogomolov, A.V. Prokofiev, A. Eychmüller, A. L. Rogach, " Electrons and photons in mesoscopic structures: Quantum dots in a photonic crystal", Jetp Letters 68, 2, 1998, 142-147.

[8] S.V. Gaponenko, V. N. Bogomolov, E. P. Petrov, A. M. Kapitonov, D. A. Yarotsky, I.I. Kalosha, A.A. Eychmueller, "Spontaneous emission of dye molecules, semiconductor nanocrystals, and rare-earth ions in opal-based photonic crystals", J. of lightwave technology 17, 11, 1999, 2128-2137.

[9] A. Rogach, A.S.F. Caruso, G. Sukhorukov, A. Kornowski, S. Kershaw, H. Möhwald, A. Eychmüller, H. Weller, "Nano and Microengineering: 3-D Colloidal Photonic Crystals Prepared from Sub-μm-sized Polystyrene Latex Spheres Pre-Coated with Luminescent Polyelectrolyte/Nanocrystal Shells.", Advanced Materials 12, 5, 2000, 333-337.

[10] A.L. Rogach, N.A. Kotov, D.S. Koktysh, J.W. Ostrander, G.A. Ragoisha, "Electrophoretic deposition of latex-based 3D colloidal photonic crystals: A technique for rapid production of high-quality opals", Chemistry of Materials 12, 9, 2000, 2721-2726.

[11] H. Mattoussi, J.M. Mauro, E.R. Goldman, G.P. Anderson, V.C. Sundar, F.V. Mikulec, M.G. Bawendi, "Self-assembly of CdSe− ZnS quantum dot bioconjugates using an engineered recombinant protein", J. American Chemical Society 122, 49, 2000, 12142-12150.

[12] X. Gao, Y. Cui, R.M. Levenson, L.W.K. Chung, S. Nie, “In vivo cancer targeting and imaging with semiconductor quantum dots”, Nature biotechnology 22, 8, 2004, 969-976.

[13] B.J. Battersby, D. Bryant, W. Meutermans, D. Matthews, M.L. Smythe, M. Trau, “Toward larger chemical libraries: encoding with fluorescent colloids in combinatorial chemistry”, J. of the American Chemical Society 122, 9, 2000, 2138-2139.

[14] C. Wadia, A.P. Alivisatos, D.M. Kammen, “Materials availability expands the opportunity for large-scale photovoltaics deployment”, Environmental science & technology 43, 6, 2009, 2072-2077.

[15] R.C. Kainthla, D.K. Pandya, K.L. Chopra, “Photo-electronic properties of solution-grown CdSe films”, Solid-State Electronics 25, 1, 1982, 73-76.

[16] D.V. Talapin, A.L. Rogach, E.V. Shevchenko, A. Kornowski, M. Haase, H. Weller, “Dynamic distribution of growth rates within the ensembles of colloidal II− VI and III−V semiconductor nanocrystals as a factor governing their photoluminescence efficiency”, J. of the American Chemical Society 124, 20, 2002, 5782-5790.

[17] X. Peng, J. Wickham, A.P. Alivisatos, “Kinetics of II-VI and III-V colloidal semiconductor nanocrystal growth:“focusing” of size distributions”, J. of the American Chemical Society 120, 21, 1998, 5343-5344.

[18] L. Qu, X. Peng, “Control of photoluminescence properties of CdSe nanocrystals in growth”, J. of the American Chemical Society 124, 9, 2002, 2049-2055.

[19] Z.A. Peng, X. Peng,” Mechanisms of the shape evolution of CdSe nanocrystals”, J. of the American Chemical Society 123, 7, 2001, 1389-1395.

[20] L. Qu, X. Peng,” Alternative routes toward high quality CdSe nanocrystals”, J. of the American Chemical Society 124, 9, 2002, 204-205.

[21] Z.A. Peng, X. Peng, “Nearly monodisperse and shape-controlled CdSe nanocrystals via alternative routes: nucleation and growth”, J. of the American Chemical Society 124, 13, 2002, 3343-3353.

[22] C.B. Murray, D.J. Norris, M.G. Bawendi, “Synthesis and characterization of nearly monodisperse CdE (E= sulfur, selenium, tellurium) semiconductor nanocrystallites”, J. of the American Chemical Society 115, 19, 1993, 8706-8715.

[23] D.V. Talapin, S. Haubold, A.L. Rogach, A. Kornowski, M. Haase, H. Weller. “A novel organometallic synthesis of highly luminescent CdTe nanocrystals”, J. of Phy Chem B 105, 12, 2001, 2260-2263.

[24] S. Kiprotich, F.B. Dejene, J. Ungula, M.O. Onani, “The influence of reaction times on structural, optical and luminescence properties of cadmium telluride nanoparticles prepared by wet-chemical process”, Physica B: Condensed Matter 480, 2016, 125-130.

[25] R.W. Buckley, Solid state chem research trends. Nova Publishers, 2007.

[26] A. Guinier, "X-ray Diffraction", Freeman, San Francisco 1963.

[27] L.L. Pan, G. Y. Li, S. S. Xiao, L. Zhao, J. S. Lian, "Bandgap variation in grain size controlled nanostructured CdO thin films deposited by pulsed-laser method", J. of Materials Science: Materials in Electronics 25, 2, 2014, 1003-1012.

[28] G. Karczewski, S. Maćkowski, M. Kutrowski, T. Wojtowicz, J. Kossut, "Photoluminescence study of CdTe/ZnTe self-assembled quantum dots", J. Applied phy lett 74, 20, 1999, 3011-3013.

[29] M. O'neil, J. Marohn, G. McLendon, "Dynamics of electron-hole pair recombination in semiconductor clusters", J. of Physical Chemistry 94, 10, 1990, 4356-4363.

[30] W. Guo, J.J. Li, Y.A. Wang, X. Peng, "Luminescent CdSe/CdS core/shell nanocrystals in dendron boxes: superior chemical, photochemical and thermal stability", J. of the American Chemical Society 125, 13, 2003, 3901-3909.

[31] A.P. Alivisatos, T.D. Harris, P. J. Carroll, M. L. Steigerwald, L. E. Brus, "Electron–vibration coupling in semiconductor clusters studied by resonance Raman spectroscopy", J. of Chem Phy 90, 7, 1989, 3463-3468.

[32] A.L. Efros, M. Rosen, Masaru Kuno, Manoj Nirmal, David J. Norris, M. Bawendi, "Band-edge exciton in quantum dots of semiconductors with a degenerate valence band: Dark and bright exciton states", Phy Review B 54, 7, 1996, 4843.

[33] C.J. Perez, A.K. Bhattacharjee, M. Chamarro, P. Lavallard, V.D. Petrikov, A. A. Lipovskii, "Photoluminescence Stokes shift and exciton fine structure in CdTe nanocrystals", Phys Review B 64, 11, 2001, 113303.

[34] W.W. Yu, L. Qu, W. Guo, X. Peng, "Experimental determination of the extinction coefficient of CdTe, CdSe, and CdS nanocrystals", Chem of Materials 15, 14, 2003, 2854-2860.

[35] J. Tauc, R. Grigorovici, A. Vancu, "Optical properties and electronic structure of amorphous germanium", physica status solidi (b) 15, 2, 1966, 627-637.

[36] F. Aldeek, L. Balan, J. Lambert, R. Schneider, "The influence of capping thioalkyl acid on the growth and photoluminescence efficiency of CdTe and CdSe quantum dots", Nanotechnology 19, 47, 2008, 475401.

Chapter 7

Effect of tellurium concentration on the structural, optical and luminescence properties of cadmium telluride nanoparticles

7.1 Introduction

Cadmium telluride (CdTe) is one of compound semiconductors in the II–VI group. They show quite unique properties which make them suitable for numerous applications in bio-imaging and medical field since they possess superior optical properties than the organic dyes [1-4]. It has a band gap energy of 1.5 eV which is found in the mid of the solar spectrum, and it known to possess a high absorption coefficient (α) ($>10^4$ cm $^{-1}$) for the visible solar spectrum [5]. In comparison to the well-known organic fluorescent dyes, the NPs display numerous significant advantages which include; narrow and Gaussian emission spectra, large fluorescence quantum yields, less susceptibility to photobleaching and tunable emission wavelength maximum [6-8].

During the preparation of II-VI semiconductor nanoparticles (NPs) by wet chemical process, it usually involves the use of trioctylphosphineoxide (TOP/TOPO), polyphosphate and trioctylphosphine, and/ or thiols as stabilizing ligands to prevent agglomeration of the particles [9]. Tellurium (Te) powder and NaBH4 has been widely used as Te source and reductant respectively in most of the aqueous approaches. This, however, requires a pretreatment to prepare the unstable tellurium precursor [10-12]. The process of preparing CdTe NPs requires nitrogen as the shielding gas at the primary stage of synthesis [13-15]. Na_2TeO can also be used as an alternative tellurium source for preparing CdTe NPs but it has a disadvantage due to its toxicity and expensive nature [16-20]. Therefore, it is very crucial to search for a unique tellurium source for the preparation of CdTe NPs. In comparison to elemental Te, Na_2TeO has the same oxidation state of Te and is relatively cheap, stable and less toxic. Lately, TeO was used as the source of Te for the preparation of CdTe quantum dots

(QDs), but some of the shortcomings of this is that it requires a long reaction time and easily produces a black precipitate of CdTeO when TeO_2 is reduced using NaBH4 in ambient conditions [21-25]. In trying to avoid the tedious processes involved in preparing tellurium source we here report on the use of potassium tellurite (K_2TeO_3) as Te source. Here, we report a simple preparation technique for the synthesis of CdTe NPs with L-cystine and K_2TeO_3 as a capping agent and tellurium source respectively. L-cystine in our study also acts as a complexing agent, stabilizer and antioxidant.

The formation of tellurium precipitates which are distributed randomly over the entire surface of the NP restricts the application of these CdTe-based compounds in the fabrication of different types of sensors [26-29]. These precipitates are formed due to the distinctiveness of CdTe phase diagram. For instance, a Te-rich composition possesses properties which are in the vicinity of the melting point and also has a strong regressive character of solidus on the Te-rich side of uniformity region [30]. The post growth stoichiometry control is, however, made difficult by these precipitates since they are known to create some technological problems during synthesis of the CdTe NPs. Precisely, the main occasional problem is the unpredictable transformation of the precipitates when exposed to high temperatures (annealing treatments) involved in ohmic contacts assembly or during epitaxial growth [31-34]. It has been noted that is not easy to avoid completely the presence of these Te precipitates by changing the growth process and the post-growth annealing treatment [32, 35 - 36]. However, some reduction in its concentration was obtained through thermal treatments in Cd vapor [29, 36, 37]. Jayathirtha et al conducted studies [30] on the how to eliminate Te precipitates by Cl doping. Studies on the effect of Te concentration in the preparation of the CdTe NPs is hereby conducted in order to identify the best Te ratio to be used in the preparation of CdTe NPs hence avoid the formation of Te precipitates.

Colloidal semiconductors have the ability of being coated on any surface and are the band gaps can be tuned by changing the size and shape of the NPs hence their numerous potential advantages [38, 39]. Synthesis of CdTe nanocrystals have been done by several groups in various environments [40-43] but reports on the influence of tellurium concentration on the structural and optical properties of CdTe nanocrystals are few to the best of our knowledge.

7.2 Experimental

7.2.1 Synthesis

All the purchased chemicals used in the present work were of analytic grade and were used without any further purification. The Cd:Te molar ratio used to prepare CdTe NPs was varied

from 1:0.1, 1:0.2, 1:0.4, 1:0.6, 1:0.8 to 1:1. Briefly, the method from our previous work [44] was followed except that the Te concentration was varied. Typically, the CdTe QDs was prepared by mixing the appropriate amount of cadmium acetate and L-cysteine in a beaker. The pH of the precursor solution was kept at 11 by an addition of sodium hydroxide. After which, 50 ml of dissolved 0.04 mmol K_2TeO_3 was added to obtain a final volume of 100 ml. After stirring for a while, an appropriate amount of sodium borohydride was added to the mixture. The mixture was transferred to a three-necked flask and refluxed at 100 oC in open air for 1 h. This produced a Cd:Te molar ratio of 1:0.2. The same method was repeated for 1:0.1, 1:0.4, 1:0.6, 1:0.8 and 1:1 Cd:Te molar ratios.

7.2.2 Characterization

The crystalline structures of CdTe NPs were analyzed by X-ray diffraction (XRD) with a Cu-Kα radiation (λα = 1.5406 Å) source and the compositions and morphology of the nanopowders were examined by Energy Dispersive Spectra (EDS) electron microscope and scanning electron microscopy (SEM) instrument respectively. Optical absorbance was estimated from Shimadzu UV/Vis evolution 100 Spectrophotometer. Photoluminescence (PL) emission was recorded using Cary Eclipse spectrophotometer with a built-in 150 W xenon flash lamp. The PL emission was taken at an excitation wavelength of 400 nm.

7.3 Results and Discussion

7.3.1 Structural and composition analysis

7.3.1.1 SEM analysis

The morphology and distribution of the particles on the surface are determined by scanning electron microscopy (SEM). Fig. 7.1 shows the SEM micrographs of CdTe NPs prepared at different Cd:Te molar ratios. The changes in shape and size observed in CdTe NPs when Te ratio is varied display the sensitivity of the growth and growth rate of the NPs to the amounts of Te used in the initial precursors. Te, therefore, is a key factor to be considered in controlling the shape and size of the CdTe NPs

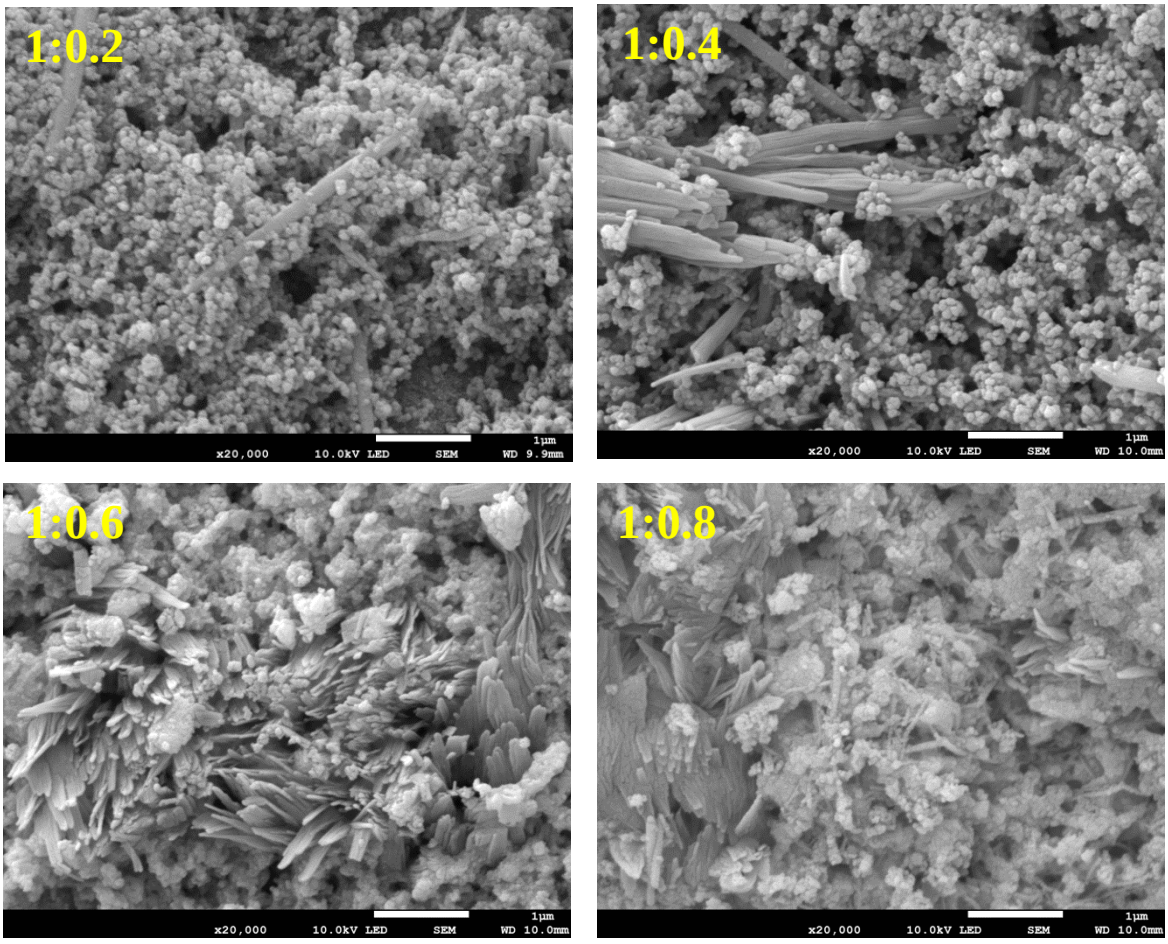

Figure 7.1 (a): Representative SEM images of CdTe samples prepared at various Cd:Te molar ratios.

.

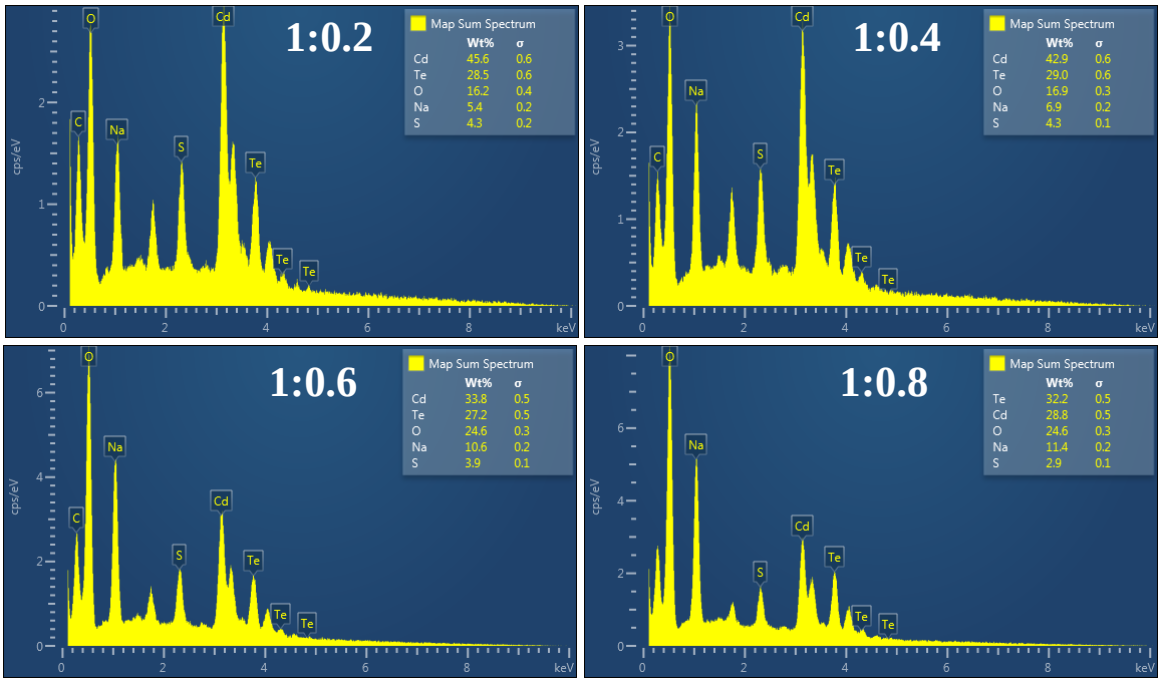

Figure 7.1 (b): Representative EDS spectra of CdTe samples prepared at various Cd:Te molar ratios.

The qualitative analysis was done using EDS incorporated in the SEM machine to determine the elemental composition of the as-prepared samples. The EDS spectra of CdTe NPs prepared at different Te molar ratio is presented in Fig. 7.1 (b).The amount of Cd was observed to decrease when Te molar ratio was increased although the Cd molar ratio was kept constant during the preparation process. However, at a molar ratio of 1:0.8 the percentage of Te was the highest as displayed in Fig. 7.1(b). This can be attributed to high volatility of Te during the synthesis process and shows that in order to achieve a stoichiometric composition small amount of Te is needed during synthesis. Other elements like O, Na and S are observed in the spectra. Na and S are trace elements from the precursors which could not be eliminated during preparation. O element could be from unreacted precursors and not from oxidation of CdTe NPs after synthesis because there are no peaks corresponding to oxidized material in the XRD pattern.

7.3.1.2 XRD Analysis

X-ray diffraction is an important technique for determining the crystal structure of the as-prepared sample. The XRD pattern of CdTe NPs (Fig. 7.2(a)) shows three diffraction peaks at the neighborhoods of 24°, 40°, and 46°, which can be readily indexed to the (111), (220), and (311) planes.

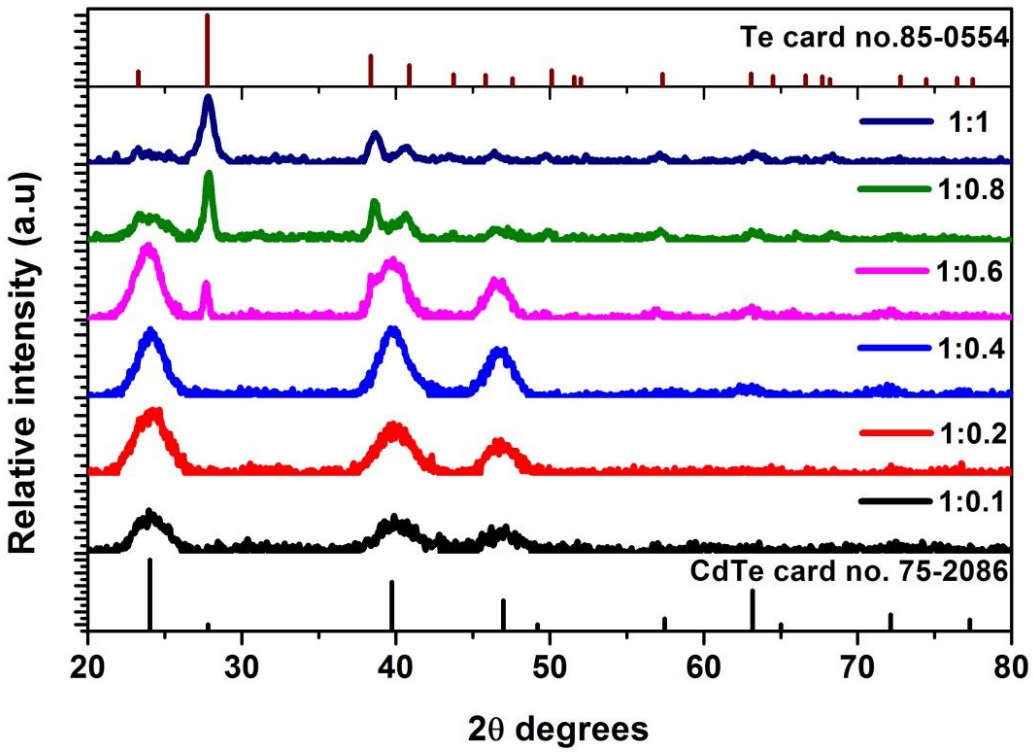

Figure 7.2(a): XRD pattern for CdTe NPs prepared at different Cd:Te molar ratios.

Such distinctive diffraction pattern indicates to formation of a typical zinc blende lattice structure (Joint Committee on Powder Diffraction Standards (JCPDS) No. 75-2086).The standard XRD pattern for cubic CdTe is given at the bottom while the standard XRD pattern for the emerging peaks at higher Te ratio assigned to hexagonal phase of Te is given at the top of Fig. 7.2(a). The CdTe NPs are all polycrystalline with three broad peaks observed in the diffractogram. The observed broad peaks are attributed to the small size of the as-obtained NPs. The values of full width at half maximum of the (111), (220) and (311) diffraction peaks were used to estimate the average crystallite sizes of the as-prepared CdTe NPs. Employing the Debye-Scherrer equation [45], the NP' results are shown inTable1. It was found that increasing the molar ratio of Te led to an increase in the size of the crystallite. It can be concluded that increasing the molar ratio of tellurium accelerated the growth of the CdTe NPs hence the observed change in crystallite sizes. At lower Te molar ratio broad peaks are observed while at higher Te molar ratio narrow diffraction peaks are observed indicates to a crystalline lattice structure. The ratio of $\frac{I_{(111)CdTe}}{I_{(200)Te}}$ are 1.9, 0.4 and 0.2 for 1:0.6, 1:0.8 and 1:1 Cd:Te molar ratios. These values indicate that for 1:0.6 molar ratio, there is a preference of (111) CdTe phase orientation while at 1:0.8 and 1:1 Cd:Te molar ratios have a (200) phase preference for Te when compared to a standard $\frac{I_{(111)CdTe}}{I_{(200)Te}}$. It also confirms that the emerging peaks at higher Te molar concentration belong to Te element. The size analyses of the NPs indicate similar distributions, however, the increased FWHM of the XRD suggest that the crystalline domains in the cadmium-rich (1:0.1) samples are smaller [46]. The calculated lattice parameters (table1) show a slight deviation from the standard bulk values. This shows that the nanocrystallites may be under some strain. Strain values provide more information on the structural properties of the as-prepared CdTe NPs, and it was calculated using the following equation [47];

$$\varepsilon = \frac{\beta \cos\theta}{4} \qquad (11)$$

Where θ is the Bragg's diffraction angle, ε is the strain of the as-prepared CdTe NPs and β is the full width at half maximum (FWHM) of the diffraction peaks. It is observed that the strain in the as-prepared CdTe NPs decreases from 7.53×10-1 to 4.68×10-1, with an increase in the Cd:Te molar ratio to 1:0.8 but increases when a 1:1 ratio is reached. The increase in strain value could be attributed to the increase in defect density or lattice distortion in the CdTe NPs [47].

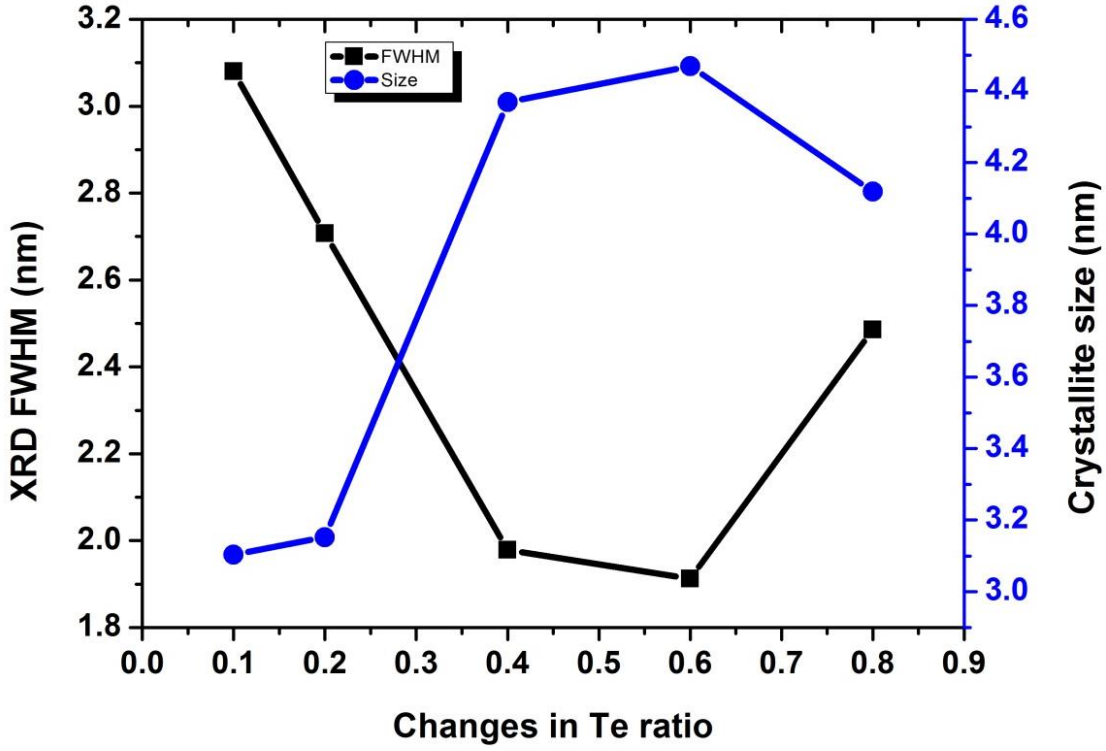

Figure 7.2(b): changes in crystallite sizes and XRD FWHM values of CdTe NPs obtained from XRD pattern for different Te ratio

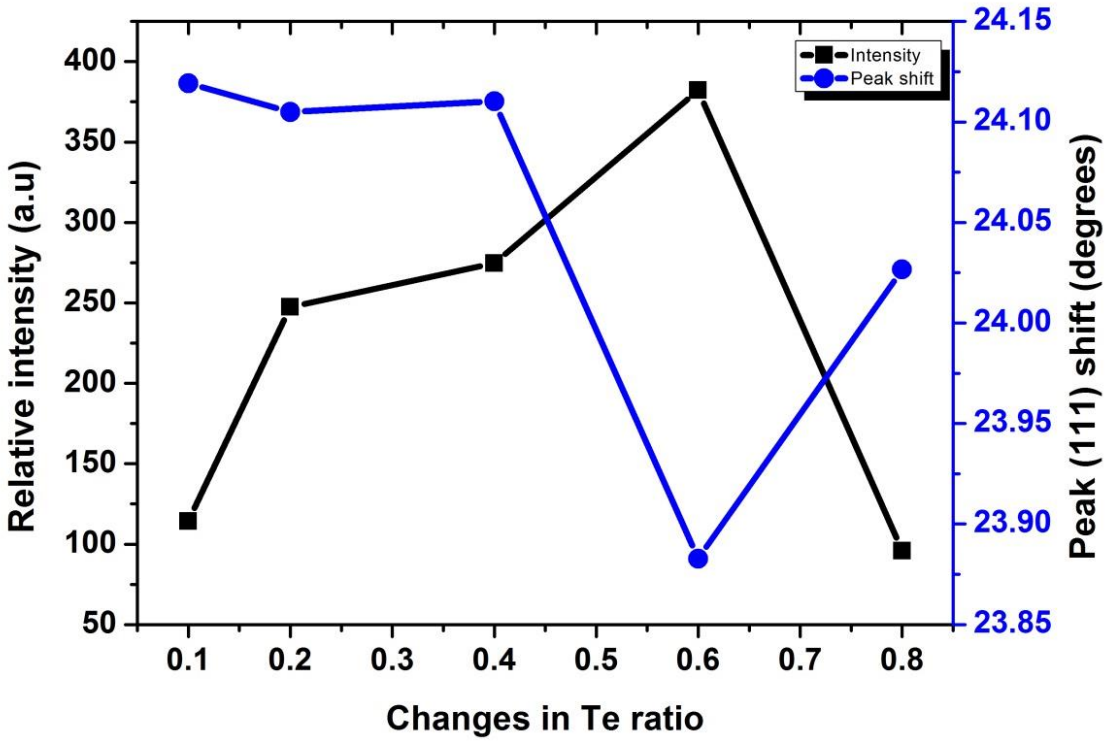

Figure 7.2(c): changes in the peak (111) position and relative intensity of the CdTe NPs with different Te ratios.

Fig. 7.2(b) displays changes in crystallite size and XRD FWHM with Te ratio. With the increase in Te ratio, the crystallite sizes increased and this could be because under Te-rich conditions, the small particles agglomerate to form the larger ones. From the literature, the development of CdTe nanowires suggests that the aggregation is driven by dipole-dipole interactions [48]. Conversely, XRD FWHM is observed to decrease with increase in the size of the crystal which explains the narrow peaks (Fig. 7.2(b)) at higher Te ratio. This displays the FWHM dependence on the size of the NPs produced. Fig. 7.2(c) depicts changes in XRD peak position for the plane (111) at various Te molar ratios. Diffraction peaks generally shift to lower diffraction angle as Te concentration is increased which was accompanied by variation in the lattice parameters. The shift in diffraction peaks to lower angle is due to increase in the lattice parameters attributed to lattice expansion (Table 1).

Table 7.1: lattice parameters, crystallite sizes and strain in the CdTe NPs for different Te ratio

Cd:Te ratio	2θ degrees for plane (111)	2θ degrees for plane (220)	2θ degrees for plane (311)	d-spacing (Å)	Lattice parameter, a=b=c (Å)	Crystallite size (nm)	Strain, ε (lines^{-2} m^{-4})
1:0.1	24.119	40.119	46.895	3.687	6.386	3.1	7.53×10^{-1}
1:0.2	24.105	39.937	46.891	3.689	6.390	3.2	6.62×10^{-1}
1:0.4	24.110	39.832	46.752	3.688	6.388	4.4	4.84×10^{-1}
1:0.6	23.883	39.629	46.607	3.723	6.448	4.5	4.68×10^{-1}
1:0.8	24.027	-	46.731	3.701	6.410	4.1	7.09×10^{-1}

7.3.2 Influence on photoluminescence properties

Controlling the formation of nanoparticles during the growth process is important in the development of novel structures. Fig. 7.3(a) displays the PL spectra and an inset of the normalized PL spectra of CdTe NPs for different Te molar ratios. There was variation in the peak position and intensity observed when Cd:Te molar ratio was increased from 1:0.1 to 1:1 (Fig. 7.3(b)). Increasing Te ratio caused a red shift in the emission wavelength from 536 to 559 nm which arises from the relocation of charges between Cd^{2+} and $Te^{2-.}$ The most intense peak was observed for NPs prepared at Cd:Te of 1:0.4.

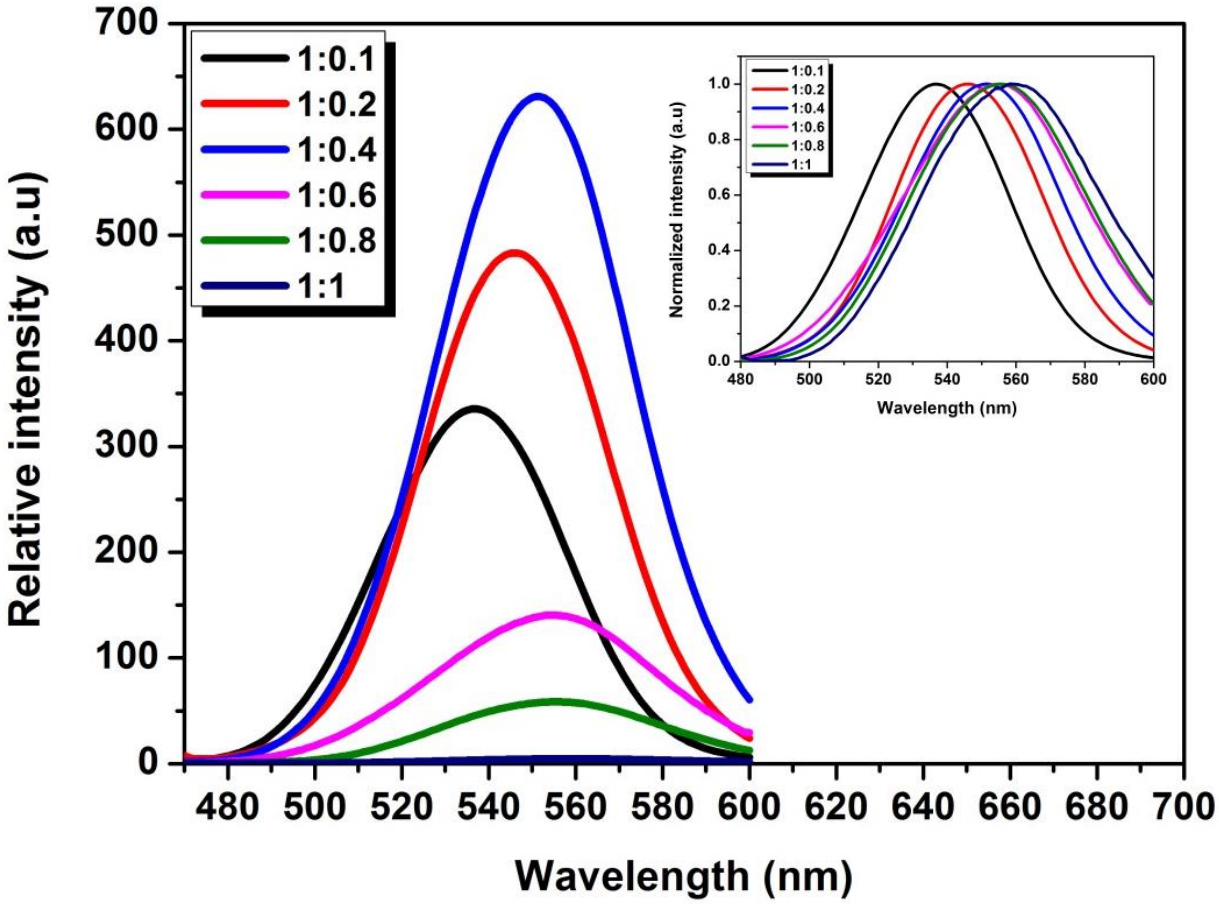

Figure 7.3(a): PL emission with an inset of normalized PL spectra of CdTe NPs prepared at different Cd:Te molar ratios.

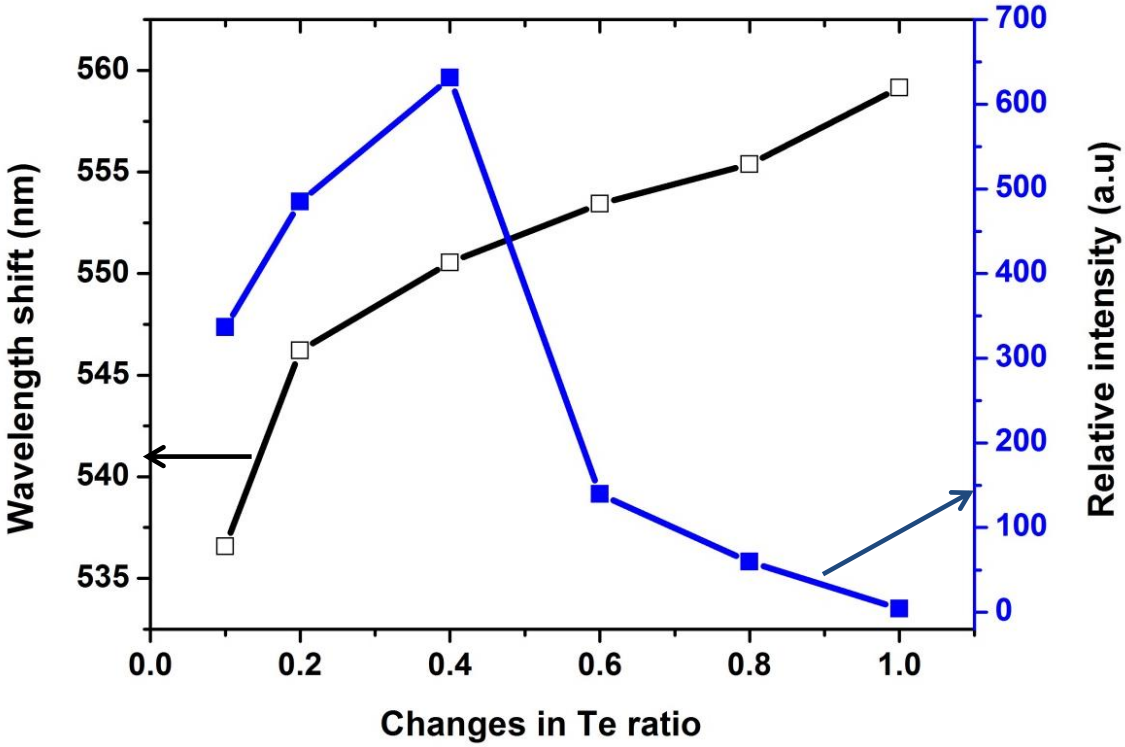

Figure 7.3(b): changes in peak position and intensity with respect to Te molar ratios.

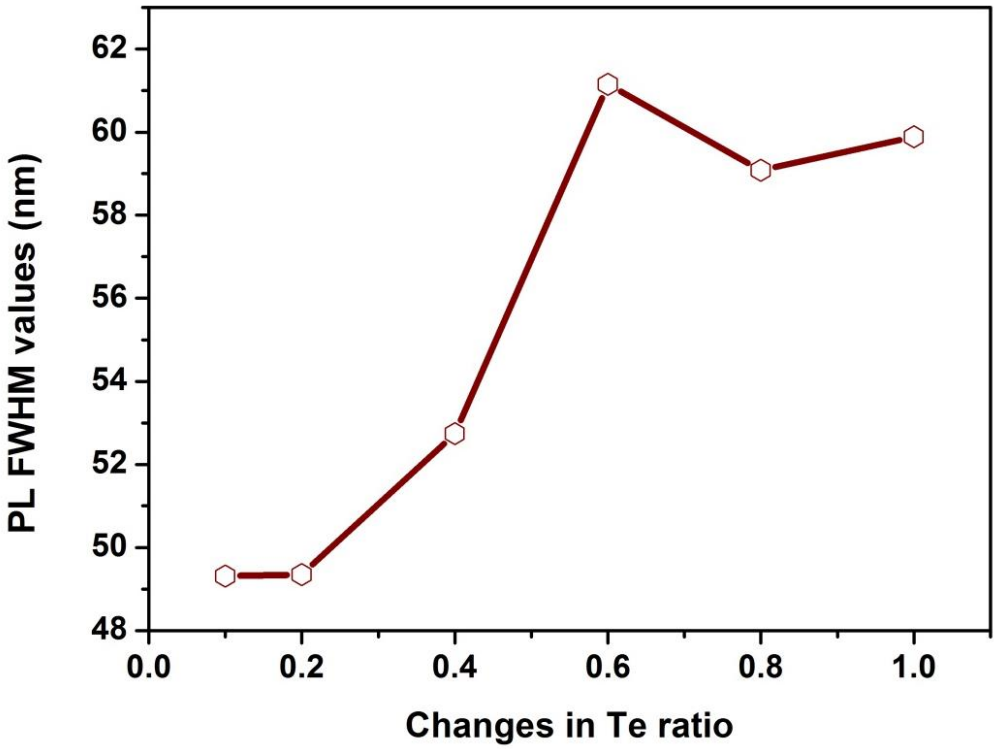

Figure 7.3(c): changes in the FWHM values of as-prepared CdTe NPs at different Te molar ratios.

In all cases, the emission peaks of the samples have identical narrow shape, which indicates monodispersed particles that are well passivated.

The red shift in emission is attributed to the growth of the CdTe NPs. This is because increasing Te ratio in the solution generally increases the resultant concentration hence faster growth rate of the NPs. The results are in good agreement with the XRD results of the growth of the NPs with increased Te ratio. The decrease in the PL intensity at higher Te ratio could be due to the presence of impurity defects or excess tellurium ions in the samples. This indicates that Te ratio has a great effect in the preparation of CdTe and a Cd:Te ratio of 1:0.4 is preferred due to its intense PL emission peak. During the PL evolution upon an increase in Te ratio, the values of PL FWHM increased gradually from 49 to 60 nm for 1:0.1 to 1:1 CdTe ratio (Fig. 7.3(c)) which is another evidence of the narrow distribution of the resultant CdTe NPs. The values of the chromaticity coordinates of as-prepared CdTe NPs have been estimated from the 1931 Commission Internationale de l'Eclairage (CIE) system. (Fig. 7.3 (d)). This system helps us visualize the variation in color emitted from the samples. The estimated coordinates are (0.257, 0.710), (0.311, 0.669), (0.338, 0.647), (0.355, 0.630), (0.364, 0.623), (0.380, 0.608) for Cd:Te ratio of 1:0.1, 1:0.2, 1:0.4, 1:0.6, 1:0.8, and 1:1 respectively.

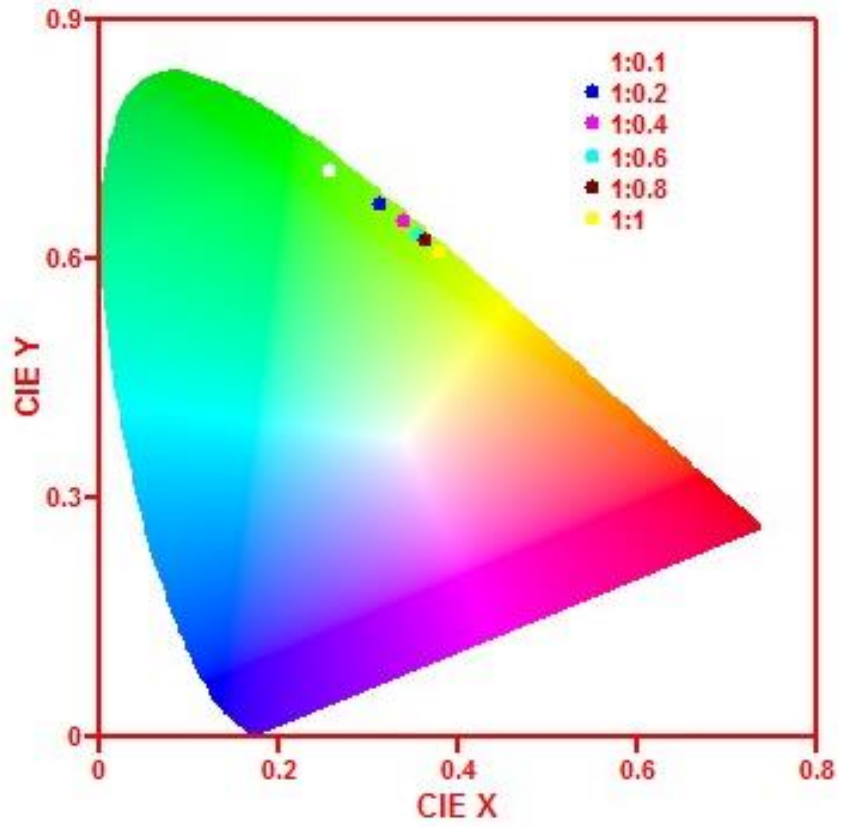

Figure 7.3 (d): CIE image obtained from PL emission data of as-prepared CdTe NPs for different Cd:Te molar ratios.

7.3.3 Influence on Ultra-violet visible properties

UV-Visible absorption spectroscopy is well known efficient technique used to monitor the optical properties of nano-sized particles. A typical absorption spectrum of CdTe NPs obtained at different Cd:Te ratios is shown in Fig. 7.4(a). A shift of absorption edges and bands to longer wavelength was observed when Cd:Te molar ratios was increased from 1:0.1 to 1:1. The observed bands red shifted from 455 to 533 nm. The red-shift of the absorption peaks clearly demonstrates the growth of the nanocrystals and formation of the CdTe QDs with various sizes at different Te concentration. When the tellurium molar ratio is increase, the growth of the CdTe NPs is accelerated hence increases the amount of absorbance which indicates that the number density of particles is greater as well. Relatively sharp absorption edges are observed from the as-prepared samples which are ascribed to the narrow size distribution of CdTe NPs formed [49]. From literature, it has been reported that size is not the only property which influences the band gap because shape also plays an important role [50]. As such the band gaps of lengthened particles depend on both their width and length although it is more sensitive to their width [50].

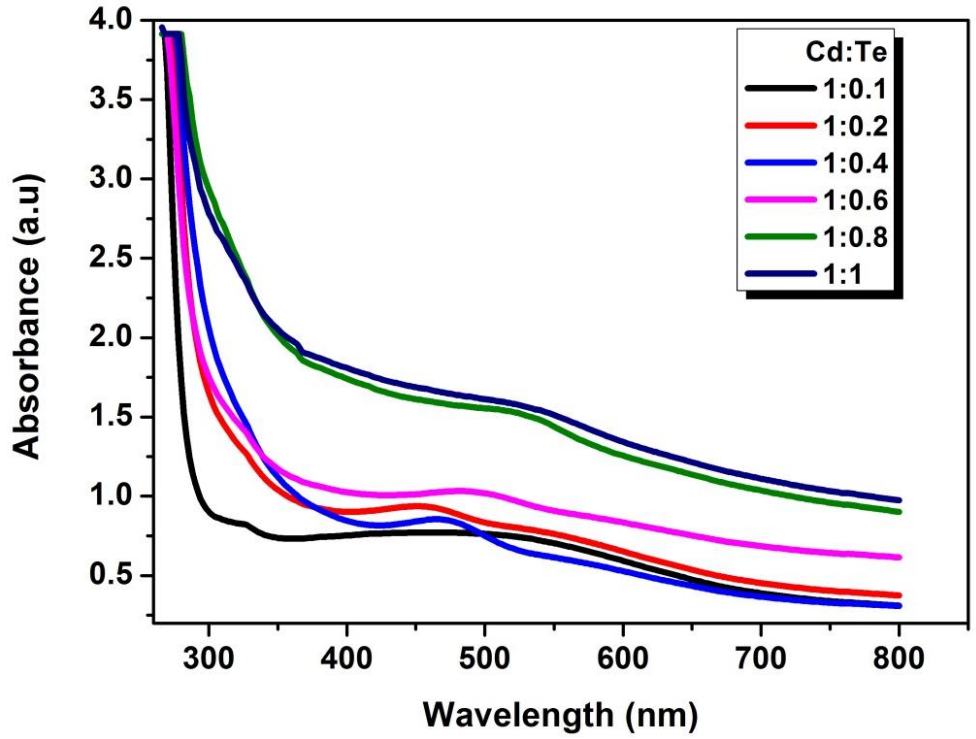

Figure 7.4(a): absorption spectra of CdTe NPs prepared at different Te molar ratios.

Therefore, both the length and the width of the particles contribute to the resultant band edge. The sizes of the NPs could be estimated from the UV–vis absorption spectra using the empirical Eq. (12) [51] where D is the diameter of the NPs and λ is the first absorption maximum. The diameters of the CdTe NPs were in the range 1 – 3 nm for different Te concentration under study which is in close agreement to those acquired from XRD studies

$$D = \left(9.8127\times10^{-7}\right)\lambda^3 - \left(1.7147\times10^{-3}\right)\lambda^2 + \left(1.0064\right)\lambda - 194.84 \qquad (12)$$

The optical energy gap (Eg) of the CdTe NPs was calculated from Tauc relation [52]. Fig. 7.4(b), it is clear that the band gap is decreased with an increase in Te ratio. This shows its dependence on the concentration of the initial precursor solution. The band gap of CdTe NPs was, however, found to be greater than the bulk band gap of the powders and thin films [53]. It is, therefore, possible to tune the band gap of CdTe by changing the concentration of precursor solutions. This supports the growth of NPs as depicted in XRD and PL results. The band edge of as-prepared CdTe NPs for different Cd:Te molar ratios indicates a red-shift with increased Te molar ratio. The graph of (Ahν) 2 plotted as a function of the photon energy (hυ) for as-prepared CdTe NPs is shown in Fig. 7.4(b). NPs prepared different Te molar ratios. There is a blue-shift in band gap energy observed when compared with that of the bulk CdTe at 810 nm (1.5 eV).

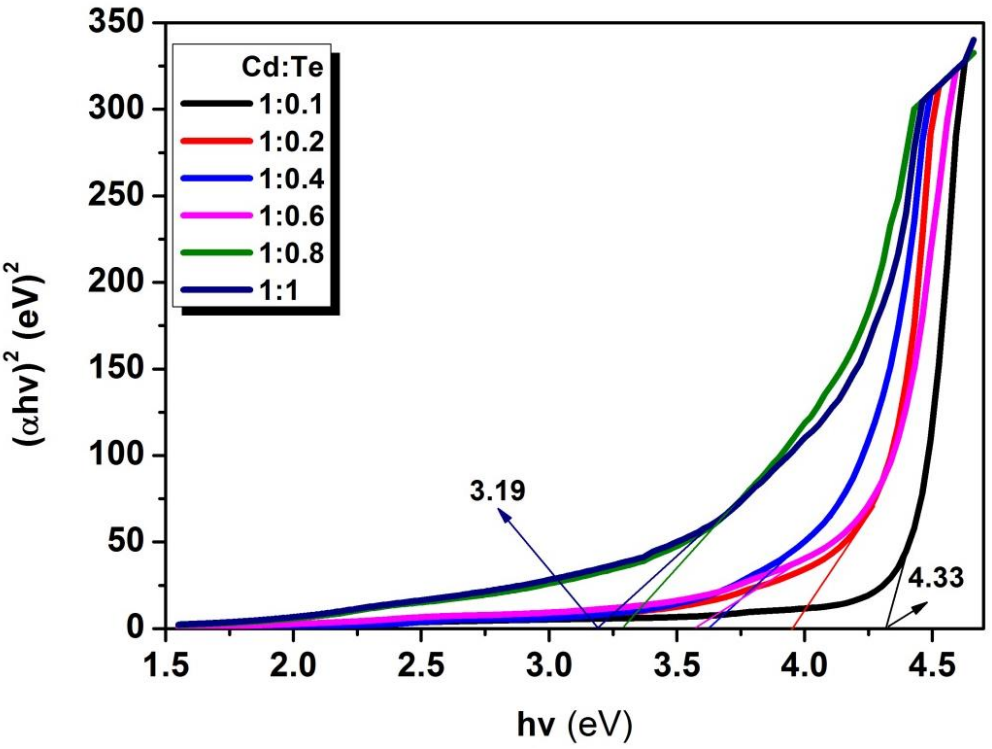

Figure 7.4 (b): Tauc plot (αhν)2 v/s hν to determine the band gap energy of CdTe

Quantum confinement effects from nanosized materials are known to cause the observed blue shift in the absorption edges of the as-obtained CdTe NPs [54]. In the as-prepared CdTe NPs sample here in reported, the average grain size estimated from XRD measurements was about 5 nm and this explains the slightly larger band gap when compared to the bulk value.

Conclusion

CdTe NPs were successfully synthesized using L-cystine as a stabilizer by a simple method at a low growth temperature of 100 ^{o}C for different Cd:Te molar ratios. The observed XRD pattern exhibited zinc blende crystal structure at low tellurium molar ratio and hexagonal Te structure at higher tellurium molar ratio. The crystallite sizes of the as-prepared CdTe NPs were all under 5nm. The SEM micrographs displayed variation in the shape of NPs with different Te molar ratios. A change from spherical to blade-like morphology was observed. The PL and UV-Vis properties showed Te concentration dependence of the as-prepared NPs. The sizes of the nanoparticles were found to increase with an increase in Te molar ratio. The optical band gap was decreased with increase in Te molar ratio.

References

[1] J.R. Sandra, J.C. Chang, O. Kovtun, J.R. McBride, I.D. Tomlinson, "Biocompatible quantum dots for biological applications", Chem. & bio 18, 2011, 10.

[2] G. Zhang, L. Shi, M. Selke, X.M. Wang, "CdTe quantum dots with daunorubicin induce apoptosis of multidrug-resistant human hepatoma HepG2/ADM cells: in vitro and in vivo evaluation", Nanoscale Res Lett 6, 2011, 418.

[3] S. Ge, C. Zhang, Y. Zhu, J. Yu, S. Zhang, "BSA activated CdTe quantum dot nanosensor for antimony ion detection", Analyst 135, 2010, 111.

[4] P. Wu, X.P. Yan, Chem. "Doped quantum dots for chemo/biosensing and bioimaging", Society Reviews 42, 2013, 5489.

[5] P. C. Sarmah, A. Rahman, "Current-voltage characteristics of Ag, Al, Ni-(n) CdTe junctions", Bulletin of Mat. Sci, 24, 2001, 411.

[6] W.C.W. Chan, S. Nie, "Quantum dot bioconjugates for ultrasensitive nonisotopic detection", Science 281, 1998, 2016.

[7] D.M. Willard, "Nanoparticles in bioanalytics", Anal. Bioanal. Chem. 376, 2003, 284.

[8] C.J. Murphy, J.L. Coffer, "Quantum dots: a primer", Appl. Spectrosc. 56, 2002, 16

[9] A. P. Alivisatos, "Perspectives on the physical chemistry of semiconductor nanocrystals", J. Phys. Chem. 100, 1996, 13226.

[10] J.F. Wang, X.T. Song, L. Li, H.F. Qian, K.Y. Chen, X.M. Xu, C.X. Cao, J.C. Ren, "Exploring feasibility for application of luminescent CdTe quantum dots prepared in aqueous phase to live cell imaging", Chin Chem. Lett 17, 2006, 675.

[11] L. Li, H. Qian, J. Ren, "Rapid synthesis of highly luminescent CdTe nanocrystals in the aqueous phase by microwave irradiation with controllable temperature", Chem. Commun 4, 2005, 528.

[12] S. Ghosh, A. Saha, "Synthesis and spectral studies of CdTe–dendrimer conjugates", Nanoscale Res Lett 4, 2009, 937.

[13] J. Yuan, W. Guo, J. Yin, E. Wang, "Glutathione-capped CdTe quantum dots for the sensitive detection of glucose", Talanta 77, 2009, 1858.

[14] F.O. Silva, M.S. Carvalho, R. Mendonca, W.A. Macedo, K. Balzuweit, "Effect of surface ligands on the optical properties of aqueous soluble CdTe quantum dots", Nanoscale Res Lett 7, 2012, 536.

[15] L.M. Sai, X.Y. Kong, "Microwave-assisted synthesis of water-dispersed CdTe/CdSe core/shell type II quantum dots", Nanoscale Res Lett 6, 2011, 399.

[16] D. Zhou, M. Lin, Z.L. Chen, H.Z. Sun, H. Zhang, H.C. Sun, B. Yang, “Simple synthesis of highly luminescent water-soluble CdTe quantum dots with controllable surface functionality”, Chem. Mat 23, 2011, 4857.

[17] C.W. Ge, M. Xu, J. Liu, J.P. Lei, H.X. Ju, “Facile synthesis and application of highly luminescent CdTe quantum dots with an electrogenerated precursor”, Chem. Commun 4, 2008, 450.

[18] H.F. Bao, E.K. Wang, S.J. Dong, “One-Pot Synthesis of CdTe Nanocrystals and Shape Control of Luminescent CdTe-Cystine Nanocomposites”, Small 2, 2006, 476.

[19] E. Ying, D. Li, S.J. Guo, S. Dong, J. Wang, “Synthesis and bio-imaging application of highly luminescent mercaptosuccinic acid-coated CdTe nanocrystals”, J PLoS One 3, 2008, e2222.

[20] Z.H. Sheng, H.Y. Han, X.F. Hu, C. Chi, “One-step growth of high luminescence CdTe quantum dots with low cytotoxicity in ambient atmospheric conditions”, Dalton Trans 39, 2010, 7017.

[21] P. Wu, X.P. Yan, “Ni 2+-modulated homocysteine-capped CdTe quantum dots as a turn-on photoluminescent sensor for detecting histidine in biological fluids”, Biosens Bioelectron 26, 2010, 485.

[22] Y.Y. Wang, K.F. Cai, J.L. Yin, X. Yao, “Facile synthesis and photoluminescence properties of water-soluble CdTe/CdS core/shell quantum dots”, Micro Nano Lett 6, 2011, 141.

[23] R.F. Wang, Y.L. Wang, Q.L. Feng, L.Y. Zhou, F.Z. Gong, Y.W. Lan, “Synthesis and characterization of cysteamine-CdTe quantum dots via one-step aqueous method”, Mat Lett 66, 2012, 261.

[24] Y.L. Wang, S.Y. Liu, L.Y. Zhou, “An alternative aqueous synthetic route to preparing CdTe quantum dots with tunable photoluminescence”, Chin Chem. Lett 23, 2012, 359.

[25] H.B. Shen, H.Z. Wang, X. Chen, J.Z. Niu, W.W. Xu, X.M. Li, X.D. Jiang, Z.L. Du, L.S. Li, “Size-and shape-controlled synthesis of CdTe and PbTe nanocrystals using tellurium dioxide as the tellurium precursor”, Chem. Mat 22, 2010, 4756.

[26] S. Sen, W.H. Konkel, S.J. Tighe, L.G. Bland, S. R. Sharma, R.E. Taylor, “Crystal growth of large-area single-crystal CdTe and CdZnTe by the computer-controlled vertical modified-Bridgman process”, J. Cryst.G. 86, 1988, 111.

[27] H.G. Brion, C. Mewes, I. Hahn, U. Schaufele, “Infrared contrast of inclusions in CdTe”, J. Cryst.G., 134, 1993, 281.

[28] H.N. Jayatirtha, D.O. Henderson, A. Burger, M.P. Volz, S"tudy of tellurium precipitates in CdTe crystals", Appl. Phy. Lett. 62, 1993, 573.

[29] H.R. Vydyanath, J.A. Ellsworth, J.B. Parkinson, J.J. Kennedy, B. Dean, C.J. Johnson, G.T. Neugebauer, J. Sepich, P.K. Liao, "Thermomigration of Te precipitates and improvement of (Cd, Zn) Te substrate characteristics for the fabrication of LWIR (Hg, Cd) Te photodiodes", J. Electron. Mat. 22, 1993, 1073.

[30] K. Peters, A. Wenzely P. Rudolph, "The p-T-x projection of the system Cd_xTe", Cryst. Res. and Tech. 25, 1990, 1107.

[31] E.D. Jones, J. Malzbender, J.B. Mullin, N. Shaw, "The diffusion of Cl into CdTe", J.Cond. Mat. 6, 1994, 7499.

[32] N.V. Sochinskii, M.D. Serrano, V.N. Babentsov, N.I. Tarbaev, J. Garrido, E. Diéguez, "Short-time annealing of as-grown p-CdTe wafers", Semicond. Sci. Techn. 9, 1994, 1713.

[33] N.V. Sochinskii, V.N. Babentsov, N.I. Tarbaev, M.D. Serrano, E. Diéguez, "The low temperature annealing of p-cadmium telluride in gallium-bath", Mat. Res. Bull. 28, 1993, 1061.

[34] M. Koralewskii, N.V. Sochinskii, M.D. Serrano, E. Diéguez, J. Garrido, G. Lifante, B. Noheda, J.A. Gonzalo, "On the ferroelectricity in $Zn_xCd_{1-x}Te$", Appl. Phy. Comm. 13, 1994, 69.

[35] N.V. Sochinskii, V.N. Babentsov, S.V. Kletskii, M.D. Serrano, E. Diéguez, "Vapor phase epitaxy of $Hg_{1-x}Cd_xTe$ on CdTe heteroepitaxial substrates", phys. stat. sol. 40, 1993, 445.

[36] J.C. Tranchart, P. Bach, "LPE growth of $Hg_{1-x}Cd_xTe$ on $Cd_{1-y}Zn_yTe$ substrates", J. Cryst. G. 32, 1976, 8.

[37] K. Mochizuki, T. Yoshida, K. Igaki, T. Shoji, Y. Hiratate, "Growth of In-doped CdTe from Te excess solution and its characteristics as a γ-ray detector", J. Cryst.G. 73, 1985, 123.

[38] Z.A. Peng, X. Peng, "Nearly monodisperse and shape-controlled CdSe nanocrystals via alternative routes: nucleation and growth", J. Am. Chem. Soc. 123, 2001, 183.

[39] Y.D. Yin, A.P. Alivisatos, "Colloidal nanocrystal synthesis and the organic-inorganic interface", Nature 437, 2005, 664.

[40] V. Esch, B. Flugel, G. Khitrova, H.M. Gibbs, X. Jiajin, K. Kang, S.W. Koch, L.C. Liu, S.B. Risbud, N. Peyghambarian, "State filling, Coulomb, and trapping effects in the optical nonlinearity of CdTe quantum dots in glass", Phys. Rev. B 42, 1990, 7450.

[41] L.C. Liu, M.J. Kim, S.H. Risbud, R.W. Carpenter, "High-resolution electron microscopy and microanalysis of CdS and CdTe quantum dots in glass matrices", Phil. Mag. B 63, 1991, 769.

[42] B. J. Potter, J.H. Simmons, "Quantum confinement effects in CdTe glass composite thin films produced using rf magnetron sputtering", J. Appl. Phys. 68, 1990, 1218.

[43] J.A.M. Neto, L.C. Barbosa, C.L. Cesar, O.L. Alves, F. Galembeck, "Quantum size effects on $CdTe_xS_{1-x}$ semiconductor-doped glass", Appl. Phys. Lett. 59, 1991, 2715.

[44] S. Kiprotich, F.B. Dejene, J. Ungula, M.O. Onani, "The influence of reaction times on structural, optical and luminescence properties of cadmium telluride nanoparticles prepared by wet-chemical process", J. of Cond. Mat. 480, 2016, 125.

[45] A. Guinier, "Elements of X-ray Diffraction", Freeman, San Francisco 1963.

[46] P. Dagtepe, V. Chikan. "Effect of Cd/Te ratio on the formation of CdTe magic-sized quantum dots during aggregation", J. of Phy. Chem. A 112, 2008, 9304.

[47] L.L. Pan, G.Y. Li, S.S. Xiao, L. Zhao, J.S. Lian, "Bandgap variation in grain size controlled nanostructured CdO thin films deposited by pulsed-laser method", J. of Mat Sci. 25, 2014, 1003.

[48] Z.Y. Tang, N.A. Kotov, M. Giersig, "Spontaneous organization of single CdTe nanoparticles into luminescent nanowires", Science 297, 2002, 237.

[49] S. Shanbhag, N.A. Kotov, "On the origin of a permanent dipole moment in nanocrystals with a cubic crystal lattice: effects of truncation, stabilizers, and medium for CdS tetrahedral homologues", J. Phys. Chem. B 110, 2006, 12211.

[50] H. Zhang, L. Wang, H. Xiong, L. Hu, B. Yang, W. Li, "Hydrothermal Synthesis for High-Quality CdTe Nanocrystals", Adv. Mat. 15, 2003, 1712.

[51] Q. Wang, D. Pan, S. Jiang, X. Ji, L. An, B. Jiang, "A solvothermal route to size-and shape-controlled CdSe and CdTe nanocrystals", J. of crystal growth 286, 2006, 83.

[52] W.W. Yu, L. Qu, W. Guo, X. Peng, "Experimental determination of the extinction coefficient of CdTe, CdSe, and CdS nanocrystals", Chem. of Materials 15, 2003, 2854.

[53] D.V. Talapin, A.L. Rogach, I. Mekis, S. Haubold, A. Kornowski, M. Haase, and H. Weller, "Synthesis and surface modification of amino-stabilized CdSe, CdTe and InP nanocrystals", Phys. Eng. Asp. 202, 2002, 145.

[54] G.D. Scholes, "Controlling the optical properties of inorganic nanoparticles", Adv. Funct. Mat. 18, 2008, 1157.

Chapter 8

A comparison investigation of optical, structural and luminescence properties of CdO_xTe_{1-x} and $CdTe_xSe_{1-x}$ nanoparticles prepared by a simple one pot method [2]

8.1 Introduction

Semiconductor nanoparticles (NPs) also known as quantum dots (QDs) attracted much attention over the past decades due to their novel size-dependent optical properties displayed by excellent luminescent properties in biological imaging [1,2], broad excitation spectra, narrow emission bandwidth [3-6], high quantum yields, reduced tendency to photobleaching compared with organic dyes and absorb throughout the visible and near-infrared spectra [7]. With these enthralling properties, QDs devices have been developed targeting applications in biological imaging, optoelectronic, photovoltaic devices and optical amplifier media for telecommunication networks [8-10].

Cadmium telluride (CdTe) is a group II-VI semiconductor with a wurtzite crystalline structure, exciton Bohr radius of 6.5 nm with bulk band gap energy of 1.5 eV at room temperature [11]. Cadmium oxide (CdO) on the other hand has a frequently accepted band gap of 2.28 eV as determined from 100 K thermoreflectance measurements of single crystal produced using a vapor transport technique [12]. Most advances in the research field have been focusing on preparing different color-emitting binary nanocrystals of different sizes by tuning the physical and chemical properties of the nanocrystal. Tunable emission of the alloyed $CdTe_xSe_{1-x}$ and CdO_xTe_{1-x} nanocrystals can be attained by playing with the particle composition alongside particle size.

Some of the existing methods for the preparation of QDs are; organometallic synthesis in highly boiling organic solvents [13,14] and the aqueous medium synthesis using thiols as

[2]Taken directly from: https://doi.org/10.1016/j.physb.2017.06.057

stabilizing agents [15, 16]. Although QDs prepared by organometallic route possess excellent luminescent properties and monodispersity, they are generally capped with hydrophobic ligands. This method, therefore, produces nanoparticles which are insoluble in water and also require high temperatures for synthesis which makes the final product incompatible with the biological systems [17, 18]. They also need to convert the organic-soluble QDs into water-soluble ones which may decrease the photoluminescence (PL) quantum yield. The water-soluble QDs can easily be prepared through this method using l-cysteine as a capping agent. This method, however, is simple, cheaper and less toxic compared with the organometallic method and furthermore, the resulting nanocrystals are water-soluble which makes them biologically compatible [19].

However, for biological use, the QDs potential cytotoxicity due to toxic chemical composition, such as heavy metals remains unanswered. Most recently, it is reported that this problem can be solved by using a proper stabilizer to modify the surface of QDs [20]. To try and alleviate the above problem an antioxidant which is known to protect cells against oxidative stress and QD-induced cytotoxicity L-cysteine has been used. It is also an aminophenol of the human body without any cytotoxin and is considered to be a more suitable stabilizer with very narrow emission spectra and long fluorescence lifetime [21, 22].

Furthermore, various experimental parameters such as reaction time, temperature, pH, and the molar ratio of reactants have considerable influence on structural, optical and photoluminescence properties of the CdTe nanoparticles (NPs) and are worth investigating. In varying these parameters, the nanoparticles (NPs) may be tuned to suit the desired applications. In this study, cysteine-capped $CdTe_xSe_{1-x}$ and CdO_xTe_{1-x} nanoparticles were prepared by a facile one-pot synthesis using potassium telluride, sodiumselenosulphate as stable tellurium and selenium (Se) sources respectively and L-cysteine as a capping agent. Capping with L-cysteine was intended to tap on the above-mentioned advantages further. The various applications of semiconductors are critically dependent on the value of the band gap energy of the material. Therefore, the ability to tune (or engineer) the band gap is essential for the fabrication of bio-imaging materials with widely varying properties. Selenium being group VI element as S, can easily make an isovalent ternary semiconductor alloys ($AB_{1-x}C_x$). It has also attracted attention because of its antioxidant properties which yield highly stable nanoparticles [23]. We report a series of high-quality cysteine-capped QDs with excellent water solubility, structural and optical properties. There is no report so far on the studies of as-prepared $CdTe_xSe_{1-x}$ and CdO_xTe_{1-x} NPs. The CdTe band gap was tuned to 2.27 eV by using oxygen and to 3.06 eV by the introduction of Se into the compound.

8.2. Experimental

8. 2.1 Synthesis

Cadmium acetate (≥99%) and L-cysteine (≥98%) were purchased at poly chem industries Durban South Africa while potassium tellurite (≥90%) and sodium borohydride (≥98%) was purchased at Aldrich chemicals. Synthesis method was adapted from previous work with few modifications done [24]. Briefly, CdO_xTe_{1-x} NPs were synthesized as follows: 2 mmol of Cd $(CH_3COO)_2$. $2H_2O$ was dissolved into 50 ml of deionized water in a beaker followed by addition of 1 mmol of L-cysteine with adjustment of pH to 11 using 1M NaOH solution. After stirring for 15 min, appropriate amounts of K_2TeO_3 and $NaSe_2SO_3$ were added to the respective precursor solutions to make $CdTe_xSe_{1-x}$ and CdO_xTe_{1-x} NPs. After this 0.8 g of $NaBH_4$ was then added into the solutions. The reactants were then transferred to individual three-necked flasks and refluxed at 100 ^oC under open air condition. As synthesis time increased, there was an observable color change from green to red and finally to black. The growths of the NPs were then monitored at different growth time.

8.2.2 Characterization

In this study, structural characterization of the CdO_xTe_{1-x} nanoparticles involved the use of powder X-ray diffractometer (XRD) and scanning electron microscope (SEM) while the optical properties; UV–Vis reflection and photoluminescence spectra for the CdO_xTe_{1-x} solution were measured at room temperature with a Nicolet evolution 100 UV-vis spectrophotometer and a Nanolog Horiba JOBYN YVOWN spectrometer, respectively at University of the Free State. PL spectra were taken at the excitation wavelength $\lambda = 350$ nm.

8.3. Results and Discussion

8.3.1 Structural and Compositional analysis

8.3.1.1 SEM analysis

Fig. 8.1 shows SEM images (scale bar = 5μm) of the representative CdO_xTe_{1-x} (a, b, c) and $CdTe_xSe_{1-x}$ (d, e and f) NPs for different reaction times. The SEM results display agglomerated morphology but the primary particles of the agglomerates are in nano scale and the XRD results confirm the same. CdO_xTe_{1-x} NPs display smooth spherical shape which

changes to oval-like while $CdTe_xSe_{1-x}$ NPs possessed spherical shapes which agglomerate at a longer time. Spherical shaped NPs are always known to be thermodynamically stable.

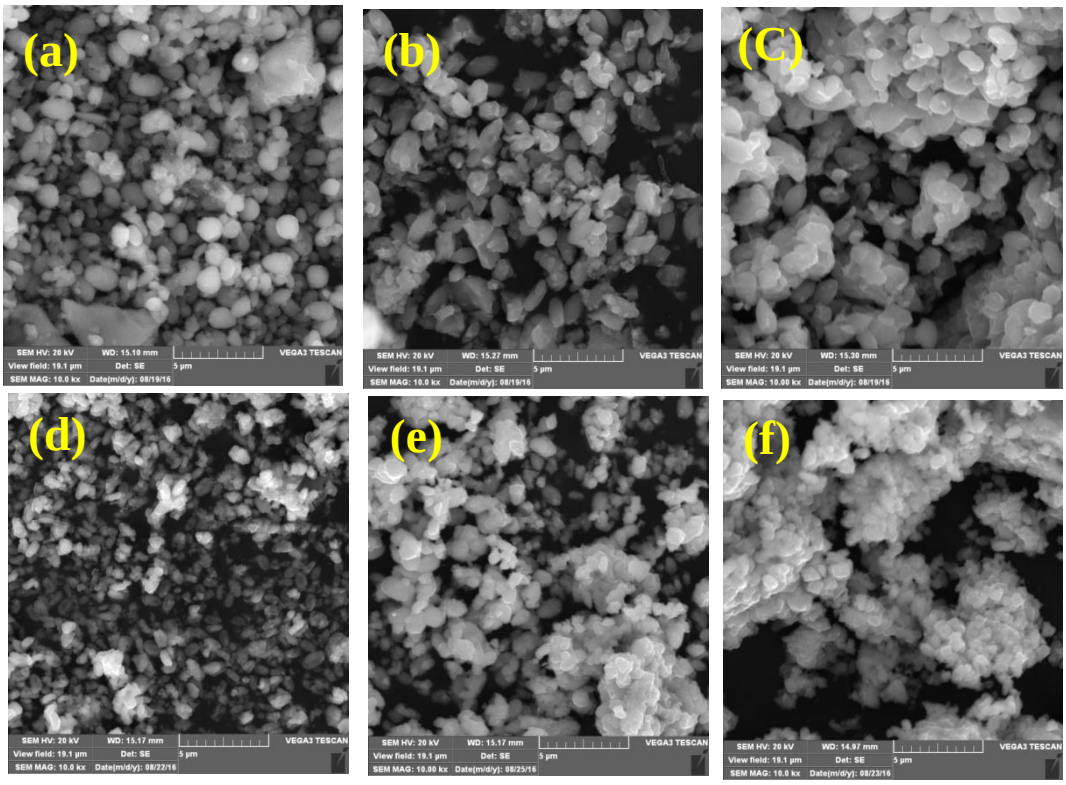

Figure 8.1: SEM micrographs of CdO_xTe_{1-x} (a, b, c) and $CdTe_xSe_{1-x}$ (d, e, f) NPs; taken at 30(a, d), 60(b, e) and 240(c, f) min of reaction time.

It is clear from the images that $CdTe_xSe_{1-x}$ NPs are smaller than CdO_xTe_{1-x} NPs. Larger particle size at a longer time could be attributed to Ostwald process which slowly leads to a reduction in the total number of particles.

8.3.1.2 XRD Analysis

The XRD can provide information both about the crystal structure and crystalline properties of the NPs. Fig. 8.2(a) shows the XRD patterns of the as-synthesized CdO_xTe_{1-x} and $CdTe_xSe_{1-x}$ NPs. Mixed phases of CdTe with CdO for CdO_xTe_{1-x} and CdTe with CdSe for $CdTe_xSe_{1-x}$ are observed. The diffraction peaks for CdO_xTe_{1-x} NPs are more indexed to CdTe wurtzite structure according to JCPDS card no. 19-0193 and the cubic phase of CdO (JCPDS 05-0640). The main peak is centered at the neighborhood of $2\theta = 33^o$. Peaks marked with asterisks (*) might be impurities from unreacted precursors like the L-cystine and/or telluride elements which could not react completely.

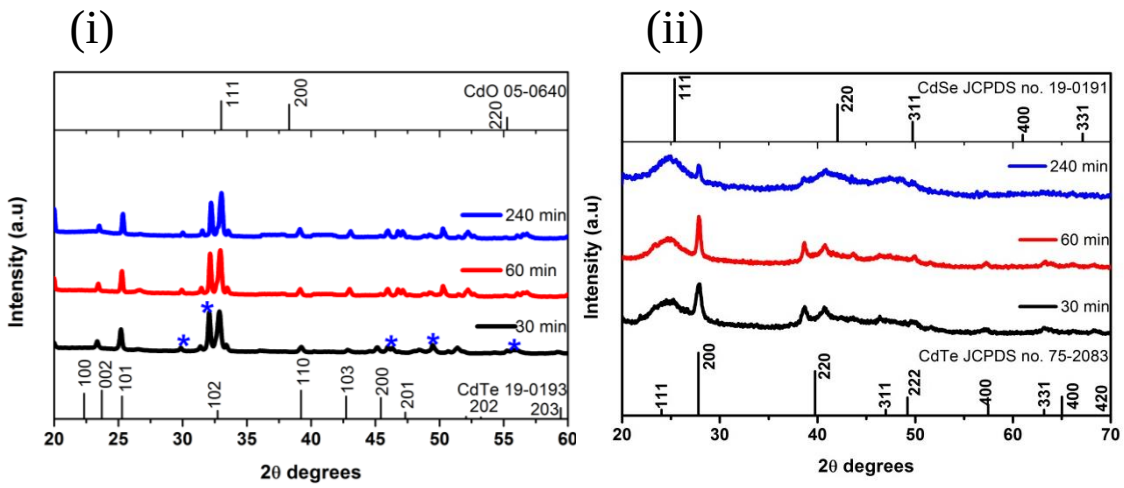

Figure 8.2 (a): XRD patterns for (i) CdO_xTe_{1-x} and (ii) $CdTe_xSe_{1-x}$ NPs synthesized at different reaction times min.

Te is very reactive and hence can easily form TeO_2 or Te element. It seems the presence of Se precursor displaces the O_2 ions. If the crystallites in a nanopowder sample have shapes e.g. plate or needle like shapes it can be very difficult to get them to adopt random orientations. In this case it seems the preferred orientation is along the peak at $2\theta = 32^o$, hence the most intense peak. On the other hand, all $CdTe_xSe_{1-x}$ diffraction peaks in the XRD patterns for the as-prepared $CdTe_xSe_{1-x}$ samples grown at different reaction times (Fig. 8.2(a) (ii)) had mixed phases well indexed to zinc blende based on the CdSe JCPDS no. 19-0191 and CdTe compared to the JCPDS NO.75-2083 for zinc blende CdTe structure. The crystallite sizes of the as-prepared nanoparticles were estimated using Debye-Scherrer formula [25].

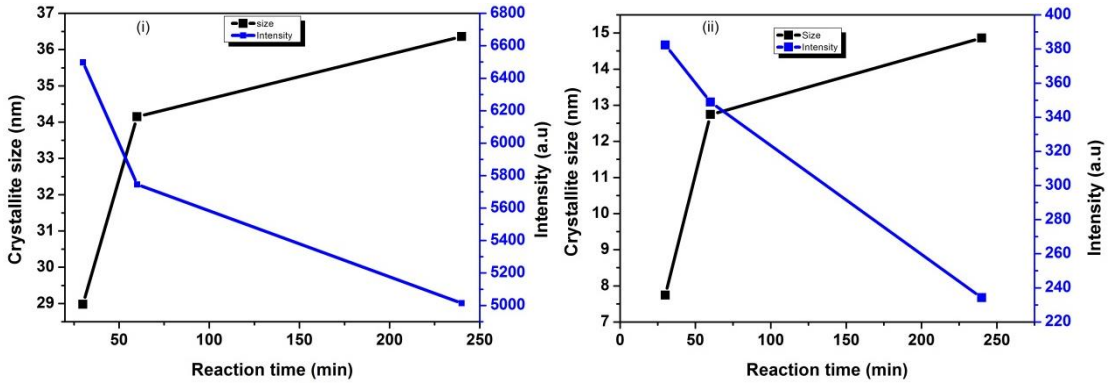

Figure 8.2 (b): Graphs showing changes in crystallite sizes and relative intensities of (i) CdO_xTe_{1-x} and (ii) $CdTe_xSe_{1-x}$ NPs with reaction time.

The crystallite sizes determined by XRD using the peak (102) were 29, 34 and 36 nm for CdO_xTe_{1-x} synthesized at 30, 60 and 240 minutes respectively while for $CdTe_xSe_{1-x}$ NPs the average crystallite sizes were estimated using CdTe peak (111) and peak (200). The obtained average values of the $CdTe_xSe_{1-x}$ NPs were 8, 13 and 15 nm for 30, 60 and 240 min reaction

time respectively. Both CdO_xTe_{1-x} and $CdTe_xSe_{1-x}$ NPs displayed an increase in crystallite sizes with reaction time. A continuous decrease in XRD peak intensities was also observed (Fig. 8.2(b)) for (102) and (111) peaks.

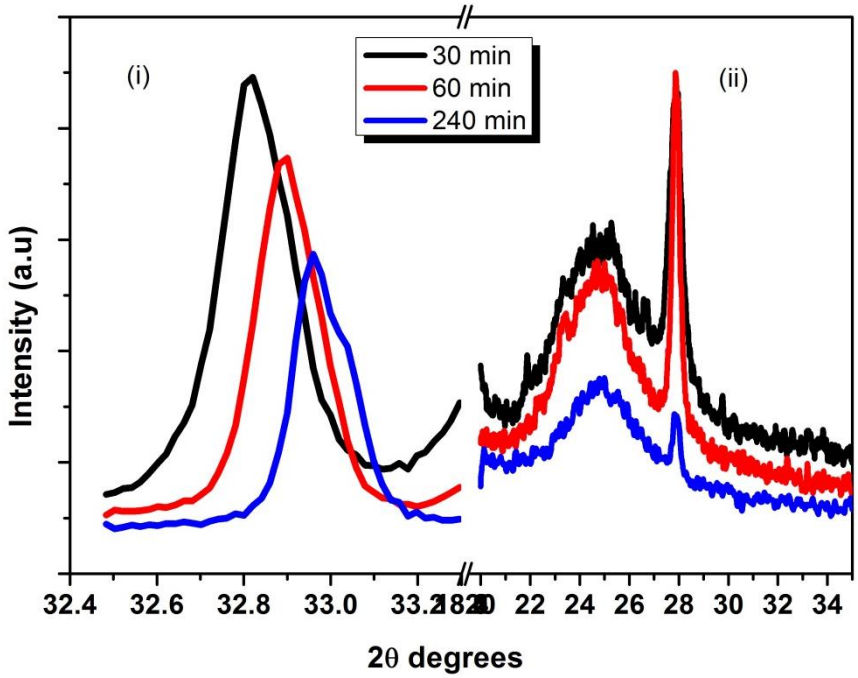

Figure 8.2(c): merged magnified XRD spectra of the as-prepared (i) CdO_xTe_{1-x} and (ii) $CdTe_xSe_{1-x}$ NPs for different reaction times.

The peak positions are observed to slightly shift to higher diffraction angle as demonstrated by peak (102) shift from 32.85 to 33.01º for CdO_xTe_{1-x} and peak (200) shift from 27.84 to 27.87º for $CdTe_xSe_{1-x}$ NPs as reaction time increase from 30 to 240 min. If excess tellurium atoms do not occupy the proper lattice positions, the crystallinity of CdO_xTe_{1-x} may be deteriorated [26] causing decrease in peak intensity of the NPs. The decrease in peak intensities can also be explained to be due to the high volatility of tellurium [27] while the peak shift with reaction time could be due to incorporation of the oxygen in the structure (for CdO_xTe_{1-x} NPs) or might be due to defects caused by some impurities present in the sample. Change of phase from polycrystalline in CdO_xTe_{1-x} to almost amorphous phase in $CdTe_xSe_{1-x}$ could be due to the random vibrations of atoms from their neutral positions due to fluctuations in their internal energy leading to lattice distortion thus reducing the perfection of the crystalline structure hence, lowering the heights of the diffraction peaks. The random distribution of atoms out of crystal lattice can also be responsible for the reduction in XRD peak intensities [25] or it could be that during XRD, severe X-ray scattering occurred on the roughened Bragg diffraction planes, weakening the diffraction signals [28, 29].

8.3.2 Influence on photoluminescence properties

Effect of reaction time on the optical properties was observed to have a great influence on the absorbance and emission of the as-prepared NPs as shown in Fig. 8.3 (a). The PL emission in CdO_xTe_{1-x} NPs could be attributed to electron hole recombination while the emission in $CdTe_xSe_{1-x}$ NPs could be attributed to defects in the as-prepared sample [30]. With an increase in reaction time the emission wavelength redshifted from approximately 510 to 566 nm for CdO_xTe_{1-x} NPs while $CdTe_xSe_{1-x}$ NPs had their emission shifting from 620 to 653 nm. Temporal evolution of the optical properties consisting of absorption and emission is indicative of the formation and growth of QDs [31]. Red shifting of the PL emission peaks could also be due to the increase in the size of NPs as explained in Ostwald ripening process [32]. The emission spectra display a good symmetry and sufficiently narrow full width at half maximum (FWHM) ranging from 41 to 65 nm for CdO_xTe_{1-x} NPs and 79 to 100 nm for $CdTe_xSe_{1-x}$ NPs. It is observed from Fig. 8.3(b) that the NPs continuously change the emission color from green to orange as reaction time increases which confirm the PL.

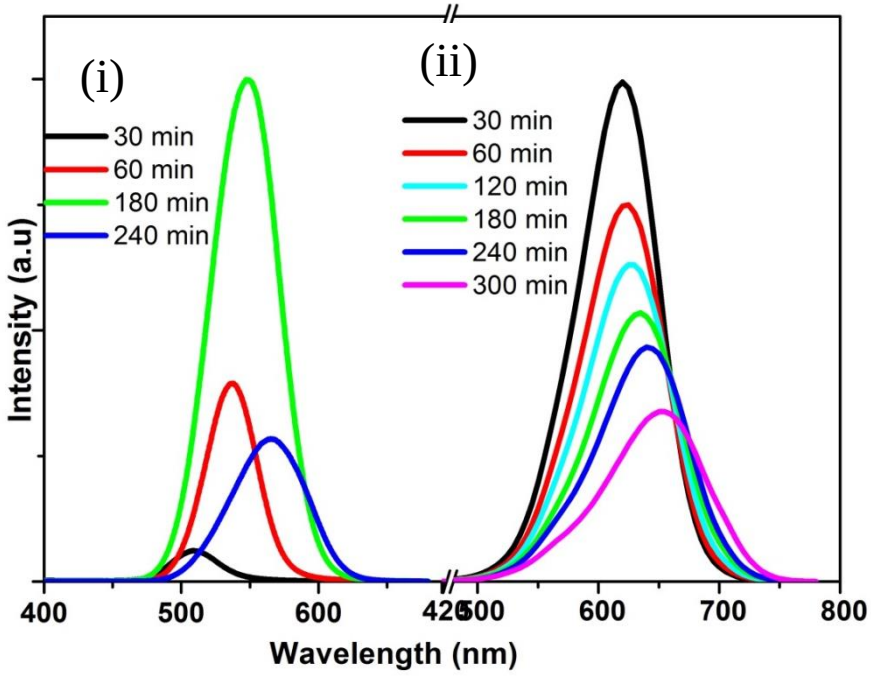

Figure 8.3(a): PL emission spectra of (i) CdO_xTe_{1-x} and (ii) $CdTe_xSe_{1-x}$ NPs prepared at various reaction times

The intensity of the PL emission spectra for CdO_xTe_{1-x} NPs increases until 180 minutes of reaction time when it starts to decrease as shown in Fig. 8.3(c) (i) which was most likely because of the oxidation of the stabilizer molecules, which resulted in reduced stabilization of the ligands and increased the surface defects of the NPs [33].

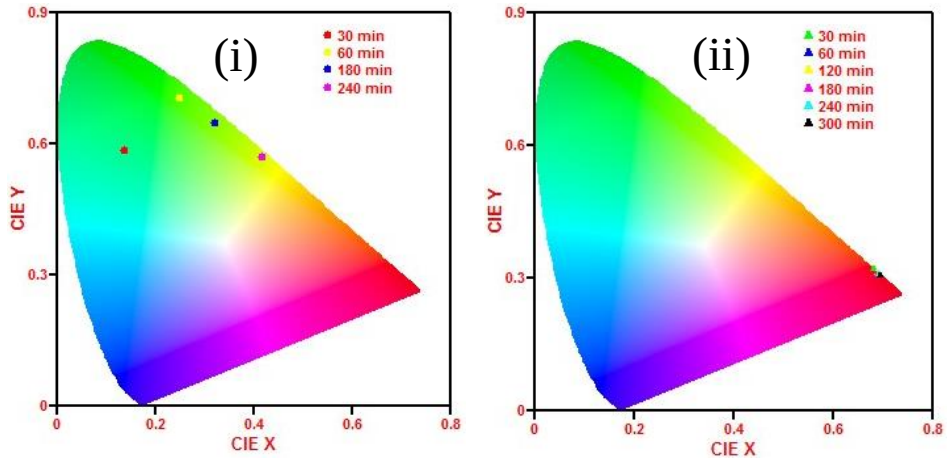

Figure 8.3 (b): PL emission International Commission on Illumination (CIE) of (i) CdO_xTe_{1-x} and (ii) $CdTe_xSe_{1-x}$ NPs prepared at various reaction times

The preformed CdTe nanocrystals exhibited an emission at 547 nm [24] which was quenched for the dislocation of the electron and hole because of the type II band gap offset, [34, 35] when reduced selenium solution was introduced into the solution. The NPs grew gradually as indicated by the redshift of the PL spectra. However, the peak intensity of the as-obtained $CdTe_xSe_{1-x}$ NPs on the other hand continuously decreased as the reaction time progressed from 15 to 300 minutes. The observed quenching in PL could be due to the large surface area to volume ratio of the NPs. It is known that the amplitude of the emission bands is increased by orders of magnitude with decreasing grain size [30]. During this period, FWHM generally broadened slowly with increasing reaction time showing a narrow size distribution of the nanoparticles.

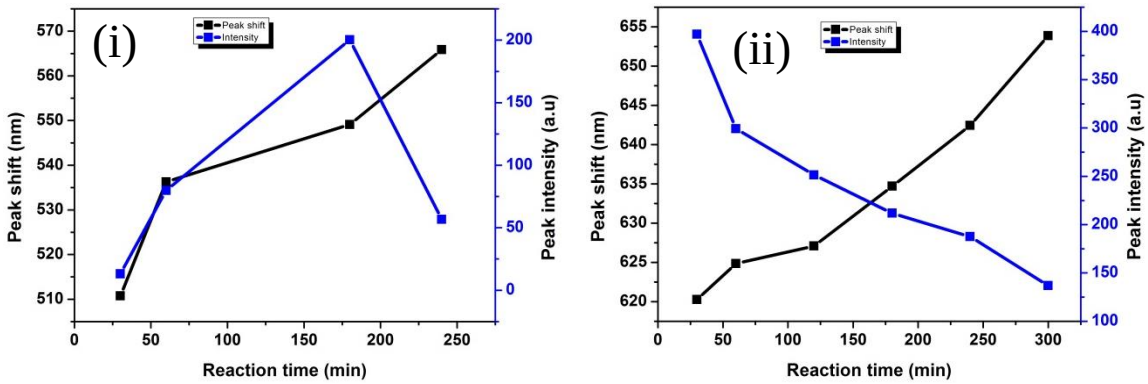

Figure 8.3 (c): Variation of PL emission wavelength and intensity (i) CdO_xTe_{1-x} and (ii) $CdTe_xSe_{1-x}$ NPs with reaction time.

8.3.3 Influence on ultra-violet visible properties

Composition and reaction time were critical for the optical properties of the as-prepared NPs. The optical properties of the NPs depended on the size of the CdO_xTe_{1-x} and $CdTe_xSe_{1-x}$ NPs formed.

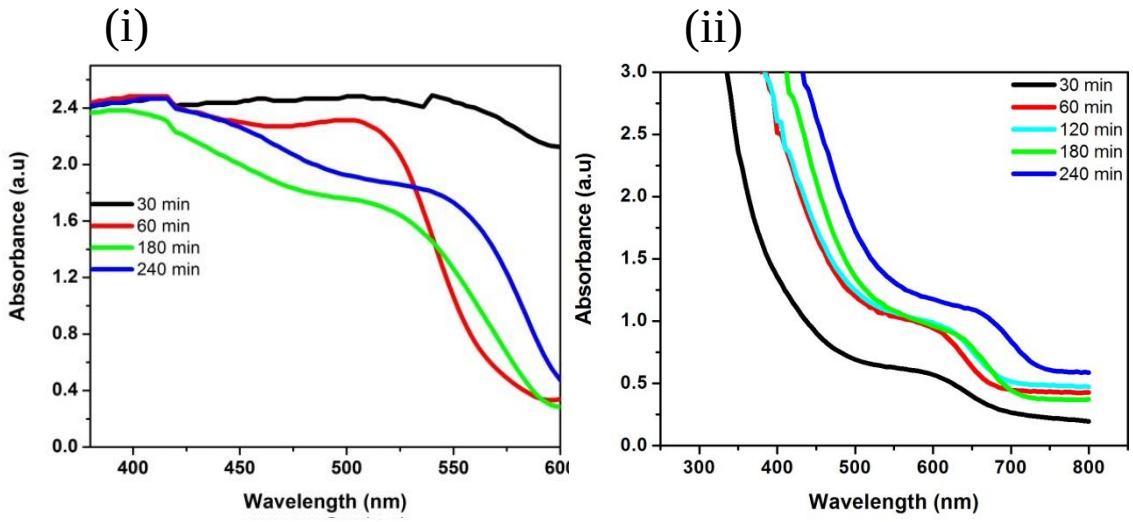

Figure 8.4(a): absorption spectra of (i) CdO_xTe_{1-x} and (ii) $CdTe_xSe_{1-x}$ NPs prepared at various reaction times.

The absorption spectra of the CdO_xTe_{1-x} NPs showed typical broad peaks in the visible region as compared to $CdTe_xSe_{1-x}$ NPs. The absorption band maxima are well resolved for CdO_xTe_{1-x} and $CdTe_xSe_{1-x}$ NPs indicating narrow size distribution of the synthesized NPs. The absorption peaks of the NPs shifted to longer wavelength as reaction time increased, Fig. 8.4 (a). There is, however, a general decrease in absorbance observed in CdO_xTe_{1-x} while an increase in absorbance is depicted by $CdTe_xSe_{1-x}$ NPs with increase in reaction time. Aggregation of the NPs led to decrease in absorption intensity, red shift and peak broadening [36]. The difference in absorption edges observed could be due to non-uniformity of the nanocrystals as confirmed by SEM images. The absorption peaks of CdO_xTe_{1-x} NPs is distributed between 505-523 nm (60-240 min) while for $CdTe_xSe_{1-x}$ NPs is between 591-658 nm (30-300 min). The red shift of the absorption edges of $CdTe_xSe_{1-x}$ could also be attributed to the inter-band gap between CdTe and CdSe parts [37,38] while red-shift observed in CdO_xTe_{1-x} NPs may be attributed to the larger particle size and thermal defects in the compound [39].

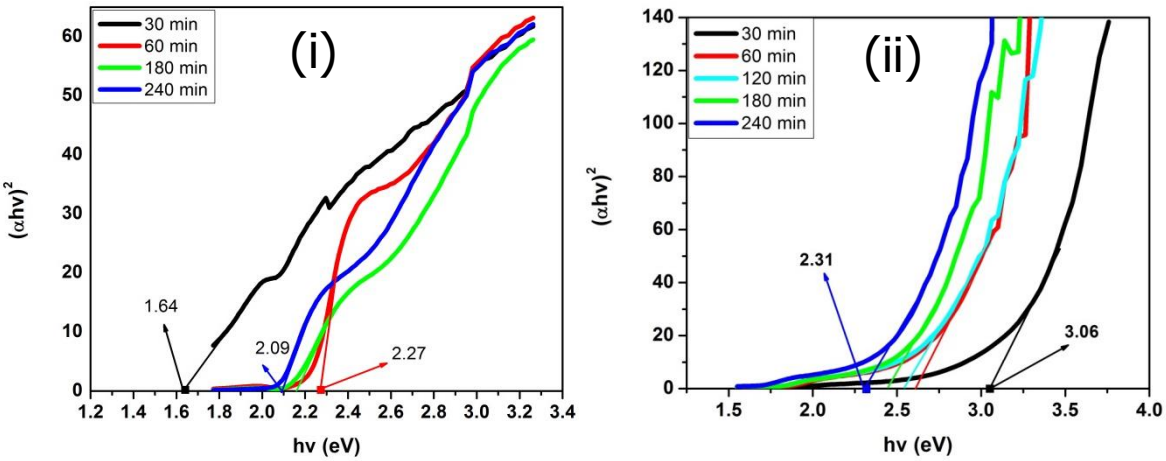

Figure 8.4(b): Tauc plot (αhv) ^{2} v/s hν to determine the band gap energy of (i) CdO_xTe_{1-x} and (ii) $CdTe_xSe_{1-x}$ NPs prepared at various synthesis time.

The band-gap energy (Eg) of the as-prepared NPs was determined based on the numerical derivative of the absorption coefficient (α). The variation in optical density with wavelength was analyzed to find out the optical energy band gap using the Tauc relation [40];

$$\alpha hv = A(hv - Eg)^n \qquad (13)$$

where A is a constant which arises from Fermi's golden rule for fundamental band-to-band electronic transitions and exponent n=1/2 for the direct allowed electronic transitions while n= 2 for allowed indirect transition and E_g is the optical energy band gap between the valence band and the conduction band. The optical band gap energies were evaluated by extrapolating the linear part of the Tauc plot to energy (hv) axis, Fig. 8.4(b). Approximately linear nature of the plot is observed towards the lower wavelength and exponentially behavior towards the higher wavelength which indicated the presence of direct optical transition. Generally, an increase in band gap energy with increasing reaction time was observed for CdO_xTe_{1-x} NPs (1.64, 2.27, 2.15 and 2.09 eV at 30, 60, 180 and 240 minutes respectively). The unexpected trend in the band gap of 30 min sample could be attributed to variation in preparation and environmental conditions. These values are higher than the bulk band gap of CdTe and lower than CdO band gap either. This trend was also observed by ref [41].This could be due to the mixed phases of both telluride and oxide which are both present in the compound formed. Conversely, the band gap of $CdTe_xSe_{1-x}$ NPs were found to be 3.06, 2.62, 2.54 , 2.44 and 2.31 eV for reaction time 30, 60, 120, 180 and 300 minutes respectively as depicted in Fig. 8.4(b) (ii). The observed decrease in the optical band gap with an increase in reaction time is due to the variation in lattice defects and stress [42].

Conclusion

Cysteine-capped CdO_xTe_{1-x} and $CdTe_xSe_{1-x}$ NPs with high luminescence properties was successfully prepared by one-step synthesis method using potassium telluride as Te source, sodium selenosulphate as Se source and $NaBH_4$ as a reductant. PL properties of the NPs were not only influenced by reaction time but also the size of the NPs formed. The spherical green-red emitting NPs with maximum intensity can be prepared at pH 11 at a reaction temperature of 100 ^oC for various reaction times. However for it to emit at the red region, longer duration of synthesis is recommended though the intensity will be very small. The XRD pattern for all $CdTe_xSe_{1-x}$ NPs samples was indexed to zinc blende structure while for CdO_xTe_{1-x} NPs the XRD results showed mixed phases of CdTe (wurtzite) and CdO (zinc blende) bulk structure. The crystallite sizes increased with increase in the growth time in both cases. The larger crystallite size in CdO_xTe_{1-x} NPs is attributed to larger the ionic radius of oxygen than the ionic radius of selenium in $CdTe_xSe_{1-x}$ NPs. UV-Vis analysis displayed well-resolved maxima which generally shifted to longer wavelengths for a prolonged duration of synthesis. There was an observable variation of energy band gaps of the as-prepared NPs with respect to reaction time. $CdTe_xSe_{1-x}$ NPs were found to possess better properties due to their small sizes than CdO_xTe_{1-x} NPs as observed from the various analysis techniques. The method of preparation, however, is low-cost and suitable for large scale production.

References

[1] C.D. Liang, L. Jia, Y.F. Xue, H. Man, P.F. Xiao, T.Y. Zhao, W.Q. Qu, P.W. Dai, L. Yan, "Chemical Synthesis and Applications of Graphene and Carbon Materials", J. Biomat, 2008, 29,4170.

[2] X.H. Gao, Y.Y. Cui, R.M. Levenson, L.W.K. Chung, S.M. Nie, "In vivo cancer targeting and imaging with semiconductor quantum dots.", J. Nat Biotech, 2004, 22, 969.

[3] W.B. Cai, D.W. Shin, K. Chen, O. Gheysens, Q.Z. Cao, S.X. Wang, S.S. Gambhir, X.Y. Chen, "Peptide-Labeled Near-Infrared Quantum Dots for Imaging Tumor Vasculature in Living Subjects", J. Nano Lett, 2006, 6, 669.

[4] J. Li, C. Wu, P. Xu, L. Shi, B. Chen, M. Selke, H. Jiang , X. Wang, "Multifunctional effects of Cys–CdTe QDs conjugated with gambogic acid for cancer cell tracing and inhibition", RSC Adv, 2013, 3, 6518.

[5] C. Bhattacharya, Z. Yu, M. J. Rishel, S. M. Hecht, "The carbamoylmannose moiety of bleomycin mediates selective tumor cell targeting", Biochem, 2014, 53, 3264.

[6] D. Li, X. Liu, G. Xie, X. Liu, "Stable and water-soluble CdTe@ SiO 2 composite nanospheres: Preparation, characterization and application in LED", Colloids Surf. A, 2013, 424, 33.

[7] T. Kabashima, Z. Yu, C. Tang, Y. Nakagawa, K. Okumura, T. Shibata, J. Lu, M. Kai, "A selective fluorescence reaction for peptides and chromatographic analysis", Pep, 2008, 29, 356.

[8] M. C. Schlamp, X. Peng, A. P. Alivisatos, "Improved efficiencies in light emitting diodes made with CdSe (CdS) core/shell type nanocrystals and a semiconducting polymer", J. Appl. Phys, 1997, 82, 5837.

[9] M. T. Harrison, S. V. Kershaw, M. G. Burt, A. L. Rogach, A. Kornowski, A. Eychmuller, H. Weller, "Colloidal nanocrystals for telecommunications. Complete coverage of the low-loss fiber windows by mercury telluride quantum dot", Pure App. Chem, 2000, 72, 295.

[10] M. Han, X. Gao, J. Z. Su, S. Nie, "Quantum-dot-tagged microbeads for multiplexed optical coding of biomolecules", Nat Biotech, 2001, 19, 631.

[11] Y. Liu, V.C.S. Reynoso, L.C. Barbosa, R.F.C. Rojas, H.L. Fragnito, C.L. Cesar, O.L. Alves, "Trap elimination in CdTe quantum dots in glasses", J. Mat. Sci. Lett, 1995, 14, 635.

[12] F.P. Koffyberg, “Thermoreflectance spectra of CdO: Band gaps and band-population effects”, Phy.Rev.B, 1976, 13, 4470.

[13] W.W. Yu, L.H. Qu, W.Z. Guo, X.G. Peng, “Experimental Determination of the Extinction Coefficient of CdTe, CdSe, and CdS Nanocrystals”, J. Chem Mat, 2003, 15, 2854.

[14] Y.S. Liu, Y.H. Sun, P.T. Vernier, C.H. Liang, S.Y.C. Chong, M.A. Gundersen, “pH-Sensitive Photoluminescence of CdSe/ZnSe/ZnS Quantum Dots in Human Ovarian Cancer Cells”, J. Phy Chem C, 2007, 111, 2872.

[15] A.M. Kapitonov, A.P. Stupak, S.V. Gaponenko, E.P. Petrov, A.L. Rogach, A. Euchmulier, “Luminescence properties of thiol-stabilized CdTe nanocrystals”, J. Phy Chem B, 1999, 103, 10109.

[16] Y.F. Liu, W. Chen, A.G. Joly, Y.Q. Wang, C. Pope, Y.B. Zhang, J.O. Bovin, P. Sherwood, “Comparison of water-soluble CdTe nanoparticles synthesized in air and in nitrogen”, J. Phy Chem B, 2006, 110,16992.

[17] C.B. Murray, D.J. Norris, M.G. Bawendi, “Synthesis and characterization of nearly monodisperse CdE (E= sulfur, selenium, tellurium) semiconductor nanocrystallites”, J. Am. Chem Soc, 1993, 115, 8706.

[18] P. Reiss, J. Bleuse, A. Pron, “Highly luminescent CdSe/ZnSe core/shell nanocrystals of low size dispersion”, Nano Lett, 2002, 2, 781.

[19] A.L. Rogach, T. Franzl, T.A. Klar, J. Feldmann, N. Gaponik, V. Lesnyak, A. Shavel, A. Eychmuller, Y.P. Rakovich, J.F. Donegan, “Aqueous synthesis of thiol-capped CdTe nanocrystals: state-of-the-art”, J. Phy Chem C, 2007, 111,14628.

[20] P.J. Laura, S.M. Sandra, W.L. Laura, A.H. Jack, “Effect of N-acetylcysteine on acetaminophen toxicity in mice relationship to reactive nitrogen and cytokine formation Toxicol”, Toxicol. Sci, 2003, 75, 458.

[21] A.O. Choi, S.J. Cho, J. Desbarats, J. Lovric, D.J. Maysinger, “Quantum dot-induced cell death involves Fas upregulation and lipid peroxidation in human neuroblastoma cells”, Nanobiotech, 2007, 5, 1.

[22] J. Lovric, H.S. Bazzi, Y. Cuie, G.R.A. Fortin, F.M. Winnik, D.J. Maysinger, “Differences in subcellular distribution and toxicity of green and red emitting CdTe quantum dots”, J. Mol. Med, 2005, 83, 377.

[23] M. Kieliszek, B. Stanisław, “Selenium: significance, and outlook for supplementation”, Nutrition 2013, 29, 713.

[24] S. Kiprotich, J. Ungula, B.F. Dejene, M.O. Onani, "The influence of reaction times on structural, optical and luminescence properties of cadmium telluride nanoparticles prepared by wet-chemical process", Phy B, 2016, 480, 125.

[25] B.D. Cullity, "Elements of X-ray Diffraction", AWPC, Inc. Massachusetts, 1967.

[26] M.Y. El Azhari, M. Azizan, A. Bennouna, A. Outzourhit, E. L. Ameziane, M. Brunel, "Preparation and characterization of CdTeO 3 thin films", Thin Solid Films , 2000, 366, 82.

[27] J.P. Nair, R. Jayakrishnan, N.B. Chaure, R.K. Pandey, "In situ Sb-doped CdTe films", Sem. sci tech, 1998, 13, 340.

[28] P.H. Dederichs, "Diffuse scattering from defect clusters near Bragg reflections", Phy. Rev. B, 1971, B4, 1041.

[29] J.W. Yeh, S.J. Lin, T.S. Chin, J.Y. Gan, S.K. Chen, T.T. Shun, C.H. Tsau, S.Y. Chou, "Formation of simple crystal structures in Cu-Co-Ni-Cr-Al-Fe-Ti-V alloys with multiprincipal metallic elements", Met mat trans A, 2004, 35, 2533.

[30] V.V. Tetyorkin, A.V. Sukach, S.V. Stariy, V.A. Boiko, "Photoluminescence studies of CdTe polycrystalline films", Quantum Elect & Opto, 2012, 15, 340.

[31] H. Mattoussi, J.M. Mauro, E. Goodman, G.P. Anderson, V.C. Sundar, F.V. Mikulec, M.G. Bawendi, "Self-assembly of CdSe− ZnS quantum dot bioconjugates using an engineered recombinant protein", J. Am. Chem. Soc. 2000,122, 12142.

[32] X. Peng, J. Wickham, A.P. Alivisatos, "Kinetics of II-VI and III-V colloidal semiconductor nanocrystal growth:"focusing" of size distributions", J. Am. Chem. Soc., 1998, 120, 5343.

[33] Y. Yu, L. Xu, J. Chen, H. Gao, S. Wang, J. Fang, S. Xu, "Hydrothermal synthesis of GSH–TGA co-capped CdTe quantum dots and their application in labeling colorectal cancer cells", Colloids Surf B, 2012, 95, 247.

[34] D.J. Milliron, S.M. Hughes, Y. Cui, L. Manna, J.B. Li, L.W. Wang, A.P. Alivisatos, "Colloidal nanocrystal heterostructures with linear and branched topology.", Nat, 2004, 430,190.

[35] P. Peng, D.J. Milliron, S.M. Hughes, J.C. Johnson, A.P. Alivisatos, R.J. Saykally, "Femtosecond spectroscopy of carrier relaxation dynamics in type II CdSe/CdTe tetrapod heteronanostructures", Nano Lett, 2005, 5, 1809.

[36] V. Poderys, M. Matulionyte, A. Selskis, R. Rotomskis, "Interaction of water-soluble CdTe quantum dots with bovine serum albumin", Nanoscale Res Lett, 2010, 6, 9.

[37] L. Carbone, S. Kudera, C. Giannini, G. Ciccarella, R. Cingolani, P.D. Cozzoli, L.J. Manna, “Selective reactions on the tips of colloidal semiconductor nanorods”, Mat. Chem, 2006, 16, 3652.

[38] R.G. Xie, U. Kolb, T. Basche, “Design and synthesis of colloidal nanocrystal heterostructures with tetrapod morphology”, Small, 2006, 2, 1454.

[39] S.D. Gunjal, Y.B. Khollam, S.R. Jadkar, T. Shripathi, V.G. Sathe, P.N. Shelke, M.G. Takwale, K.C. Mohite, “Spray pyrolysis deposition of p-CdTe films: Structural, optical and electrical properties”, Sol. Energy 2014, 106, 56.

[40] U.P. Khairnar, D.S. Bhavsar, R.U. Vaidya, G.P. Bhavsar, “Optical properties of thermally evaporated cadmium telluride thin films”, Mat. Chem. Phys, 2003, 80, 421.

[41] P.H. Jefferson, S. A. Hatfield, T.D. Veal, P. D. C. King, C.F. McConville, J. Z. Pérez, V. M. Sanjosé, “Bandgap and effective mass of epitaxial cadmium oxide”, App Phy Lett 2008, 92, 022101.

[42] Y.C. Lin, B.L. Wang, W.T. Yen, C.T. Ha, C. Peng, “Effect of process conditions on the optoelectronic characteristics of ZnO: Mo thin films prepared by pulsed direct current magnetron sputtering”, Thin Solid Films, 2010, 518, 4928.

Chapter 9

Future work

- Investigation on the effect of other different reaction parameters should be done so as to establish the perfect conditions for the preparation of CdTe NPs and be able to obtain a wide range of spectrum of colors and also to improve the stability of the NPs.
- Different synthesis techniques should be explored. With the current synthesis technique multiple phases of CdTe NPs are formed in the process. This is affecting the PL intensity as well as the crystal structure and morphology. A technique should be found that is both fast, cheap and that is producing high quality, pure CdTe QDs.
- Investigation should be done using other techniques other than those applied in this study in order to get more detailed information on the various properties of the NPs which will enhance their performance in applications.
- Studies on effect of shell growth on the preformed CdTe NPs should be done so as to obtain a wide spectrum of colors especially the NIR emissions. It would be even more exciting to investigate the effect of shell growth on different core materials.
- Effect of annealing temperatures on the optical, structural and luminescent properties of the as-prepared samples should also be put into consideration. This may have some good effect in obtaining pure NPs. Also different inert gasses can be used during synthesis process to prevent the formation of multi-phased CdTe QDs.
- Research could also be done on growing CdTe and $CdTe_xSe_{1-x}$ thin films and studying the effect of growth conditions.
- Investigation on different other dopants on the structural and luminescent properties of CdTe NPs should be conducted.

List of Figures

List of Tables

Publications

The following papers have been submitted for publication by the following authors;
Kiprotich S., Dejene B.F., Onani M.O.

1. The influence of reaction times on structural, optical and luminescence properties of cadmium telluride nanoparticles prepared by wet-chemical process (published). https://doi.org/10.1016/j.physb.2015.08.062
2. A comparison investigation of optical, structural and luminescence properties of CdO_xTe_{1-x} and $CdTe_xSe_{1-x}$ nanoparticles prepared by a simple one pot. (Published) https://doi.org/10.1016/j.physb.2017.06.057
3. High luminescent L-cysteine capped CdTe quantum dots prepared at different reaction times (Published). https://doi.org/10.1016/j.physb.2017.07.037
4. Effect of growth temperature on the structural, optical and luminescence properties of CdTe nanoparticles (Submitted to Journal of material science).
5. Effect of tellurium concentration on the structural, optical and luminescence properties of CdTe nanoparticles (submitted to Journal of luminescence).

Conferences

- **6th South African Conference of Photonic Materials (SACPM)** Mabula (RSA) 3rd - 8th May 2015, The influence of reaction times on structural, optical and luminescence properties of cadmium telluride nanoparticles prepared by wet-chemical process; Kiprotich S., Dejene B.F., Ungula J. and Onani M.O.

- **61st Annual conference of the South African institute of Physics (SAIP)** University of capetown (UCT), Capetown (RSA) 4th - 8th July 2016, Effect of refluxing growth time on optical, structural and luminescent properties of ZnTe quantum dots, Kiprotich S., Dejene B.F. and Onani M.O.

- **7th South African Conference of Photonic Materials (SACPM)** Amanzi (RSA) 27th - 31st March 2017, A comparison investigation of optical, structural and luminescence properties of CdO_xTe_{1-x} and $CdTe_xSe_{1-x}$ nanoparticles prepared by a simple one pot; Kiprotich S., Dejene B.F. and Onani M.O.

- **7th South African Conference of Photonic Materials (SACPM)** Amanzi (RSA) 27th - 31st March 2017, High luminescent L-cysteine capped CdTe quantum dots prepared at different reaction times; Kiprotich S., Dejene B.F. and Onani M.O.

Glossary

Some common terminologies used

(i). Luminescence

Luminescence is explained to be a process where the electronic states of substance is excited by some kind of external energy source and that excitation energy is given out as light of different wavelengths. Luminescence can also include both fluorescence and phosphorescence [1]. When a higher energy photon is absorbed, a lower energy photon is emitted a process is referred to as a Stokes process. During this Stokes process, the excess energy is absorbed by the solid and appears as lattice vibrational (heat) energy [2]. This kind of luminescence refers to the luminous emission which is not thermal in origin and is thus a form of cold body radiation. This process, however, differentiates between luminescence and incandescence. Incandescence is generation of light by a body at high temperatures. In luminescence, when the electrons overcome their ground state (lowest state) by absorbing excess energy inform of radiations, they gain enough energy to enter into an excited state (highest state). However, the stability of this excited state electron is altered and hence jumps back to the ground state and gives out energy inform of light in the process. In most cases the excitation energy is usually higher than the energy of light emitted (wavelength). Some of the natural luminescence cases are experienced from fire-flies, glow worms and in certain bacteria and aquatic animals. Luminescence is classified into two general groups; first, depending on the type of excitation sources (chemical reactions, electrical energy, subatomic motions, or stress on a crystal) for example electroluminescence, thermoluminescence, cathodoluminescence, photoluminescence or bioluminescence and second depending on the extent in which they glow for instance, fluorescence and phosphorescence.

(ii). Absorption

Absorption can be defined as the intake of energy in the form of electromagnetic radiation (UV or visible light) by a certain material and keeps it within itself. Absorption of energy in luminescent materials takes place by either the host lattice or by intentionally doped impurities [3].

(iii. Excitation

This term is also referred to as "photo-excitation", it is defined as the process in which a sample is illuminated by light of certain specific wavelength which is then absorbed by the

sample and divulges into the material the extra energy. This extra drive into the material elevates the electrons to higher energy states called the excited states.

(iv). Emission

When electrons are excited, they gain energy which makes them unstable. The unstable electrons returns to equilibrium state releasing excess energy in the process. This process is called emission. The process could be radiative (emission of light) or non-radiative (no light is emitted). The photoluminescence wavelength (energy of the emitted light) is usually related to the difference in energy levels between the two electron states involved in the transition, that is, between the excited state and the ground state. The energy of the emitted radiation is always less than that of the absorbed radiation [2].

(v). Transition

The term transition refers to the movement or transfer of electrons from one energy level to another due to either absorption or emission. Release of energy or take up of energy (Excitation and emission) occurs due to electronic transitions at the center [3].

(vi). Relaxation

Relaxation is a process in which after excitation, the nuclei adjust their positions to the new excited state, so that the inter-atomic distances equal the equilibrium distances belonging to the excited state. There is usually no emission observed during relaxation. The system can return to the ground state spontaneously under emission of radiation from the lowest level of the excited state. The emission occurs at a lower energy than the absorption due to the relaxation process. The energy difference between the maximum of the lowest excitation band and that of the emission band is called Stokes shift [4].

References

[1]. R.C. Ropp, M. A. Aia, C. W. W. Hoffman, T. J. Veleker, and R. W. Mooney. “X-ray powder diffraction patterns of strontium phosphates”, Analytical Chemistry 31, 1959, 1163.

[2]. C.R. Ronda, “Luminescence from Theory to Applications”, Willy-VCH, Germany, 2008.

[3]. G. Michael, R. Renata, P. Gérard, “Modern Luminescence Spectroscopy of Minerals and Materials”, 2005, 20

[4]. K. Zweibel, J. Mason, and V. Fthenakis. SCIENTIFIC AMERICAN-AMERICAN EDITION- 298, 2008, 48.